KU LEUVEN

ARENBERG DOCTORAL SCHOOL
Faculty of Science

Trajectories

From quantum mechanics to general relativity

Kasper Meerts

Supervisor:
Prof. dr. Christian Maes

Dissertation presented in partial fulfillment of the requirements for the degree of Doctor of Science (PhD): Physics

September 2023

Trajectories

From quantum mechanics to general relativity

Kasper MEERTS

Examination committee:
Prof. dr. Pavlik Lettinga, chair
Prof. dr. Christian Maes, supervisor
Prof. dr. Wojciech De Roeck
Prof. dr. Thomas Hertog
Dr. Ward Struyve
Prof. dr. Roderich Tumulka
(Eberhard-Karls University, Tübingen)
Prof. dr. Júlia Komjáthy
(Technische Universiteit Delft)

Dissertation presented in partial fulfillment of the requirements for the degree of Doctor of Science (PhD): Physics

September 2023

© 2023 KU Leuven – Faculty of Science
Uitgegeven in eigen beheer, Kasper Meerts, Celestijnenlaan 200D box 2415, B-3001 Leuven (Belgium)

Alle rechten voorbehouden. Niets uit deze uitgave mag worden vermenigvuldigd en/of openbaar gemaakt worden door middel van druk, fotokopie, microfilm, elektronisch of op welke andere wijze ook zonder voorafgaande schriftelijke toestemming van de uitgever.

All rights reserved. No part of the publication may be reproduced in any form by print, photoprint, microfilm, electronic or any other means without written permission from the publisher.

Preface

Hoewel dit de eerste woorden van deze thesis zijn na de titel, zullen het ironisch genoeg ongeveer de laatste zijn die ik schrijf als doctoraatsstudent, nu dit vier jaar lange avontuur langzaamaan ten einde komt. Het is een moment om te reflecteren over wat ik allemaal geleerd en meegemaakt heb, en om mijn dankbaarheid te uiten aan iedereen die me heeft bijgestaan tijdens deze rit. Ik prijs me gelukkig dat ik zoveel mensen mag bedanken die een verschil voor me hebben betekend. Het heeft heel wat voeten in de aarde gehad om tot hier te komen, en dat was me alleen nooit gelukt.

Eerst en vooral wil ik vanuit het diepste van mijn hart mijn promotor bedanken, Christian Maes. Bedankt, Christ. Het lijdt geen twijfel dat zonder jou mijn academische carriere nooit van start was gegaan. Bedankt voor de vele kansen en het vertrouwen, en dat de deur van je kantoor altijd openstond. Ik heb genoten van de vele gesprekken en uitwisseling van gedachten, het was een eer om met je samen te kunnen werken.

Verder zou ik mijn andere academische collega's willen bedanken, zonder wie mijn publicaties nooit tot stand waren gekomen. Ik ben Ward Struyve enorm veel dank verschuldigd voor zijn hulp en de ideeën die hebben bijgedragen tot mijn werk. Bedankt aan Dieter, Aaron en Simon voor de fijne samenwerking. Thank you Faezeh and Irene for being great office mates. And to my colleague Gui obrigado as well.

I would also like to thank the other members of my examination committee, Pavlik Lettinga, Thomas Hertog, Wojciech De Roeck, Roderich Tumulka and Júlia Komjáthy, for taking the time to read and assess my thesis.

Verder ben ik dankbaar voor het ITF en iedereen die daar werkt in het algemeen, en Anneleen en Filip in het bijzonder. Het was een hele fijne werkomgeving en ik zal ze missen.

Buiten de academische wereld wil ik natuurlijk in de eerste plaats mijn ouders bedanken, aan wie ik alles te danken heb. Mama en papa, duizendmaal dank. Ik besef hoe dankbaar ik mag zijn voor de mogelijkheid te hebben gekregen om (zo lang) te kunnen studeren en voor alle steun onderweg, en waardeer dit immens.

Verder ben ik dankbaar dat ik zo'n grote familie heb, met zoveel lieve en oprechte mensen die er voor elkaar zijn, met name mijn meter en mijn broer.

Ook wil ik mijn allerliefste Saffrijn, die mij sinds het laatste kwart van deze tocht vergezelt, bedanken om er altijd voor me te zijn. We zien mekaar graag?

Finally I would like to express my sincere gratitude to my friends and all other people who at some point supported me, compelled me to take action, or simply listened to me. Thank you for always believing in me, even though I kept insisting to the point of annoyance that I could not do it. In no particular order, Ymke, Катя, the fellas, Benjamin, Теодор, Jacob, Yuán and everyone I have forgotten to mention, thank you, спасибо, bedankt, merci, хвала, xièxie, tak!

Abstract

In this work, we investigate a number of physical systems, where we will consistently focus on the paths that particles follow. Trajectories are a known concept in classical mechanics, in fact, the essence of this field can be summarized as figuring out the paths particles take, given the forces acting on them. In quantum mechanics, applying this concept proves to be much more challenging, but it can also lead to a deeper understanding.

To begin with, we revisit canonical quantization of gravity, where we employ point particles for matter. These theories are typically plagued by the problem of time, a conceptual conflict over this notion between quantum field theory on one hand and general relativity on the other, resulting in equations that do not describe evolution through time. We postulate equations of motion for both the point particles and the spatial metric itself, based on the continuity equation associated to the Wheeler-DeWitt equation. These equations of motion yield the classical trajectories of both the particles and the metric, along with an additional non-local term derived from the modulus of the wave function, the quantum potential. In addition, this allows us to define a conserved energy-momentum tensor.

Next, we turn our attention to another quantum theory, that of the Dirac electron. Here, we find a connection with a concept from nonequilibrium statistical mechanics, active matter. Specifically, we observe that the electron can be seen as a run-and-tumble particle, switching between chiralities. These trajectories are used to illustrate the two-slit experiment. Furthermore, they also serve to explore concepts such as the arrival times of particles at detectors.

Finally, we shift our focus to a very different type of particle, the photon. We consider a photon gas that exchanges energy with the environment, where the dominant process is assumed to be inverse Compton scattering. We review the derivation of the Kompaneets equation, a nonlinear Fokker-Planck equation for the dynamics of this system, and generalize the process to a nonlinear Langevin dynamics. This is applied in simulations with the goal of enabling or facilitating extensions to nonequilibrium, which are also briefly illustrated. One motivation considered for this is the processes of the early universe, shortly after the Big Bang, where we question whether this nonequilibrium environment could have left traces on the cosmic microwave background radiation. We also briefly study

another application of nonequilibrium, resetting, where the photon is regularly abruptly lowered in frequency. Several possibilities for resetting are discussed and simulated.

Beknopte samenvatting

In dit werk onderzoeken we een aantal fysische systemen, waar we telkens de aandacht zullen vestigen op de trajecten die de deeltjes volgen. Trajecten zijn bekend als concept in de klassieke mechanica, in feite kan de essentie van dit vak samengevat worden als het uitzoeken van de paden die deeltjes afleggen, gegeven de krachten die er op werken. In kwantummechanica blijkt het veel uitdagender dit concept toe te passen, maar ook hier kan het tot een dieper inzicht leiden.

Om te beginnen hernemen we de canonische kwantisatie van zwaartekracht, waar we puntdeeltjes aanwenden voor de materie. Deze theorieën worden normaal geplaagd door het probleem van de tijd, een conceptueel conflict over dit begrip tussen kwantumveldentheorie enerzijds en algemene relativiteit anderzijds, dat tot gevolg heeft dat de vergelijkingen die het systeem beschrijven geen tijdsevolutie aangeven. Wij postuleren bewegingsvergelijkingen voor zowel de puntdeeltjes als de ruimtelijke metriek zelf, gestoeld op de continuiteitsvergelijking geassocieerd aan de Wheeler-DeWitt vergelijking. Deze bewegingsvergelijkingen leveren ons opnieuw de klassieke trajecten van zowel de deeltjes als de metriek op, met daarbij als toevoeging een niet-lokale term die afgeleid is van de modulus van de golffunctie, het kwantumpotentiaal. Dit laat ons ook toe een behouden energie-impuls-tensor te definieren.

Vervolgens richten we onze aandacht op een andere kwantumtheorie, die van het Dirac elektron. Hier vinden we een connectie met een begrip uit de niet-evenwicht statistische mechanica, actieve materie. We zien namelijk dat het elektron kan worden aanzien als een *run-and-tumble* deeltje, dat wisselt tussen chiraliteiten. Deze trajecten worden gebruikt ter illustratie van het twee-spleten experiment. Verder dienen ze ook om concepten zoals de aankomstijden van de deeltjes bij detectoren te verkennen.

Tenslotte verleggen we onze focus naar een heel ander soort deeltje, het foton. We beschouwen een fotongas dat energie uitwisselt met de omgeving, waar het dominante proces inverse Comptonverstrooiing wordt geacht te zijn. We herzien de afleiding van de Kompaneets vergelijking, een niet-lineaire Fokker-Planck vergelijking voor de dynamica van dit systeem, en veralgemenen het proces tot een niet-lineare Langevin dynamica. Deze wordt toegepast in simulaties. Het doel is om uitbreidingen naar niet-evenwicht toe mogelijk te maken of te

vergemakkelijken, wat ook kort geillustreerd wordt. Een motivatie die hiervoor in acht wordt genomen zijn de processen van het vroege universum, kort na de Oerknal, waar we ons de vraag stellen of deze niet-evenwicht omgeving sporen kan nagelaten hebben op de kosmische achtergrondstraling. We bestuderen ook kort een andere toepassing van niet-evenwicht, resetting, waar het foton regelmatig abrupt verlaagd wordt in frekwentie. Verscheidene mogelijkheden van resetting worden besproken en gesimuleerd.

Conventions and notation

$g_{\mu\nu}$	metric tensor
γ_{ij}	spatial metric
∂_x	partial derivative with respect to x
$\dot{x}$	derivative of x with respect to time
$\mathcal{Q}$	quantum potential density
$\psi^\dagger$	Hermitian conjugate
$\overline{\psi}$	Dirac conjugate, defined as $\overline{\psi} = \psi^\dagger \gamma^0$
χ	chirality, can be $+1$ or -1
$\mathbf{v}$	a 3-vector
$\hat{\mathbf{n}}$	a unit vector
x	dimensionless frequency, defined as $x = \hbar\omega / k_B T$
$n(\mathbf{k})$	photon occupation number
k_B	the Boltzmann constant, approximately $1.38 \times 10^{-23}\,\mathrm{J\,K^{-1}}$
$\langle . \rangle$	expected value

Contents

Preface i

Abstract iii

Beknopte samenvatting v

Conventions and notation vii

Contents ix

List of Figures xiii

1 Introduction 1
- 1.1 Nonequilibrium . . . 2
- 1.2 Wave mechanics . . . 6
  - 1.2.1 Outline . . . 7
- 1.3 Photon stochastic processes . . . 8
  - 1.3.1 Outline . . . 10

I Wave mechanics 13

2 Wave mechanics for gravity with point-particles 15
- 2.1 Introduction . . . 16
- 2.2 Geometrodynamics coupled to point-particles . . . 17
- 2.3 Wave mechanics for 3-metric and particles . . . 20
- 2.4 Hamiltonian form of the quantum dynamics . . . 21
- 2.5 Discussion and outlook . . . 23
- 2.A Functional derivatives in the ADM formalism . . . 24

3 Diffraction and interference with run-and-tumble particles 25
- 3.1 Introduction . . . 26
- 3.2 Spacetime activity . . . 28
- 3.3 Zig-zag theory of the Dirac electron . . . 28
- 3.4 Trajectory visualization . . . 32
  - 3.4.1 Single slit diffraction . . . 34

3.4.2 Double slit interference . . . 39
3.5 Arrival times . . . 44
3.6 Back to classical run-and-tumbling . . . 48
3.7 Conclusions . . . 49

II Photon stochastic processes 51

4 On the derivation of the Kompaneets equation 53
4.1 Introduction . . . 54
4.2 Detailed balance with stimulated emission . . . 57
4.3 Kramers-Moyal expansion . . . 59
4.4 The Boltzmann-Master equation . . . 62
4.5 Diffusion approximation to the Boltzmann Equation . . . 64
4.6 Extending the Kompaneets equation . . . 69
4.7 Conclusions and outlook . . . 71
4.A Expansion of the transition rates . . . 71
4.B Klein-Nishina differential cross section . . . 72
4.C Computation of integrals . . . 74
4.C.1 Integral I_1 . . . 74
4.C.2 Integral I_2 . . . 75
4.C.3 The integrals and the Thomson cross section . . . 76
4.C.4 Nonequilibrium case . . . 77

5 Photon frequency diffusion process 81
5.1 Introduction . . . 81
5.2 Kompaneets equation . . . 83
5.3 Mesoscopics of Compton scattering: Kompaneets stochastic process 86
5.3.1 Jump process in reciprocal space . . . 87
5.3.2 Diffusion limit . . . 89
5.3.3 Tagged photon nonlinear Markov process . . . 90
5.4 Simulation of the Kompaneets process . . . 91
5.5 Bremsstrahlung and double Compton scattering . . . 95
5.6 Extension of the Kompaneets process . . . 97
5.7 Simulation of the extended Kompaneets process . . . 100
5.7.1 Adding low-frequency diffusion . . . 100
5.7.2 Adding frequency-dependent drift . . . 101
5.8 Conclusions . . . 102
5.A Itô's lemma and the Kompaneets process . . . 105
5.B Data availability statement . . . 106

6 Resetting photons 107
6.1 Introduction . . . 107

6.2 The Kompaneets process 109
6.2.1 Kompaneets equation 109
6.2.2 Tagged photon stochastic process 111
6.3 Resetting the Kompaneets process 112
6.4 Simulation results and discussion 115
6.5 Conclusions 118

Epilogue **122**

7 Conclusions and outlook **123**

Bibliography **127**

List of publications **143**

List of Figures

3.1 Spatial setup, with electrons exiting the wall from slits to arrive at the screen. 32
3.2 The desired boxcar function with width $2\sigma_y$ representing the single slit and its approximation by a sum (3.16) of 13 shifted Gaussians. 35
3.3 Near-field behavior of the trajectories for a single slit, without the curling and tumbling (keeping only the first term in (3.7)). 36
3.4 Single slit trajectories with random initial positions distributed according to the Born rule for the initial wave function (3.10) with the boxcar function (3.16) in the y-direction. Pictured on the left and the right are respectively the far-field and near-field behaviors. 37
3.4 (continued) 38
3.5 The y-dependence of the tumbling rates when $\hat{\mathbf{s}} = \hat{\mathbf{y}}$. The blue curve corresponds to the tumbling rate from + to − chirality, and vice versa for the orange curve. In black is shown $|\psi|^2$. For a single slit, the profile is linear as shown in (a). For two slits, (b)-(d), oscillations appear as the wave function starts to show more peaks farther away from the wall. 39
3.6 Patterns on the screen, for $\hat{\mathbf{s}} = (\hat{\mathbf{x}} + \hat{\mathbf{y}} + \hat{\mathbf{z}})/\sqrt{3}$. The single slit is on the left and the double slit is on the right. 40
3.7 Double slit trajectories with random initial positions distributed according to the Born rule for the initial wave function (3.10) with the Gaussian superposition (3.17) in the y-direction. Pictured on the left and the right are respectively the far-field and near-field behaviors. 42
3.7 (continued) 43
3.8 Double slit trajectories for particles starting at $x = 0$ and $z = 0$, with the same initial positions in (a)-(c), and $\hat{\mathbf{s}} = (\hat{\mathbf{x}}+\hat{\mathbf{y}}+\hat{\mathbf{z}})/\sqrt{3}$. Comparison of the different dynamics. 45
3.9 Three-dimensional views towards wall. Particles start from $x = 0$ and $z = 0$. 46

3.10 Trajectory of a single particle with $\hat{\mathbf{s}} = \hat{\mathbf{y}}$ traversing the given distance. Unlike in the other figures, we only plot a point where a tumble happens, and not the (mostly straight) parts of the trajectories in between, as this would completely wash out the image. 47
3.11 Arrival times in the case of a single Gaussian wave function (3.11) and $\hat{\mathbf{s}} = \hat{\mathbf{x}}$. In both plots, the dotted vertical line indicates the time at which the center of the wave packet reaches the screen. 48
3.12 Leaving quantum mechanics: the tumbling rates are given by (3.19) and not derived from a wave function. 49

5.1 The spectral probability density ρ_t in function of the dimensionless frequency x with plots for $t = 0.05, 0.5$ and 5, respectively dotted, dashed and solid. We compare the Kompaneets process (5.21) on the left with a numerical solution of the Kompaneets equation on the right. The initial condition (not shown here) was taken to be a sum of two Gaussians centered around $x = 2$ and $x = 6$ with standard deviations of respectively 2 and 1, and weights of respectively 1/3 and 2/3. 93
5.2 The spectral probability density ρ_t in function of the dimensionless frequency x for the Kompaneets process (5.21), with plots for $t = 1, 2, 3$ going from right to left. The dotted line indicates the initial "hot Planck" condition corresponding to the occupation field $n_0(x) = n_{\mathrm{BE}}(x/2)/8$ for which $Z = 1$. Notice the fast thermalization to a Wien-like tail, followed by a slow final thermalization at lower frequencies ($x < 6$). 94
5.3 Similar to Fig. 5.2, but with $Z = 0.1$, *i.e.*, with the initial occupation field $n_0(x) = n_{\mathrm{BE}}(x/2)/80$. There is a marked difference (going like x^2 at low frequency) with the dashed line representing the Planck density, as there is particle conservation. There is only the fast thermalization to a(n almost) Wien density because of the absence of low-frequency activity, $x^2 n_t(x) \ll 1$ at low x. 95
5.4 "Stationary" spectral density for $Z = 1.1$. The dashed line is the Planck density. Notice the formation of a condensate around the origin. In that case, there is also the appearance of non-physical negative frequencies. The condensate and the non-physical behavior may be remedied by considering radiative processes like Bremsstrahlung. 96
5.5 Solid line corresponds to the simulation of (5.33) using (5.31) for $c = 0.10, b = 0$. The dashed line is the Planck law. The dotted line depicts the supposed stationary distribution (5.36). 102

5.6 Profile of effective temperature corresponding to Fig. 5.5 and defined in (5.37). The very-low frequency regime is dominated by the *ad hoc* cutoff and procedures replacing Bremsstrahlung and double Compton scattering, as explained in the text. For low frequency $1 < x < 5$ the effective temperature is significantly higher than the Planck-value. 103
5.7 Stationary density profile when adding the frequency-dependent drift with $b = 0.1$ and $k = 0.4$, keeping $c = 0$ in (5.31). Again a deviation is seen from the Planck law (dashed line), with the simulation almost completely overlapping with the stationary solution. 104

6.1 Frequency distribution for the Kompaneets process for $t = 0.0, 0.5, 1.0, 1.5$ and 2.0. The initial condition is a "hot Planck Law" at a temperature three times the temperature T used in the dynamics, corresponding to the rescale $x \to x/3$ of the dimensionless frequency. There is a fast pre-thermalization for the moderate and high frequencies, followed by a slower relaxation at the lower frequency scale. See more details in [74]. 113
6.2 Stationary distribution for a resetting rate of $r = 10^{-2}$ and a divisor $d = 100$. For comparison, the dotted line gives the Planck distribution 116
6.3 Comparison between three methods of resetting, overlaid on top of the Planck distribution (dotted straight line). The three simulations have the same resetting rate $r = 0.01$, while the resetting parameters are $d = 200$, $x_0 \approx 0.027$ and $\lambda_0 \approx 74$, all giving approximately equal first moment $\langle x \rangle \approx 0.014$. 118
6.4 Stationary distributions at low frequencies for four resetting rates r. In each case, as the curves move down, the divisor $d = 25, 50, 100, 200, 400$. 119
6.5 Spectral probability density at the origin in function of the rate r for various divisors d. 119

"Desire, to know why, and how, curiosity; such as is in no living creature but man: so that man is distinguished, not only by his reason; but also by this singular passion from other animals; in whom the appetite of food, and other pleasures of sense, by predominance, take away the care of knowing causes; which is a lust of the mind, that by a perseverance of delight in the continual and indefatigable generation of knowledge, exceedeth the short vehemence of any carnal pleasure."

Leviathan, Thomas Hobbes

1 Introduction

We are built for recognizing and reproducing patterns. All brains in general are designed for this task, but humans have a unsurpassed aptitude for it. Without conscious effort, simply being exposed repeatedly to stimuli leads us to be able to predict the continuation and act in anticipation. Obviously, this capability was and is tremendously advantageous for survival in the natural world, but humans have stretched it to far beyond what nature could have prepared us for, abstracting the concept of a stimulus away completely. A child does not need to be taught anything about genitives or relative clauses to perfectly master all the intricacies of their mother tongue in a few years time, solely through exposure to the language. Although there is a tremendous amount of theory behind it, the main aspect of becoming proficient in chess simply consists of acquiring and internalizing hundreds, if not thousands, of patterns through practice, with the conscious mind at most guiding this instinct towards the most likely profitable avenues. And everyone working in a professional field, like physicists, will develop an intuition that allows them to take a guess at the answer of professionally relevant problems without having to solve them, or at least reducing it to far fewer steps than a novice might need to solve it. It is what allows us to drive cars, read books or play video games. It is what lead us to invent music, art, architecture, and of course, science.

Although among the sciences mathematics without any doubt epitomizes pattern recognition & reproduction, physics certainly comes as close as you can get while remaining in contact with the real world. And this leads us to what might be

one of the central mysteries of Nature: why does this work so astonishingly well? It is perhaps not too surprising that we turned out to be capable of intuitively understanding some phenomena that happen at our level, like simple mechanics or optics, though even here it is remarkable how simple the fundamental processes turned out to be, but our deep understanding of Nature stretches all the way from the edge of the observable universe, 45.7 billion light years away, to the tiniest wisps of matter and energy that are described by quantum fields. In both cases we had to give up many of the concepts we find intuitively pleasing, like simultaneity or the concept of clearly delineated particles, yet whatever came in its place has without a fault eventually turned out to be simple and satisfying. The word "eventually" is used here, because even though we are usually able to use our mathematical and other explanatory tools to reduce a new concept to its essence, sometimes it takes a while, sometimes what we found is just the harbinger of a new pattern, which will emerge when, in due course, a sufficient amount of new phenomena are studied.

Closely related to these capabilities is also our propensity towards their application. We are not just good at it, the process is also enjoyable. At times this means we can entertain ourselves with tasks that either have no real utility or for which we already know the outcome, simply to tickle our brain and feel some sense of reward, e.g. solving a crossword puzzle or replaying a song so often you start to know the lyrics by heart. But when we do not know where we are going, we call it curiosity, and it longs to be satisfied. Our insatiable desire to know and understand, and the joy that comes from not just knowing and understanding, but also the journey towards uncovering these mysteries, regardless of eventual success, are what makes physics such a wonderful undertaking.

And with these thoughts, we delve into the main body of research.

1.1 Nonequilibrium

One very fundamental and mysterious feature of our universe is the presence of phenomena that are far away from equilibrium. Perhaps most saliently, in the existence of life (and therefore, us), but nonequilibrium is present on all scales, from quantum nonequilibrium in Bohmian mechanics[43], to magnetic domains[23], to the machinery keeping cells alive, to glassy systems[4], all the way up to the supernovae that introduced all the heavy elements to the universe. It is often postulated that during the early stages of the Big Bang, geometric degrees of freedom were out of equilibrium, and remain to this day sources of low entropy that contribute to the remarkable (self-)organization of matter

that we see today, as well as delaying the inevitable entropic decay of ourselves towards cold and boring uniformity. Other fundamental questions, like the origin of the Second Law, are embedded in this same realm. To gain insights in these mechanisms, it is crucial to go far beyond the usual energy-entropy balances, and come to terms with more statistical-dynamical inquiries. This general introduction outlines how the present thesis embraces this challenge.

Nonequilibrium phenomena manifest across a wide range of scales, both in length, energy and time. They span various fields such as biology, climate science, early-universe cosmology, and the role of quantum entanglement in transport processes. The study of these phenomena gives rise to a number of subdomains within physics, with statistical mechanics playing a prominent role.

For instance, the locomotion of bacteria like *E. coli* can be effectively described by using the principles of active matter physics, specifically run-and-tumble dynamics. Reaction-diffusion models find applications in ecology and microbiology, such as in the modeling of mitosis. Irreversible thermodynamics and macroscopic fluctuation theory serve as frameworks for climate models, with geophysics, fluid dynamics and oceanography as distinct subdomains. Models involving high-temperature conductivity are being developed, leveraging the concept of entanglement in spin-fluids, such as the SYK-model. The diverse range of nonequilibrium phenomena is highlighted by these and many other examples, but this also makes it clear that we have a need for a systematic classification. In general, we identify three main categories, each with subclasses that may intersect with one another.

The first category pertains to relaxation. Since the inception of statistical mechanics (together with the first dynamical understandings of temperature), people have been reflecting on the convergence towards equilibrium. Despite being a very common occurrence, relaxation continues to stimulate discussions and new findings. Within this category, there are fundamental questions that arise, such as the origins of the second law of thermodynamics and the rationale behind the Gibbs ensembles. Additionally, there are more specific and contemporary themes to consider. For instance, the physics of glasses, where relaxation appears to be exceptionally slow, likely due to kinetic constraints. Furthermore, there are instances where relaxation is hindered by localization (and quantum interference) effects, or there may be different regimes of pre- and postthermalization. Theories of nucleation and metastability find their place within this framework. In this study, we will exclusively focus on the convergence to equilibrium as it pertains to the Kompaneets equation, concerning the relaxation of the photon occupation number towards the Planck law by Compton scattering with thermal electrons.

The second category involves steady processes that sustain currents within

a system, maintained by (weak) coupling with various equilibrium reservoirs. These reservoirs can be mechanical, chemical or thermal baths that "frustrate" the system, giving so-to-speak conflicting signals. This concept of frustration is well-defined only at certain levels of description, but it holds significant importance in comprehending the relationship between transport and dissipation. Time-dependent systems that achieve a steady condition when averaged over longer times, as well as transformation between different regimes of this steady nonequilibrium, can also be considered within this category.

The third class of nonequilibrium phenomena, which somewhat complements the previous two, involves systems that are not globally driven by external forces, neither in the bulk nor at the boundaries. Instead they possess individual sources of low-entropy "fuel". These systems are commonly referred to as active particles, or active matter, and are observed in biological systems, morphing matter and biomimetics. As it happens, active matter can also be viewed as strongly coupled systems or systems in contact with nonequilibrium reservoirs, as in the second category above.

The previous classification does not provide a strict division of phenomena in the realm of nonequilibrium physics. Another approach is to consider the different approaches and methodologies in this field, depending on the scales of description or the specific goals. In a broader sense still, self-organized, responsive, and adaptive structures like those in morphing and active matter, are the subject of nonequilibrium studies. Clearly the investigation of self-assembly and biomimetic and biohybrid structures are of growing importance.

Indeed, nonequilibrium statistical mechanics goes beyond reconciling thermodynamics and mechanics, aiming to extend and refine both of them, for example by understanding the nature of fluctuations. This brings us to a branch of mathematics that has been fundamental in numerous developments in the past century, including in particular the study of stochastic processes. Specifically, realizing the power of large numbers has shaped much of the Gibbs formalisms serving as the framework of equilibrium statistical mechanics, which has, in turn, been a rich source of inspiration for condensed matter theory and quantum field theory. Key concepts like entropic and fluctuation forces can then summarize much of equilibrium statistical mechanics. Major successes include the theory of emergent phenomena, phase transitions, critical phenomena and the arrow of time. Productive exchanges between high-energy physics and condensed matter communities have given rise to discussions on spontaneous symmetry breaking, universality, renormalization and scale invariance. Today, other fields such as biology and computer science also benefit from these techniques, using inference schemes developed from nonequilibrium statistical mechanics.

The question then becomes in what sense the methodology of nonequilibrium

statistical mechanics differs from that in equilibrium, where the dynamics and kinetics become significantly more important. More precisely, energy-entropy balances, which play a central role in equilibrium, become less significant and the challenge lies in finding alternative approaches. In other words, nonequilibrium statistical mechanics cannot simply be reduced to thermodynamics or field theory. It requires major changes and goes beyond the traditional notions present in equilibrium regimes, where a Hamiltonian is available and we busy ourselves with counting states. The connection with dynamical systems becomes stronger, and the focus shifts to properties that are not solely energetic or dissipative (i.e. related to entropy production).

The present thesis is an exploration of that "dynamical point of view" on nonequilibrium phenomena, beginning with the consideration of *trajectories*. If we are to speak about such notions as (dynamical) activity, a time-symmetric quantity, or about kinetics, it is beneficial to study the fluctuation dynamics of the system and do statistics on the level of trajectories. This approach aligns with recent advancements in experimental physics, where optical and high-resolution techniques provide a closer look into the sub-mesoscopic world. Optical tweezers and femtosecond imaging, for example, allow for the precise monitoring and manipulation of materials, enabling the unraveling of mesoscopic trajectories with unprecedented accuracy.

We are of course used to the idea of trajectories in classical mechanics (as well as their apparent fall from grace in quantum mechanics). One can sum up the main task in this field as determining particle trajectories given forces and initial conditions. However, in fields like colloidal physics, where forces are more statistical in nature, the concept of trajectories becomes less obvious. For example, how exactly Brownian motion is observed depends on the resolution of the measuring apparatus, as we cannot follow the actual true microscopic trajectory of the particle. And as mentioned before, things become really hairy in quantum mechanics. What are we even to make of the path of photons? While we may use the term "trajectory" colloquially, it remains problematic...

The problems, possibilities and advantages of adopting a trajectory-centered perspective are discussed in various ways throughout this thesis. We take the opportunity to relate them to the various chapters, after giving a short introduction to the subjects at hand. Because it concerns two somewhat distinct research projects, this dissertation is split in two Parts, though they share the same spirit of the aforementioned trajectory-based approach.

1.2 Wave mechanics

Sometimes, new discoveries and theories can make you notice problems you never knew you had, assumptions you never knew you held, and worldviews you never knew you subscribed to. Back in the good old days when physics was still classical, the concept of an *ontology* never came up. It was obvious our theories were basically approximations to how things really were, and that the concept of measurement, though interesting for all kinds of practical reasons, was simply outside of the purview of the laws of physics. Even if everyone closed their eyes at night, the Moon would still be there without anyone to observe it.

The first cracks in this worldview probably occurred after the development of electromagnetism, where the exact nature of the electric and magnetic fields started raising some questions, culminating with the development of Jefimenko's equations, which together with the Lorentz force law just barely don't make the entire concept of electromagnetic fields superfluous[89]. Regardless, in this context, everybody at least still agrees electrons and other charged particles exist.

However, with quantum mechanics taking its modern form, a lot of these concepts we take for granted seemed to become untenable. Instead of particles moving on the stage set by nature, the true state of a system was instead best represented as something as intangible and abstract as a Hilbert space. Moreover, a discrepancy arose between the behavior of classical systems, where we observe definite outcomes as a result of a deterministic (at least in principle) evolution, and quantum systems, where at best we can assign a probability to each possible outcome, even with theoretical full knowledge of the system. We instead find the system is best described to be in in a superposition of many possibilities, yet after observing the system it is always found to be in a definite state. Furthermore, this also meant an act of measurement had now become an inevitably active process, where a (conscious) observer makes the wavefunction "collapse", leading to only one of the outcomes to manifest itself.

How exactly the observer is involved, the true nature of the collapse, what exactly constitutes a measurement, how the system "chooses" what value an observable takes, and other questions constitute the so-called *measurement problem*.

Naturally, as soon as these questions started to arise, an even larger number of answers was proposed as well. We refer to the different conceptual frameworks used to understand the fundamental principles and the mathematical formalism of quantum mechanics as *interpretations*. Although this nomenclature would seem to imply all interpretations share the same mathematical machinery and offer the same experimental predictions, only differing in how they explain in

what sense this mathematical theory corresponds to reality, this is not necessarily true anymore, with some interpretations truly being physically different theories, whereas for others the difference is merely philosophical.

Regardless, for most practical purposes all of this has little importance, leading some people to adopt a "shut up and calculate" ethos. Closely related to that is the Copenhagen Interpretation, which is still in some sense the standard as taught to students, even though as a nondeterministic theory it is obviously incomplete. We will not waste the reader's time by expounding all other kinds of interpretations, and simply limit ourselves to the one relevant to the matter: *de Broglie-Bohm theory*, also called pilot wave theory, the causal interpretation, or Bohmian mechanics.

Bohmian mechanics provides an ontology for quantum mechanics consisting of a universal wavefunction and particles, which have a definite position in space and time[60]. Therefore, the universe has an objective configuration at all times. The equation of motion of this configuration is twofold:

$$\frac{dX}{dt} = v^{\Psi}(X(t)) \qquad \text{(guiding equation)}$$

$$\mathrm{i}\hbar\frac{\partial\Psi}{\partial t} = \mathcal{H}\Psi. \qquad \text{(Schrödinger equation)}$$

Here, X denotes a spatial configuration of the particles and Ψ the universal wavefunction. The guiding equation is summed up by a velocity function v^{Ψ}, which will depend on the wavefunction, which itself evolves according to the Schrödinger equation of ordinary quantum mechanics. Clearly both equations are deterministic and so must be the evolution of the configuration.

Much has and can be written about the implications of this interpretation. Curiously, it even has a concept of *quantum nonequilibrium*, which, though it in some sense parallels nonequilibrium statistical mechanics, is nonetheless not relevant for this work. We will focus, however, on the fact that with their definite positions and deterministic equations of motion, the particles will have trajectories through space-time.

1.2.1 Outline

In the first Part, we will present two projects in quantum mechanics, where we hope a trajectory-based approach can lead to more visual and methodological perspectives on some issues.

In Chapter 2, we hark back to one of the earliest methodological attempts at quantizing classical mechanical systems, canonical quantization, and apply it

to geometrodynamics, revisiting old ideas by e.g. Wheeler and DeWitt. The aim is to add some matter in the form of non-relativistic point particles and solve the problem of time using ideas from Bohmian mechanics, yielding definite trajectories for both the particles through physical space, and the metric through the space of all three-dimensional metrics.

In Chapter 3, we delve into the connection between two seemingly distinct fields of study: active matter and the Dirac electron. Our aim is not only to establish the relationships between these fields but also to provide illustrations and visualizations that demonstrate how they contribute to relevant kinetic information, particularly in nonequilibrium scenarios. It is worth noting that in standard quantum mechanics, there is no straightforward quantum mechanical operator for "time" or "duration", which fall somewhat outside of the typical measurement postulates. On the other hand, time is a crucial observable for understanding nonequilibrium phenomena. By employing trajectories, which stem from the de Broglie-Bohm pilot wave theory, we are however able to discuss and explore arrival-times and distributions.

1.3 Photon stochastic processes

One of the most famous successes in early quantum mechanics, and a very fruitful application of equilibrium thermodynamics, was the unraveling of the spectrum of black-body radiation in the early 19th century. Once this theory had been established, a natural follow-up question posed itself: how does the system actually get to this state, how does it behave before it reaches equilibrium?

Unlike, for example, the motion of molecules in a fluid described by the Boltzmann equation, radiation cannot achieve equilibrium by itself, as the equations governing its evolution are strictly linear, and no exchange of energy is possible between different modes of frequency, direction or polarization. At least, this is true when we restrict ourselves to energies below several GeV, before two-photon physics starts playing a role.

Therefore, to effect any kind of time-evolution, we need to introduce some kind of matter which will serve as an intermediary between the radiation and itself, or more usually, which will exert its own influence on it. Though usually the cavity is imagined to be empty, and it is the walls that are transferring thermal energy into the radiation, we will take a different approach here, in which the walls can be taken to be either perfectly reflective, or even completely absent, if periodic boundary conditions are assumed. Instead, if we imagine a mote of dust to be floating in the cavity, it will absorb and emit radiation until some kind of equilibrium is achieved. Thinking on a more microscopic level, we can imagine

an electron (or any other kind of charged particle) instead, which, lacking the internal degrees of freedom a composite particle has, can only scatter radiation. It is this process that we will turn our attention to.

In what follows in Part II, the setup for the radiation is always the same. We consider a box with sidelength L, which we will assume to be much larger than the characteristic length scales of the process involved. We shall assume periodic boundary conditions to hold, for ease of computation, though the volume of the box should be so large that the exact conditions at the boundary should not matter. We can then number our fundamental modes, delocalized plane waves, with a triplet of natural numbers

$$\mathbf{k} = \frac{2\pi}{L}(i,j,k) \qquad \text{for } (i,j,k) \in \mathbb{Z}^3 \setminus \{(0,0,0)\}, \tag{1.1}$$

as well as a polarization $s = \pm$.

The state of the radiation is then summed up by the photon occupation numbers, which for every mode $(\mathbf{k}, s)$ give the number of photons in it, $n_{\mathbf{k},s} \in \mathbb{N}$. Assuming again L is large, and taking into account the interactions we will be considering are usually indifferent of polarization, we will immediately go to a continuum limit and refer to the photon occupation number with a function $n(\mathbf{k}, t)$ instead, which is an averaged value of the occupation number over nearby modes, meaning it will be a positive real number.

The main mechanism of interaction between the matter and radiation will be assumed to be inverse Compton scattering, which basically corresponds to an elastic collision between a massive and a massless particle. Considering a photon of frequency ω traveling in direction $\hat{\mathbf{n}}$ colliding with an electron of momentum $\mathbf{p}$, labelling the same quantities after the collision with an apostrophe $'$, we find that[107]

$$\omega' - \omega = \frac{c\mathbf{p}\cdot(\hat{\mathbf{n}}' - \hat{\mathbf{n}}) - \hbar\omega(1 - \hat{\mathbf{n}}\cdot\hat{\mathbf{n}}')}{\gamma m_e c^2 - c\mathbf{p}\cdot\hat{\mathbf{n}}' + \hbar\omega(1 - \hat{\mathbf{n}}\cdot\hat{\mathbf{n}}')}\,\omega. \tag{1.2}$$

As we will mostly be interested in a low-energy regime, where both the photon and electron kinetic energy are much smaller than $m_e c^2$, to leading order this equation simplifies to

$$\omega' - \omega \approx \frac{c\mathbf{p}\cdot(\hat{\mathbf{n}}' - \hat{\mathbf{n}}) - \hbar\omega(1 - \hat{\mathbf{n}}\cdot\hat{\mathbf{n}}')}{m_e c^2}\,\omega. \tag{1.3}$$

Two remarks come to mind when seeing this equation. First of all, we can easily identify the two terms in the numerator as respectively due to the Doppler effect and Compton recoil. If at some point equilibrium is to be achieved, these two contributions will have to cancel out on average. Second of all, shifting our attention to the denominator, we see that the average shift in frequency will be very small, due to the factor $m_e c^2$.

The latter remark in particular is crucial in making the modeling of this setup mathematically tractable, as it implies we can replace this possibly very complicated stochastic process with a diffusion process, i.e. performing a so-called *diffusion approximation*[79]. Without using so many words, A. S. Kompaneets was the first to undertake this affair in 1956[99], yielding the eponymous Kompaneets equation

$$\frac{\partial n}{\partial t} = n_e \sigma_T c \frac{k_B T}{m_e c^2} \frac{\partial}{\partial \omega} \omega^4 \left\{ \frac{\partial n}{\partial \omega} + \frac{\hbar}{k_B T} n(1+n) \right\}, \tag{1.4}$$

which is a partial differential equation for the photon occupation number $n(t, \omega)$. Here n_e, m_e, σ_T and T are respectively the spatial density, mass, scattering cross-section and temperature of the charged particle that makes up the background, again assumed to be electrons.

Defining a unitless frequency $x = \hbar\omega / k_B T$ and time $y = n_e \sigma_T c \; k_B T / m_e c^2$, the equation can be distilled to its essence

$$\frac{\partial n}{\partial y} = \frac{1}{x^2} \frac{\partial}{\partial x} x^4 \left\{ \frac{\partial n}{\partial x} + n(1+n) \right\}. \tag{1.5}$$

This diffusion equation is nonlinear due to the status of photons as identical bosons.

1.3.1 Outline

In the second Part, we consider stochastic processes on the level of individual photons, and we will eventually "tag" a single photon, whose trajectory through momentum space will become our main interest. The aim of this project is to investigate potential deviations from the Planck law, which serves as our equilibrium starting point. Unlike other particles, photons do not interact with each other, but they can be brought into nonequilibrium conditions when they interact with matter. This matter can be taken to be electrons, which themselves can be driven to far-from-equilibrium states, interacting through effects like Compton scattering or radiative processes. Additionally, mechanical disturbances can also be considered, such as vibrating or randomly expanding cavities.

Furthermore, there are two more specific applications of these concepts. The first concept explores whether there are any indications of nonequilibrium properties in the cosmic microwave background, signatures of the nonequilibrium features of the primordial plasma. This investigation considers experiments like ARCADE[68, 152] or LOFAR. The second application focuses on creating

artificial disruptions of time-reversal symmetry in cold gases, included photon gases.

In Chapter 4 we revisit the derivation of the Kompaneets equation, the nonlinear Fokker-Planck-like equation associated to the simplest photon stochastic process, as first derived by A.S. Kompaneets. We clarify some of the issues and fill in some of the gaps. The aim is not just to polish the original derivation, but also to serve as a useful point of departure to understand how nonequilibrium conditions could reflect on the Planck law. First steps are taken towards a diffusion approximation.

Next, in Chapter 5, we introduce a photon frequency diffusion process. Although the individual trajectories of photons through time and space are never considered, which would make little sense anyway as they are ill-defined, we can still follow the evolution of the momentum of a single "tagged" photon, i.e. its trajectory in reciprocal space. To this end, we start by introducing a multi-photon dynamics on this space, incorporating near-neighbor hopping. The inherent nonlinearity of the dynamics due to the photon's bosonic nature has to be taken into account. We apply the diffusion approximation to the resulting master equation, yielding what we will call the Kompaneets process, the nonlinear Langevin dynamics associated to the Kompaneets equation. We confirm the correctness of the equations by comparing simulations of the process to numerical integrations of the Kompaneets equation. Afterwards, we wish to explore nonequilibrium effects, motivating their introduction into the process. Modifications to the Planck law are probed, with our attention aimed mostly at the lower ranges of frequencies.

Afterwards, in Chapter 6 we explore a completely different type of nonequilibrium conditions, where starting from the frequency diffusion process as derived before, we now add *resetting*, where photons lower their frequency at random times. The physical origins of this resetting are discussed, and modifications are made to the simulations to incorporate the resetting into the process. Various implementations of the resetting method, rate and parameters are considered.

Part I

Wave mechanics

This result is too beautiful to be false; it is more important to have beauty in one's equations than to have them fit experiment.

Paul Adrien Maurice Dirac

2

Wave mechanics for gravity with point-particles

Abstract

We consider non-relativistic point-particles coupled to Einstein gravity and their canonical quantization. From the resulting Wheeler-DeWitt wave equation we determine a quantum version of geometrodynamics, where the coupled evolution of particle positions and 3-metric is guided by the wave function. We find that this quantum dynamics implies a quantum extension of the Einstein equations. The conserved energy-momentum tensor now contains a quantum contribution. This conceptually simple setup is promising both for deriving semiclassical and weak field approximations to the quantum Einstein equations and is thus important for the development of quantum corrections to computational general relativity.

This chapter was first published in [110], with coauthors C. Maes and W. Struyve. The author of this thesis performed the calculations, wrote the first draft, and contributed to later revisions.

2.1 Introduction

The problem of quantum gravity can be approached from many sides. One of the major theoretical concerns however is to avoid an observer-based description as is the hallmark of e.g. the Copenhagen version of quantum mechanics. The point is indeed that our theory must give a consistent physical cosmology, which does not suppose outside observers. Fundamental theories must directly address the beables of nature, and not the observables [10].

We formulate a theory which achieves this, involving geometry and matter as dynamical variables. More specifically, we develop a quantum modification of *geometrodynamics*, which describes the time-evolution of the 3-metric, just as in the Hamiltonian formulation of Einstein's gravity, coupled to non-relativistic point particles. This is a Bohmian dynamics where the velocity of the 3-metric and the particle positions is determined by a wave function which itself satisfies a Schrödinger-type equation — the Wheeler-DeWitt equation — obtained from quantizing Einstein's gravity. From this quantum geometrodynamics, a modification to the Einstein equations is derived in the form of an extra contribution to the energy-momentum tensor.

This extends the results of [58] which applied to a matter field. While field beables are suitable for bosonic matter, point-particles are the natural beables for fermionic matter [159]. So the present work allows the study of non-relativistic fermionic matter in the context of quantum gravity. The spin degrees of freedom will not be taken into account (the fermionic nature is then reflected only in the anti-symmetry of the wave function). Introducing spin could be done in the non-relativistic domain via the Pauli theory. Non-relativistic particles rather than relativistic particles are considered which makes the analysis simpler. Yet, clearly, many aspects of quantum gravity involve the effects of gravity for non-relativistic particles, see e.g. [2, 20, 111]. At any rate, the extension to relativistic particles could be done using e.g. [162].

This work serves as a starting point to find quantum corrections to classical gravity, in particular applicable to the recently booming field of computational (classical) general relativity. It can be used to develop semi-classical approximations [161, 160] or weak field approximations, perhaps relevant for the study of of quantum modifications to gravitational waves. Another avenue is to investigate the status of space-time singularities in quantum gravity [64, 54].

The outline of the paper is as follows. The next Section recalls the ADM formalism for classical gravity. It gives us the Hamiltonian formulation with constraints which can be quantized to lead to the appropriate Wheeler-DeWitt equation. In Section 2.3, we obtain the velocity field that determines the

quantum dynamics for particles positions and three-metric. From that dynamics we derive the quantum Einstein equations, with a conserved energy-momentum tensor containing a quantum contribution. We conclude with discussion and outlook in Section 2.5.

2.2 Geometrodynamics coupled to point-particles

To formulate the classical theory, in particular the Hamiltonian form, the ADM formalism [3, 96, 19, 32] is employed. It is supposed that spacetime can be foliated in terms of space-like hypersurfaces such that the spacetime manifold is diffeomorphic to $\mathbb{R} \times \Sigma$, with Σ a 3-surface. Coordinates $x^\mu = (t, \mathbf{x})$ can be chosen such that the time coordinate t labels the leaves of the foliation and $\mathbf{x}$ are the coordinates on Σ. Units are chosen such that $\hbar = c = 1$. In terms of these coordinates and following the conventions of [32], the metric and its inverse are

$$g_{\mu\nu} = \begin{pmatrix} -N^2 + N_i N^i & N_i \\ N_i & h_{ij} \end{pmatrix}, \qquad g^{\mu\nu} = \begin{pmatrix} -\frac{1}{N^2} & \frac{N^i}{N^2} \\ \frac{N^i}{N^2} & h^{ij} - \frac{N^i N^j}{N^2} \end{pmatrix}, \tag{2.1}$$

where N and N^i are respectively the lapse and the shift vector, and h_{ij} is the Riemannian metric on Σ, with determinant h. Spatial indices are raised and lowered by this spatial metric.

The total action is

$$\mathcal{S}_{\text{cl}} = \int dt\, L_{\text{cl}} = \int d^4x\, \mathcal{L}_{\text{cl}} = \mathcal{S}_G + \mathcal{S}_M, \tag{2.2}$$

which adds to the Einstein-Hilbert action $\mathcal{S}_G$ of gravity, with $\kappa = 8\pi G$,

$$\mathcal{S}_G = \frac{1}{2\kappa} \int d^4x \sqrt{-g}\, (R - 2\Lambda), \tag{2.3}$$

the action $\mathcal{S}_M$ for a non-relativistic particle in a gravitational field $g_{\mu\nu}$, using (2.1),

$$\begin{aligned} \mathcal{S}_M = &-m \int dt N(t, \mathbf{X}(t)) \\ &+ \frac{m}{2} \int dt \frac{h_{ij}(t, \mathbf{X}(t))}{N(t, \mathbf{X}(t))} \left[\dot{X}^i(t) + N^i(t, \mathbf{X}(t))\right] \left[\dot{X}^j(t) + N^j(t, \mathbf{X}(t))\right]. \end{aligned} \tag{2.4}$$

The latter, with the first terms corresponding to the rest mass contribution, is derived as the non-relativistic limit of the relativistic particle action. As in

classical electrodynamics [156], a smearing could be introduced to avoid the singular nature of point-particles, but that is something we will not pursue here.

The action $\mathcal{S}_{\rm cl}$ can also be expressed in terms of phase space variables. The canonically conjugate momenta are

$$P_i = \frac{\partial L_{\rm cl}}{\partial \dot{X}^i} = \frac{m}{N(\mathbf{X})}\left[\dot{X}_i + N_i(\mathbf{X})\right], \qquad \pi^{ij} = \frac{\partial \mathcal{L}_{\rm cl}}{\partial \dot{h}_{ij}} = -\frac{\sqrt{h}}{2\kappa}(K^{ij} - Kh^{ij}), \tag{2.5}$$

with

$$K_{ij} = \frac{1}{2N}(2D_{(i}N_{j)} - \dot{h}_{ij}), \qquad K = K_{ij}h^{ij}, \tag{2.6}$$

the extrinsic curvature. Indices of the particle position and momentum are raised and lowered with the metric $h_{ij}(\mathbf{X})$. (The conjugate momentum is a tensor density of weight -1). In terms of these variables, the action reads

$$\mathcal{S}_{\rm cl} = \int dt \int_\Sigma d^3x \dot{h}_{ij}\pi^{ij} + \int dt \dot{X}^i P_i - \int dt H, \tag{2.7}$$

where H is the Hamiltonian, given by

$$H = \int_\Sigma d^3x \left(N\mathcal{H} + N^i\mathcal{H}_i\right), \tag{2.8}$$

with

$$\mathcal{H} = \mathcal{H}_G + \mathcal{H}_M, \qquad \mathcal{H}_i = \mathcal{H}_{Gi} + \mathcal{H}_{Mi} \tag{2.9}$$

and

$$\mathcal{H}_G = 2\kappa G_{ijkl}\pi^{ij}\pi^{kl} + \mathcal{V}, \qquad \mathcal{H}_M(\mathbf{x}) = \delta(\mathbf{x} - \mathbf{X})\left(m + \frac{P_iP^i}{2m}\right), \tag{2.10}$$

$$\mathcal{H}_{Gi} = -2h_{ik}D_j\pi^{jk}, \qquad \mathcal{H}_{Mi}(\mathbf{x}) = -\delta(\mathbf{x} - \mathbf{X})P_i, \tag{2.11}$$

where $G_{ijkl} = (h_{ij}h_{kl} + h_{il}h_{jk} - h_{ij}h_{kl})/2\sqrt{h}$ is the DeWitt metric, D_i is the covariant derivative corresponding to h_{ij}, and $\mathcal{V} = \sqrt{h}(2\Lambda - R^{(3)})/2\kappa$ is the gravitational potential density. We write $V(t) = \int_\Sigma d^3x N(t,\mathbf{x})\mathcal{V}(h(t,\mathbf{x}))$.

In terms of these variables, the classical equations of motion are

$$\dot{X}^i = \frac{N(\mathbf{X})}{m} P^i - N^i(\mathbf{X}), \tag{2.12}$$

$$-\dot{P}_i = \partial_i N \left(m + \frac{1}{2m} P^k P_k \right) + \frac{N}{2m} \partial_i h^{kl} P_k P_l - \partial_i N^k P_k, \tag{2.13}$$

$$\dot{h}_{ij} = 2N 2\kappa G_{ijkl} \pi^{kl} + 2D_{(i} N_{j)}, \tag{2.14}$$

$$\begin{aligned} -\dot{\pi}^{ij}(\mathbf{x}) = {} & N(\mathbf{x}) 2\kappa \frac{\partial G_{mnkl}}{\partial h_{ij}(\mathbf{x})} \pi^{mn}(\mathbf{x}) \pi^{kl}(\mathbf{x}) + \frac{\delta V}{\delta h_{ij}(\mathbf{x})} \\ & + \frac{\delta}{\delta h_{ij}(\mathbf{x})} \int_\Sigma d^3 y \left(-2 N_k D_l \pi^{kl} \right) + \delta(\mathbf{x} - \mathbf{X}) \frac{N(\mathbf{X})}{2m} P^i P^j, \end{aligned} \tag{2.15}$$

$$\mathcal{H} = 0, \qquad \mathcal{H}_i = 0. \tag{2.16}$$

The last two equations are the Hamiltonian and diffeomorphism constraint. While equation (2.15) can be worked out more, that is not necessary for our purposes. For the full expression, see e.g. [176, 19].

Together, Equations (2.14)–(2.16) constitute the Einstein field equations

$$G_{\mu\nu} - \Lambda g_{\mu\nu} = \kappa T_{\mu\nu}, \tag{2.17}$$

where $G_{\mu\nu} = R_{\mu\nu} - \frac{1}{2} R g_{\mu\nu}$ is the Einstein tensor and is the energy-momentum tensor, with components

$$\begin{aligned} T^{00}(t, \mathbf{x}) &= \frac{1}{N(t,\mathbf{x})^2 \sqrt{h(t,\mathbf{x})}} \left[m + \frac{P_k(t) P^k(t)}{2m} \right] \delta(\mathbf{x} - \mathbf{X}(t)), \\ T^{0i}(t, \mathbf{x}) = T^{i0}(t, \mathbf{x}) &= \frac{P^i(t)}{N(t,\mathbf{x}) \sqrt{h(t,\mathbf{x})}} \delta(\mathbf{x} - \mathbf{X}(t)) - N^i(t,\mathbf{x}) T^{00}(t,\mathbf{x}), \\ T^{ij}(t, \mathbf{x}) &= \frac{1}{\sqrt{h(t,\mathbf{x})}} \left[\frac{P^i(t) P^j(t)}{m} - \frac{2 P^{(i} N^{j)}}{N(t,\mathbf{x})} \right] \delta(\mathbf{x} - \mathbf{X}(t)) \\ & \quad + N^i(t,\mathbf{x}) N^j(t,\mathbf{x}) T^{00}(t,\mathbf{x}), \end{aligned} \tag{2.18}$$

which is most easily derived using $T^{\mu\nu} = -\frac{2}{\sqrt{-g}} \frac{\delta \mathcal{S}_M}{\delta g_{\mu\nu}}$ and the relations (2.42) derived in Appendix 2.A.

2.3 Wave mechanics for 3-metric and particles

The ADM formalism of Einstein gravity is the starting point for canonical quantization [96]. In the present case, this results in a wave functional $\Psi(\mathbf{X}, h)$ which is a function of the 3-metric h and the particle coordinates $\mathbf{X}$ which satisfies the Wheeler-DeWitt equation

$$\widehat{\mathcal{H}}\Psi \equiv \widehat{\mathcal{H}}_G\Psi + \widehat{\mathcal{H}}_M\Psi = 0, \tag{2.19}$$

and diffeomorphism constraint

$$\widehat{\mathcal{H}}_i\Psi \equiv \widehat{\mathcal{H}}_{Gi}\Psi + \widehat{\mathcal{H}}_{Mi}\Psi = 0, \tag{2.20}$$

with

$$\widehat{\mathcal{H}}_G = -2\kappa G_{ijkl}\frac{\delta}{\delta h_{ij}}\frac{\delta}{\delta h_{kl}} + \mathcal{V}(h,\phi), \qquad \widehat{\mathcal{H}}_M(\mathbf{x}) = \delta(\mathbf{x}-\mathbf{X})\left(m - \frac{\nabla^2}{2m}\right), \tag{2.21}$$

$$\widehat{\mathcal{H}}_{Gi} = 2h_{ik}D_j\frac{\delta}{\delta h_{jk}}, \qquad \widehat{\mathcal{H}}_{Mi}(\mathbf{x}) = \delta(\mathbf{x}-\mathbf{X})\nabla_i, \tag{2.22}$$

where ∇_i corresponds to the covariant derivative D_i evaluated at $\mathbf{X}$, with $\nabla_i\psi = \partial_i\psi$, and $\nabla^2 = \nabla_i\nabla^i$. We have chosen the Laplace-Beltrami ordering for matter, but not for gravity. Other choices are of course possible [100, 40, 58].

Writing $\Psi = |\Psi|e^{\mathrm{i}S}$, we define the guidance equations for $(\mathbf{X}, h)$ as

$$\dot{X}^i = \frac{N(\mathbf{X})}{m}\nabla^i S(h,\mathbf{X}) - N^i(\mathbf{X}), \tag{2.23}$$

$$\dot{h}_{ij} = 2N2\kappa G_{ijkl}\frac{\delta S}{\delta h_{kl}} + D_iN_j + D_jN_i. \tag{2.24}$$

This amounts to a Bohmian dynamics, developed in other contexts in [17, 81, 168, 134]. As in the classical case, the dynamics involves a lapse and shift function. Together with the 3-metric they determine a 4-metric defined by (2.1). Classically, the choice of lapse and shift do not change the 4-geometry (i.e. the coordinate independent content of the metric). However, this is no longer the case for the quantum dynamics; different choices of the shift vector give the same geometry, but lapse functions do not (unless they merely differ by a factor which depends only on time). Put differently, the dynamics depends on the particular choice of foliation of spacetime [134]. That does not necessarily imply the predictions of the quantum theory depend on that choice. (The Bohmian dynamics in Minkowski space-time may also violate Lorentz invariance at the fundamental level, yet the statistical predictions are Lorentz invariant [9, 56].)

2.4 Hamiltonian form of the quantum dynamics

To derive the quantum Einstein equations, we first derive a Hamiltonian form of the dynamics. Defining

$$P_i = \nabla_i S, \qquad \pi^{ij} = \frac{\delta S}{\delta h_{ij}}, \tag{2.25}$$

the quantum dynamics (2.23)–(2.24) obtains the form

$$\dot{X}^i = \frac{N(\mathbf{X})}{m} P^i - N^i(\mathbf{X}), \quad \dot{h}_{ij} = 2N 2\kappa G_{ijkl}\pi^{kl} + 2D_{(i}N_{j)}, \tag{2.26}$$

which agrees with the classical dynamics (2.12) and (2.14).

The constraint (2.19) implies that

$$2\kappa G_{ijkl}(\mathbf{x})\frac{\delta S}{\delta h_{ij}(\mathbf{x})}\frac{\delta S}{\delta h_{kl}(\mathbf{x})} + \mathcal{V}(\mathbf{x}) + \frac{\nabla_i S \nabla^i S}{2m}\delta(\mathbf{x}-\mathbf{X}) + \mathcal{Q}(\mathbf{x}) = 0, \tag{2.27}$$

where $\mathcal{Q}$ is the quantum potential density, given by

$$\mathcal{Q} = \mathcal{Q}_G + \mathcal{Q}_M, \tag{2.28}$$

with

$$\mathcal{Q}_G = -2\kappa G_{ijkl}\frac{1}{|\Psi|}\frac{\delta|\Psi|}{\delta h_{ij}\delta h_{kl}}, \qquad \mathcal{Q}_M(\mathbf{x}) = -\delta(\mathbf{x}-\mathbf{X})\frac{\nabla^2|\Psi|}{2m|\Psi|}. \tag{2.29}$$

From the other constraint (2.20) we find that

$$2D_j\frac{\delta S}{\delta h_{ji}(\mathbf{x})} + \delta(\mathbf{x}-\mathbf{X})\nabla^i S = 0. \tag{2.30}$$

Hence, using the definition (2.25), we have that

$$\mathcal{H} + \mathcal{Q} = 0, \qquad \mathcal{H}_i = 0. \tag{2.31}$$

These are the classical constraint equations (2.16) modified by $\mathcal{V} \to \mathcal{V} + \mathcal{Q}$.

Finally, taking the time-derivative of (2.25) and using (2.27), (2.30) and defining $Q(t) = \int_\Sigma d^3x N(\mathbf{x},t)\mathcal{Q}(\mathbf{x},t)$, it follows that

$$-\dot{P}_i = \partial_i N\left(m + \frac{P^k P_k}{2m}\right) + \frac{N}{2m}\partial_i h^{kl}P_k P_l - \partial_i N^k P_k + \partial_i Q, \tag{2.32}$$

$$\begin{aligned}-\dot{\pi}^{ij}(\mathbf{x}) =& N(\mathbf{x})2\kappa\frac{\partial G_{mnkl}}{\partial h_{ij}(\mathbf{x})}\pi^{mn}(\mathbf{x})\pi^{kl}(\mathbf{x}) + \frac{\delta}{\delta h_{ij}(\mathbf{x})}(V+Q) \\ &+ \frac{\delta}{\delta h_{ij}(\mathbf{x})}\int_\Sigma d^3y\left(-2N_k D_l\pi^{kl}\right) + \delta(\mathbf{x}-\mathbf{X})\frac{N(\mathbf{X})}{2m}P^i P^j,\end{aligned} \tag{2.33}$$

which are the classical equations (2.13), (2.15), modified by $V \to V + Q$. In this way, a Hamiltonian form of the dynamics is obtained, given by (2.26), (2.31)-(2.33).

A crucial advantage of this Hamiltonian formulation is that it can be derived from the action

$$\mathcal{S} = \mathcal{S}_{\rm cl} + \mathcal{S}_Q, \tag{2.34}$$

with

$$\mathcal{S}_Q = -\int dt\, Q = -\int dt \int_\Sigma d^3x\, N\, \mathcal{Q}. \tag{2.35}$$

The Bohmian dynamics is not completely determined by this action as it also entails (2.25) which should be imposed here as an additional constraint. Actually, it is sufficient to assume that (2.25) holds on a certain leaf of the foliation [132], because then it will hold on all leaves of the foliation.
From (2.34) we now immediately get the quantum Einstein equations by varying with respect to $g_{\mu\nu}$:

$$G_{\mu\nu} - \Lambda g_{\mu\nu} = \kappa \left(T_{\mu\nu} + T_{Q\mu\nu}\right), \tag{2.36}$$

with $T^{\mu\nu}$ the classical energy-momentum tensor given in (2.18) and

$$T_Q^{\mu\nu} = -\frac{2}{\sqrt{-g(x)}} \frac{\delta \mathcal{S}_Q}{\delta g_{\mu\nu}(x)}$$

a quantum contribution given by

$$T_Q^{00}(t,\mathbf{x}) = \frac{1}{N(t,\mathbf{x})^2 \sqrt{h(t,\mathbf{x})}} \mathcal{Q}(t,\mathbf{x}), \tag{2.37a}$$

$$T_Q^{0i}(t,\mathbf{x}) = T_Q^{i0}(t,\mathbf{x}) = -N^i(t,\mathbf{x}) T_Q^{00}(t,\mathbf{x}), \tag{2.37b}$$

$$\begin{aligned} T_Q^{ij}(t,\mathbf{x}) =& N^i(t,\mathbf{x}) N^j(t,\mathbf{x}) T_Q^{00}(t,\mathbf{x}) \\ & - \frac{2}{N(\mathbf{x},t)\sqrt{h(\mathbf{x},t)}} \frac{\delta}{\delta h_{ij}(\mathbf{x})} \int_\Sigma d^3y N(\mathbf{y},t) \mathcal{Q}(\mathbf{y},t). \end{aligned} \tag{2.37c}$$

This tensor has the same form as in the scalar field case of [58], but with a different quantum potential. Defining $\widetilde{\mathcal{Q}} = \mathcal{Q}/\sqrt{h}$, it can be written more compactly as

$$T_Q^{\mu\nu}(x) = g^{\mu\nu}(x) \widetilde{\mathcal{Q}}(x) - \frac{2}{\sqrt{-g(x)}} \delta_i^\mu \delta_j^\nu \int_\Sigma d^3y \sqrt{-g(\mathbf{y},t)} \frac{\delta \widetilde{\mathcal{Q}}(\mathbf{y},t)}{\delta h_{ij}(\mathbf{x})}. \tag{2.38}$$

Note that if $\widetilde{\mathcal{Q}}$ is constant, then it acts as a cosmological constant. This feature has been explored in [157, 133, 53].

So far, we have just considered a single particle. The generalization to many particles is straightforward. The wave functional now depends on all the particle positions. i.e., $\Psi = \Psi(\mathbf{X}_1, \ldots, \mathbf{X}_n, h)$ and satisfies the constraints (2.19) and (2.20), with

$$\widehat{\mathcal{H}}_M(\mathbf{x}) = \sum_k N(\mathbf{x})\delta(\mathbf{x}-\mathbf{X}_k)\left(m_k - \frac{\nabla_k^2}{2m_k}\right), \qquad \widehat{\mathcal{H}}_{Mi}(\mathbf{x}) = \sum_k \delta(\mathbf{x}-\mathbf{X}_k)\nabla_{ki}, \tag{2.39}$$

where k is the particle label. The dynamics for the metric remains (2.24), while that of the particles is

$$\dot{X}^i_k = \frac{N(\mathbf{X}_k)}{m_k}\nabla^i S(\mathbf{X}_1, \ldots, \mathbf{X}_n, h) - N^i(\mathbf{X}_k). \tag{2.40}$$

The form of the quantum Einstein equations also remains unchanged, with the proviso that the matter part of the quantum potential is now

$$\mathcal{Q}_M(\mathbf{x}) = -\sum_k \delta(\mathbf{x}-\mathbf{X}_k)\frac{\nabla_k^2|\Psi|}{2m_k|\Psi|}. \tag{2.41}$$

2.5 Discussion and outlook

A direct consequence of the very structure of the quantum Einstein equations (2.36) is that the energy-momentum tensor $T_{\mu\nu} + T_{Q\mu\nu}$ is covariantly conserved. Namely, the left-hand-side of (2.36) is covariantly conserved as an identity. Therefore, the right-hand-side is also covariantly conserved. As a consequence, the status of energy conservation is the same as in classical general relativity [58]. In the context of spontaneous collapse theories, difficulties with the non-conservation of the energy-momentum tensor (in the semi-classical approximation) are circumvented by resorting to uni-modular gravity [90].

This work will be of interest to develop a semi-classical or weak field approximations, but that is work in progress. Namely, one goal would be to derive an approximation where gravity is treated classically and the particles quantum mechanically. Our energy-momentum tensor would then act as the source in the classical Einstein field equations. As explained in detail in [160], care has to be taken of the gauge invariance (in this case the invariance under spatial diffeomorphisms), by separating gauge degrees of freedom from gauge

invariant degrees of freedom. This is easily done in the case of electromagnetism using for example the transverse degrees of freedom of the electric field [160]. Presumably something similar can be done in the case of gravity, by passing to the weak field limit and considering the transverse traceless degrees of freedom, perhaps following the ideas of [1].

2.A Functional derivatives in the ADM formalism

To find the Einstein and stress-energy tensor we need to be able to take functional derivatives with respect to the metric components. However, because the specific decomposition we use mixes various parts of the metric this takes some care. We will start by going the other way around and calculate the functional derivatives with respect to the lapse, shift and spatial metric.

$$\frac{\delta}{\delta N} = \frac{\delta}{\delta g_{00}}\frac{\partial g_{00}}{\partial N} = -2N\frac{\delta}{\delta g_{00}}$$

$$\frac{\delta}{\delta N^k} = \frac{\delta}{\delta g_{00}}\frac{\partial g_{00}}{\partial N^k} + \frac{\delta}{\delta g_{0i}}\frac{\partial g_{0i}}{\partial N^k} + \frac{\delta}{\delta g_{i0}}\frac{\partial g_{i0}}{\partial N^k} = 2h_{ik}N^i\frac{\delta}{\delta g_{00}} + 2h_{ik}\frac{\delta}{\delta g_{0i}}$$

$$\begin{aligned}\frac{\delta}{\delta h_{ij}} &= \frac{\delta}{\delta g_{00}}\frac{\partial g_{00}}{\partial h_{ij}} + \frac{\delta}{\delta g_{0k}}\frac{\partial g_{0k}}{\partial h_{ij}} + \frac{\delta}{\delta g_{k0}}\frac{\partial g_{k0}}{\partial h_{ij}} + \frac{\delta}{\delta g_{ij}}\frac{\partial g_{ij}}{\partial h_{ij}} \\ &= N^iN^j\frac{\delta}{\delta g_{00}} + N^i\frac{\delta}{\delta g_{0j}} + N^j\frac{\delta}{\delta g_{i0}} + \frac{\delta}{\delta g_{ij}}\end{aligned}$$

We can solve these for the functional derivatives

$$\frac{\delta}{\delta g_{00}} = -\frac{1}{2N}\frac{\delta}{\delta N} \tag{2.42a}$$

$$\frac{\delta}{\delta g_{0i}} = \frac{h^{ik}}{2}\frac{\delta}{\delta N^k} + \frac{N^i}{2N}\frac{\delta}{\delta N} \tag{2.42b}$$

$$\frac{\delta}{\delta g_{ij}} = \frac{N^iN^j}{2N}\frac{\delta}{\delta N} - N^{(i}h^{j)k}\frac{\delta}{\delta N^k} + \frac{\delta}{\delta h_{ij}} \tag{2.42c}$$

Naar links!
Naar rechts!
Nog een keer!
Naar links!
Naar rechts!

Rob Kemps

3

Diffraction and interference with run-and-tumble particles

Abstract

Run-and-tumble particles, frequently considered today for modeling bacterial locomotion, naturally appear outside a biological context as well. Here, we consider them in a quantum mechanical relation, using a wave function to drive their propulsion and tumbling. Such quantum-active motion realizes a jittery motion of Dirac electrons (as in the famous *Zitterbewegung*): the Dirac electron *is* a run-and-tumble particle, where the tumbling is between chiralities. We visualize the electron trajectories in single and double slit experiments and discuss their dependence on the spin-direction. In particular, this yields the time-of-arrival statistics of the electrons at the screen. Finally, we observe that away from pure quantum guidance, run-and-tumble particles with suitable spacetime-dependent parameters produce an interference pattern as well.

This chapter was first published in [109], together with C. Maes and W. Struyve. The author of this thesis wrote the code for the simulations and created the visualizations, and also contributed to the writing of the manuscript.

3.1 Introduction

Active media constitute an important topic of current research efforts in nonequilibrium statistical mechanics. The mechanism of self-propulsion, e.g. by consuming stored or ambient energy, is central and combines interestingly with repulsive interactions showing collective behavior such as phase separation or flocking, [138]. For biophysical applications, models often imitate bacterial motion and biological motors. Major examples include active Brownian motion [151, 139] and run-and-tumble models [148]. The latter describe particles (like *E. coli* in polymeric fluids [126]) with flagellar self-propulsion where the 'free run' is interrupted by tumbling events where the orientation is updated.
Such models of active media often have a longer history however; see e.g. [178]. The origin of run-and-tumble processes goes back to the problem of electromagnetic wave propagation in a double transmission line (the transatlantic cable of the 1850's) such as summarized in the telegraph equation of Oliver Heaviside and William Thomson, and to the corresponding telegraph process as pioneered by Mark Kac [91]. Choosing suitable boundary conditions [112], independent-particle models simulating running and standing waves are easily obtained. In the present paper, we explore and visualize a newer relation with the Dirac theory [113] of the electron.

According to the usual formulation of the Dirac theory, an electron is described by a spinor. By decomposing the Dirac spinor into its left- and right-handed chiral component, the theory can be seen as one of interacting Weyl particles. That is, the electron is viewed as a massless Weyl particle with a chirality that flips between left- and right-handed. That interpretation is strongly suggested in particular by the Standard Model of particles physics, according to which electrons are fundamentally massless and hence Weyl particles, acquiring an effective mass through the interaction with the Higgs field. Roger Penrose describes this view in detail in [130] referring to it as the *zig-zag picture*, writing: "So are these zigs and zags real? For my own part, I would say so; they are as real as the "Dirac electron" is itself real..." [130, p. 632]. That perspective has in fact a longer history, probably starting with Richard Feynman who suggested and formulated a path-integral version for the Dirac equation in two-dimensional spacetime where the electron paths go back and forth at the speed of light [67, 150, 33].

That zig-zagging of electrons, as they flip between right-handed and left-handed chirality, is made manifest in the pilot-wave theory and makes the topic of the present study. Then, most interestingly, the electron dynamics becomes that of a run-and-tumble particle with propulsion speed and tumbling rates depending on the left- and right-handed chirality component of the Dirac spinor. In that way, we connect an interesting model of nonequilibrium statistical

mechanics, the active motion of run-and-tumble particles, with Dirac theory. As a result, we can visualize the electron dynamics in the case of diffraction and interference phenomena, studying the effect of the spin direction. The explicit connection with the (stochastic) run-and-tumble model indeed allows simulating the electron path in the nonrelativistic Pauli approximation. The availability of particle trajectories also allows a straightforward determination of arrival times on the screen after exiting the double-slit, something that is difficult to achieve otherwise [120]. The numerical method employs a Cash-Karp algorithm in Julia [34, 12]; see [116] for the publicly available code.

The outline of the paper is as follows. In the next section, we start with the general setup of run-and-tumble particles with spacetime-dependent propulsion speeds and tumbling rates, as a slight extension of the usual practice for active particles in nonequilibrium statistical mechanics. In Section 3.3, we show how the run-and-tumble dynamics for a Dirac particle can be obtained in the pilot-wave approach. Following [51, 42, 158], this is done by identifying the continuity equation for the Dirac electron, when viewed as combination of chiral Weyl electrons, with the Master equation for run-and-tumble particles. The dynamics contains what we call a "curling" and a "tumbling" component, which both depend on the spin. We study the effects of these components, comparing with previous studies in [131, 82, 77, 145, 147, 146] where either the curling or the tumbling aspects were ignored. The main part of the present paper is the application of these ideas to the simulation of diffraction and interference experiments. This is done within the non-relativistic limit of the Dirac theory, which is given by the Pauli theory. In Section 3.4, we visualize the trajectories of the electrons producing the typical patterns upon hitting the screen. The simulation allows to speak here precisely about arrival times as well, as we illustrate in Section 3.5. We add in Section 3.6 that diffraction and interference patterns can be obtained away from the strict quantum context, within the dynamics of run-and-tumble particles more generally. Here also, an implicit relation between pure quantum processes such as in spin-orbit coupling and (classical) run-and-tumble particles was formulated before. References with such analogies and similar inspiration include [106, 28]. The recent [13] gives a mathematical (spectral) analysis of the zig-zag process within classical probability. We conclude in Section 3.7.

3.2 Spacetime activity

We consider independent active particles in three spatial dimensions, that alternatingly follow one of two spacetime-dependent velocity fields $\mathbf{v}_\pm(\mathbf{x},t)$,

$$\dot{\mathbf{x}}_t = \mathbf{v}_{\chi_t}(\mathbf{x}_t,t) \tag{3.1}$$

for position $\mathbf{x}_t$ at time t. The variable $\chi_t = \pm$ (we think of it as chirality, with right-handed particles having $\chi = +$, left-handed particles having $\chi = -$) follows an inhomogeneous Markov jump process with transition rate $a(\mathbf{x},t)$ to jump from $- \longrightarrow +$ and rate $b(\mathbf{x},t)$ to jump $+ \longrightarrow -$ when $\mathbf{x}_t = \mathbf{x}$. Then, the resulting Master equation for the densities $\rho(\mathbf{x},t;\chi)$ of left- and right-handed movers is

$$\frac{\partial\rho}{\partial t}(\mathbf{x},t;\chi) + \nabla\cdot\big(\mathbf{v}_\chi(\mathbf{x},t)\rho(\mathbf{x},t;\chi)\big) = r(\mathbf{x},t;-\chi)\rho(\mathbf{x},t;-\chi) - r(\mathbf{x},t;\chi)\rho(\mathbf{x},t;\chi) \tag{3.2}$$

for the tumbling field $r(\mathbf{x},t;\pm)$ with $r(\mathbf{x},t;\chi=-) = a(\mathbf{x},t)$ and $r(\mathbf{x},t;\chi=+) = b(\mathbf{x},t)$. Initial conditions should be added for the initial distribution of the particles (e.g. at time $t = 0$ near $\mathbf{x} = 0$ in what follows). That extension of the usual run-and-tumble dynamics is strictly continued in Section 3.6. The relation with quantum mechanics appears next.

As to be explained in the following section, the wave function (spinor) that solves the Dirac or Pauli equation will determine $\mathbf{v}_\pm(\mathbf{x},t)$ and $r(\mathbf{x},t;\chi)$, such that (3.2) is exactly the continuity equation for the corresponding quantum probability density. If the initial positions of the particles are thrown according to the Born rule, they will move following (3.1) with some initial χ_0, such that at all times they follow the quantum statistics.
In that sense we may speak about quantum-active motion where the "fuel" is provided by a quantum evolution, yet without breaking time-reversal invariance (more on that below).

3.3 Zig-zag theory of the Dirac electron

The Dirac equation is the relativistic version of the Schrödinger equation for electrons. We are interested in trajectories that can be associated with a Dirac electron, as pioneered by David Bohm [18], and in the connection with run-and-tumble dynamics. We follow [158] for the choice of decomposition of the wave function with the resulting continuity equations for left-handed and right-handed (so called Weyl) electrons. The basic idea is that all fermionic particles are fundamentally chiral and massless, as suggested by the Standard

Model. The electron mass m couples the Weyl electrons which results in the tumbling of chiralities; the tumbling rate will be seen to be proportional to $mc^2/\hbar$. Between any two consecutive tumbling events the electrons move at the speed of light c, but the tumbling results in an average velocity smaller than this. We now proceed with the mathematical details for that decomposition in four spacetime dimensions.

A single electron in four spacetime dimensions has a wave function $\psi(\mathbf{x},t) \in \mathbb{C}^4$ satisfying the (free) Dirac equation

$$(i\hbar\gamma^\mu\partial_\mu - mc)\psi = 0 \tag{3.3}$$

written in terms of the gamma-matrices γ^μ. Assuming the Weyl (or chiral) basis for the gamma matrices, the wave function can be written as a bispinor, a pair of two component Weyl spinors $\psi = (\psi_-, \psi_+)^T$, describing respectively a left-handed and a right-handed spinor. The Dirac equation (3.3) can then be rewritten as two coupled equations of these spinors,

$$i\hbar\,\sigma^\mu\partial_\mu\psi_+ = mc\psi_-, \qquad i\hbar\,\overline{\sigma}^\mu\partial_\mu\psi_- = mc\psi_+ \tag{3.4}$$

where $\sigma^\mu = (\mathbb{1}, \boldsymbol{\sigma})$ and $\overline{\sigma}^\mu = (\mathbb{1}, -\boldsymbol{\sigma})$ for Pauli matrices $\boldsymbol{\sigma}$. Thereupon, the Dirac current

$$j^\mu = \overline{\psi}\gamma^\mu\psi \quad \text{with} \quad \overline{\psi} = \psi^\dagger\gamma^0, \ \text{satisfying} \quad \partial_\mu j^\mu = 0$$

follows the decomposition $j^\mu = j^\mu_+ + j^\mu_-$ for

$$j^\mu_+ = \psi^\dagger_+\sigma^\mu\psi_+, \qquad j^\mu_- = \psi^\dagger_-\overline{\sigma}^\mu\psi_-$$

They do not satisfy a continuity equation separately, but have a source

$$\partial_\mu j^\mu_\pm = \pm F, \quad \text{with} \quad F = 2\frac{mc}{\hbar}\,\mathrm{Im}\,\psi^\dagger_+\psi_-$$

That last equation can be written out explicitly in the way of (3.2),

$$\begin{aligned} \partial_t\rho_+ + \nabla\cdot(\mathbf{v}_+\rho_+) &= a\rho_- - b\rho_+ \\ \partial_t\rho_- + \nabla\cdot(\mathbf{v}_-\rho_-) &= b\rho_+ - a\rho_- \end{aligned} \tag{3.5}$$

for the densities $\rho_+ = j^0_+ = \psi^\dagger_+\psi_+$ and $\rho_- = j^0_- = \psi^\dagger_-\psi_-$, where

$$\mathbf{v}_+ = c\,\frac{\psi^\dagger_+\,\boldsymbol{\sigma}\,\psi_+}{\psi^\dagger_+\psi_+}, \qquad \mathbf{v}_- = -c\,\frac{\psi^\dagger_-\,\boldsymbol{\sigma}\,\psi_-}{\psi^\dagger_-\psi_-}$$

$$a = 2\frac{mc^2}{\hbar}\,\frac{\left(\mathrm{Im}\,\psi^\dagger_+\psi_-\right)^+}{\psi^\dagger_-\psi_-}, \qquad b = 2\frac{mc^2}{\hbar}\,\frac{\left(\mathrm{Im}\,\psi^\dagger_-\psi_+\right)^+}{\psi^\dagger_+\psi_+} \tag{3.6}$$

(equations (22)–(23) in [158].) Here we used that $F = F^+ - (-F)^+$ for $F^+ = \max\{F, 0\}$.

As in the theory of stochastic processes, the natural next step is to interpret the above equations (3.5)–(3.6) as the Master equation for an ensemble of run-and-tumble particles, following the setup of Section 3.2. They are here interpreted as two different massless manifestations of the Dirac electron, "zig" and "zag," i.e., as the Weyl electrons [130].

We consider therefore the stochastic dynamics of the electron position $\mathbf{x}_t$ as in (3.1). The speed $|\mathbf{v}_\pm| = c$ is invariably equal to the speed of light. (That follows from the fact that $j^\mu_+ j_{+\mu} = j^\mu_- j_{-\mu} = 0$.) What changes discontinuously at every transition $\chi \to -\chi$ is the direction of the particle, as the velocity changes from $\mathbf{v}_\chi$ to $\mathbf{v}_{-\chi}$. The tumbling (and change of effective velocity field) is a consequence of the coupling between left- and right-chirality and indeed occurs at a rate proportional to the mass. Note in any case that the factor $2mc^2/\hbar$ in the expressions (3.6) for a and b is known as the angular frequency of the *Zitterbewegung*[1], here realized as the tumbling of the particle. The resulting dynamics is a time-dependent Markov process $(\mathbf{x}_t, \chi_t)$ and that dynamics is such as to reproduce at every moment the correct densities $\rho_\pm$.

The dynamics is also time-reversal invariant, in contrast with models of run-and-tumble particles where there is dissipation (in consuming fuel), [69]. Given a trajectory $\omega = (\mathbf{x}(t), \chi_t), t \in [-s, s]$, its time-reversal $\theta\omega$ is $(\theta\omega)_t = (\mathbf{x}(-t), \chi_{-t}), t \in [-s, s]$. If ω is a possible trajectory from applying the rules (3.6) with solution $\psi(t, \mathbf{x})$, then the time-reversed trajectory $\theta\omega$ can be generated from applying those rules to the solution $i\gamma^1\gamma^3\psi^*(\mathbf{x}, t)$. That time-reversal operation $\psi(\mathbf{x}, t) \to i\gamma^1\gamma^3\psi^*(\mathbf{x}, t)$ [78], or $\psi_\pm(\mathbf{x}, t) \to -\sigma_2\psi^*_\pm(\mathbf{x}, t)$, is anti-unitary, and indeed implies that $\mathbf{v}_\pm(\mathbf{x}, t) \to -\mathbf{v}_\pm(\mathbf{x}, -t)$. Probabilities for trajectories arise here from the initial condition where the positions are drawn according to the Born rule and from the random tumbling events. Since the transformation takes $|\rho_\pm(\mathbf{x}, s)|^2 \to |\rho_\pm(\mathbf{x}, -s)|^2$ and also maps $a(\mathbf{x}, t) \to b(\mathbf{x}, -t)$, $b(\mathbf{x}, t) \to a(\mathbf{x}, -t)$, there is statistical reversibility [57], i.e. formally, the probability densities for ω and at $\theta\omega$ are equal.

To model the slit experiment it is natural to use Gaussian wave functions. However, for the Dirac theory the Gaussian solution is not of closed form [78]. For numerical simplicity, we therefore consider the non-relativistic limit of the

[1]The Zitterbewegung [22, 149, 78] is actually due to the interference of positive and negative energy wave functions (for the trajectories see [80, 81]). As such it should be distinguished from the zig-zag motion considered here which is due to the fundamental massless nature of the particles.

Dirac theory (3.4)-(3.6), given by the Pauli theory, which after all is realistic for the interference experiments with electrons as in the pioneering works [117, 171]. We further assume that the spin decouples from the translational degrees of freedom, so that the Pauli spinor is of the form $\phi(t,\mathbf{x}) = \psi(t,\mathbf{x})\,\xi$, where now ψ is a scalar function governed by the Schrödinger equation, and ξ a constant spinor. We define the spin polarization vector $\hat{\mathbf{s}} = \xi^\dagger \boldsymbol{\sigma} \xi$, where $\boldsymbol{\sigma}$ are still the Pauli matrices.

Then, the zig-zag model goes as follows [158]. The velocity field for (3.1) turns out to be[2]

$$\mathbf{v}_\chi = \frac{\hbar}{m}\,\mathrm{Im}\,\frac{\boldsymbol{\nabla}\psi}{\psi} + \frac{\hbar}{m}\,\mathrm{Re}\,\frac{\boldsymbol{\nabla}\psi}{\psi} \times \hat{\mathbf{s}} + \chi\, c\, \hat{\mathbf{s}} \tag{3.7}$$

That velocity field thus consists of three terms written in the right-hand side of (3.7). The first corresponds simply to the velocity field associated with solutions of the free Schrödinger equation. For example, for a plane wave with wave vector $\mathbf{k}$, that first term in (3.7) would be $\hbar\mathbf{k}/m$. The second term with the curl produces a whirling orthogonal to the spin; we will refer to it as the "curling". The third term corresponds to the "tumbling" (as the chirality χ flips). This is the dominant one in (3.7) as being a light speed component in the direction of the spin vector. We will see that between tumbling events the particle indeed approximately moves in straight lines at speed c. The jumps between chiralities $\chi \to -\chi$ happen at a rate

$$r(\mathbf{x},t,\chi) = [\chi\tau(t,\mathbf{x})]^+ \tag{3.8}$$

where

$$\tau(t,\mathbf{x}) = -c\frac{\boldsymbol{\nabla}|\psi|^2}{|\psi|^2}\cdot\hat{\mathbf{s}} = -2c\,\mathrm{Re}\,\frac{\boldsymbol{\nabla}\psi}{\psi}\cdot\hat{\mathbf{s}} \tag{3.9}$$

The trajectories of the Dirac electron are thus well approximated (for non-relativistic speeds) by that running and tumbling as summarized in (3.7)–(3.9) to be substituted in (3.1). (The dynamics is still time-reversal invariant, with now $\psi(\mathbf{x},t) \to \psi^*(\mathbf{x},-t)$ and $\xi \to -\sigma_2\xi^*$.)

The dynamics without the curling and tumbling term corresponds to the one originally suggested by de Broglie and Bohm to describe non-relativistic particles without spin [17, 81]. Relativistic considerations suggest the addition of the spin-dependent curling term [17], whereas the standard model suggests also the addition of the tumbling term [42, 158].

[2]In the non-relativistic limit actually an extra term appears in the velocity field [158]. However, this term makes that the distribution $|\psi|^2$ is not exactly preserved by the zig-zag dynamics, but only up to relevant order. Here, we have chosen to drop this term in order to guarantee preservation of the distribution $|\psi|^2$. See [158] for further discussion.

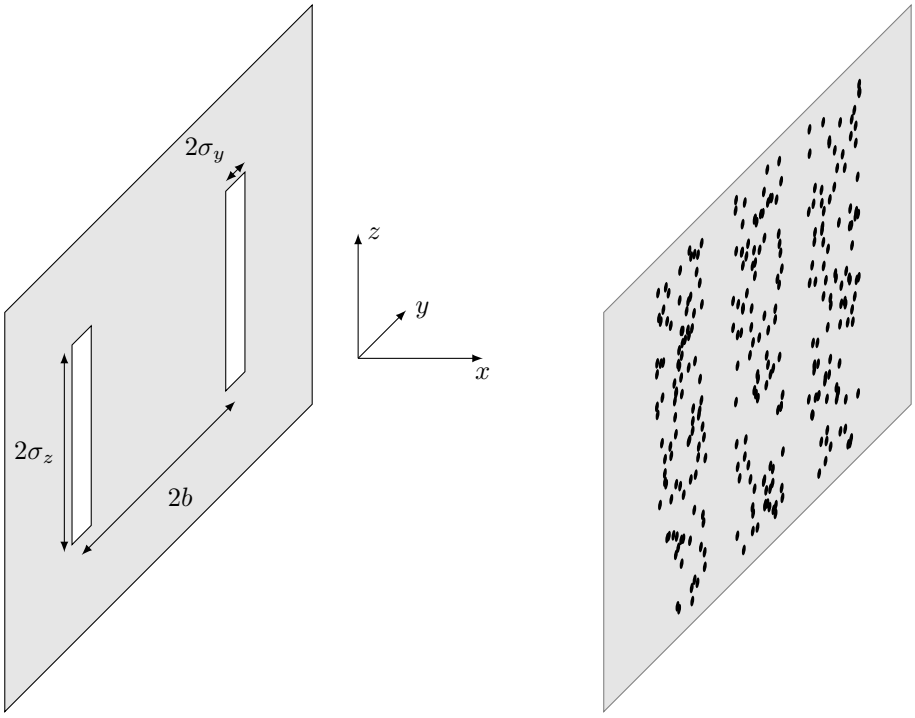

Figure 3.1: Spatial setup, with electrons exiting the wall from slits to arrive at the screen.

3.4 Trajectory visualization

The issue of visualization (*Anschaulichkeit*) has been subject of major discussion among the pioneers of quantum mechanics. The ultimate goal, often "refuted[3]", is to derive and to show the trajectories of quantum particles, thus shedding light on the underlying causal connections leading to the empirical findings. In the present section we visualize diffraction and interference with Pauli electrons, following the theoretical framework above.

The physical setup for the simulated experiments is as seen in Fig. 3.1. The Cartesian coordinates are such that the distance from the slit(s) to the screen is measured in the x-direction, the slits are separated from each other in the y-direction and the z-direction goes along the (vertical) direction of the slit(s).

[3]It was, for example, the motivation for the Heisenberg paper (1927) on the uncertainty relations.

We model the wave function right after it exits the slit(s) as

$$\psi^G(t, \mathbf{x} \equiv (x, y, z)) = \psi_x(t, x)\psi^S(t, y)\psi_z(t, z), \tag{3.10}$$

where

$$\psi_x(t, x) = \frac{1}{\left(2\pi\sigma_x^2\left(1 + i\frac{\hbar t}{2m\sigma_x^2}\right)^2\right)^{1/4}} \times \exp\left[-\frac{(x - v_0 t)^2}{4\sigma_x^2\left(1 + i\frac{\hbar t}{2m\sigma^2}\right)} + \frac{i}{\hbar}\left(mv_0 x - \frac{mv_0^2}{2}t\right)\right] \tag{3.11}$$

with

$$\frac{\partial\psi_x}{\partial x}(t, x) = \left(-\frac{x - v_0 t}{2\sigma_x^2\left(1 + i\frac{\hbar t}{2m\sigma_x^2}\right)} + \frac{i}{\hbar}mv_0\right)\psi_x(t, x) \tag{3.12}$$

is a Gaussian packet with standard deviation σ_x moving with speed v_0 in the positive x-direction. We localize the wave function in the x-direction as much as possible, but not so much that the uncertainty in momentum space overwhelms the bulk velocity of the wave packet, i.e. $\Delta p_x \ll mv_0$. The uncertainty principle $\Delta x \Delta p_x = \hbar/2$ implies therefore that $\sigma_x = \Delta x$ has a lower limit of a few times $\hbar/2mv_0$: we take $v_0 = c/10$ and $\sigma_x = 50\hbar/mc$.

For the z-direction, $\psi_z(t, z)$ is similarly a Gaussian wave packet with standard deviation σ_z, to be specified later, but with zero speed. The form of the packet $\psi^S(t, y)$ will depend on whether we consider one or two slits.

The wave function ψ^G is separable in the coordinates x, y, z. Therefore, if the spin is aligned along one of the coordinate axes, the motion in that direction will decouple from the motion in the other directions. For example, suppose $\hat{\mathbf{s}} = \hat{\mathbf{x}}$, then $\mathbf{v}_\chi = (v_{\chi,x}, v_{\chi,y}, v_{\chi,z})$ equals

$$v_{\chi,x} = \frac{\hbar}{m}\,\mathrm{Im}\left(\frac{1}{\psi_x}\frac{\partial\psi_x}{\partial x}\right) + \chi\, c \tag{3.13}$$

$$v_{\chi,y} = \frac{\hbar}{m}\,\mathrm{Im}\left(\frac{1}{\psi^S}\frac{\partial\psi_y}{\partial y}\right) + \frac{\hbar}{m}\,\mathrm{Re}\left(\frac{1}{\psi_z}\frac{\partial\psi_z}{\partial z}\right) \tag{3.14}$$

$$v_{\chi,z} = \frac{\hbar}{m}\,\mathrm{Im}\left(\frac{1}{\psi_z}\frac{\partial\psi_z}{\partial z}\right) - \frac{\hbar}{m}\,\mathrm{Re}\left(\frac{1}{\psi^S}\frac{\partial\psi^S}{\partial y}\right) \tag{3.15}$$

The motion in the y-and z-direction are thus coupled and corresponds to the motion without tumbling. The motion in the x-direction has the tumbling but

no curling. Hence, a plot of the projection of the trajectories in the (y, z)-plane would give the same trajectories with or without keeping the tumbling in the dynamics. When $\hat{\mathbf{s}} = (\hat{\mathbf{x}} + \hat{\mathbf{y}} + \hat{\mathbf{z}})/\sqrt{3}$, as we will often consider in the following, the motion along the different directions is coupled.

We are then ready to numerically integrate the stochastic dynamics described by (3.1). We choose to implement the following algorithm in Julia, [12]. We employ the Cash-Karp method, [34], an adaptive Runge-Kutta method, giving a fourth order approximation with a fifth-order error estimate. The latter is used to adaptively adjust the time step for the local truncation error to a reasonable value, say 10^{-12}. In addition, an upper limit is set for the product of the time step $\mathrm{d}t$ with the tumbling rate r: $r\ \mathrm{d}t < 2^{-7}$. If surpassed, the time step is lowered and the step is retried. For every Runge-Kutta step, the tumbling rate is sampled at the beginning and at the end of the step, the mean of these two values will then provide an approximation to the mean value of the rate over the step. If that mean tumbling rate does not exceed the threshold, the step is accepted, and a random number is chosen uniformly from 0 to 1. Only if the product of the time step and the rate exceeds that random number, the chirality of the particle is inverted. In either case, we continue on to the next step, until the particle hits the screen or the maximum number of iterations is reached.
The code is publicly available; see [116]. The plots are made in natural units where $\hbar = c = m = 1$. Since the distance traveled by the particle is usually much greater than the width of the wave function in the y-direction, we rescale the y-axis to comfortably fit all the data on the page. The same scale is used when different dynamics or spin orientations are explicitly compared.

3.4.1 Single slit diffraction

To model the sharp edge of the slit, we would ideally use a boxcar function. However, although an analytical solution for the Schrödinger equation exists with these initial conditions, making use of the imaginary error function, the high-frequency components of its derivative pose numerical difficulties. Instead we can make a decent approximation by taking the y-component in (3.10) to be the sum

$$\psi^S(t, y) = \mathcal{N} \sum_{\ell=-K}^{K} \psi_y \left(t, y - \frac{\sigma_y}{K}\ell\right) \tag{3.16}$$

where $\mathcal{N}$ is an irrelevant normalization factor, and each ψ_y is of the form (3.11) with $v_0 = 0$ and with standard deviation $\sigma_y/\sqrt{2}K$. For this diffraction experiment we take a square slit, assuming $\sigma_y = \sigma_z = 20\hbar/mc$ is the half width of the slit; see Fig. 3.2. For our simulations we take $K = 6$. Furthermore,

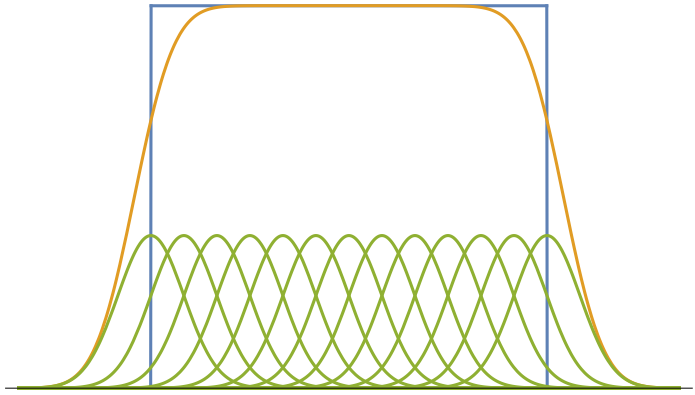

Figure 3.2: The desired boxcar function with width $2\sigma_y$ representing the single slit and its approximation by a sum (3.16) of 13 shifted Gaussians.

knowing that the electron velocity is $0.1c$, the de Broglie relation tells us that its wavelength will be $20\pi\hbar/mc$, which is comparable to the full width of the slit. Therefore the near field will extend over at most a few times this distance.

We are ready to apply (3.7)–(3.9) in (3.1). To start, in Fig. 3.3 we give the so called Bohmian trajectories, i.e. the trajectories without including the curling and tumbling. We plotted there the near-field behavior in the sense that the horizontal dimension of the picture covers only $100\hbar/mc$.

An (xy)-projection of the trajectories including all terms in (3.7) is shown in Figs. 3.4 (a),(b) and (c) for different choices of spin orientation $\hat{\mathbf{s}}$. We also compare there the far-field behavior (Fraunhofer diffraction) with the near-field behavior (Fresnel diffraction). The left panels in Fig. 3.4 show the far-field behavior with the screen at a distance $1000\hbar/mc$ from the slit. The right panels give the near-field trajectories at one tenth of this distance. The left vertical line is the placement of the wall (in the y-direction). Because of the spreading of the wave function, the slits are not always visible on the largest scale. On the right, the location of the screen is indicated with a vertical line. Each time we show 25 trajectories for the far field and 5-10 trajectories for the near field, started from sampling initial positions according to the Born rule. Note that some trajectories cross the barrier of the slits. That is an artifact of our modeling due to the wave function having tails in these regions. For a wave function that vanishes in these regions, there would be no such crossings. The particles tend to explore the support of the wave function, especially in the direction of the spin, in contrast to the trajectories without curling and tumbling, cf. Fig. 3.4d.

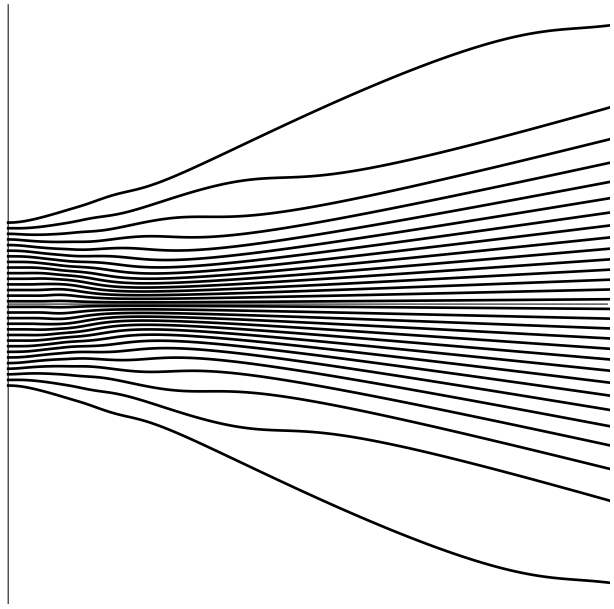

Figure 3.3: Near-field behavior of the trajectories for a single slit, without the curling and tumbling (keeping only the first term in (3.7)).

The particles will tend to keep moving at approximately the light speed in a certain direction until they reach a region of low density $|\psi|^2$. As is clear from the formulae (3.8)–(3.9), in such regions the jump rate increases, giving more chance for a velocity flip to occur. This is also clarified through Fig. 3.5a where the tumbling rate is plotted for ψ_y a Gaussian of the form (3.11) with $v_0 = 0$.

Taking the spin to point towards $(\hat{\mathbf{x}}+\hat{\mathbf{y}}+\hat{\mathbf{z}})/\sqrt{3}$, the distribution of the positions at impact (first crossing) of the particles on the screen is shown in Fig. 3.6, on the left. Notice the secondary maxima, characteristic of diffraction. This distribution is not just simply equal to $|\psi|^2$. First of all, the wave function changes over time and some trajectories may take more time than others to reach the screen. Second, it is also the first crossing of the screen that is recorded; due to the zig-zag a trajectory may cross the screen several times. (We have here ignored what exactly the effect of a physical screen is on the trajectories.)

In Fig. 3.6c, on the left, the distribution of the y coordinate is plotted in function of the arrival time, which clearly illustrates the time-dependence of the pattern. The arrival time for each particle trajectory is the time when the particle first hits the screen (at a certain fixed distance from the slit(s)). Note that the pattern, perhaps surprisingly, appears asymmetric around $y = 0$, with offset

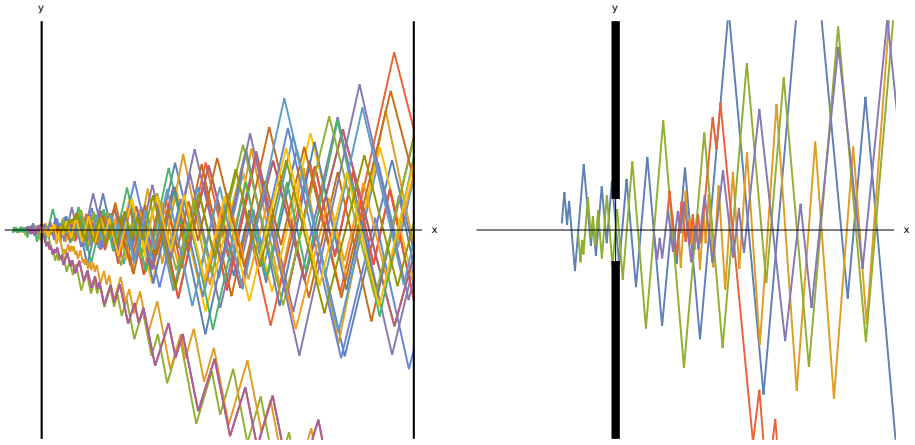

(a) $\hat{\mathbf{s}} = \hat{\mathbf{y}}$

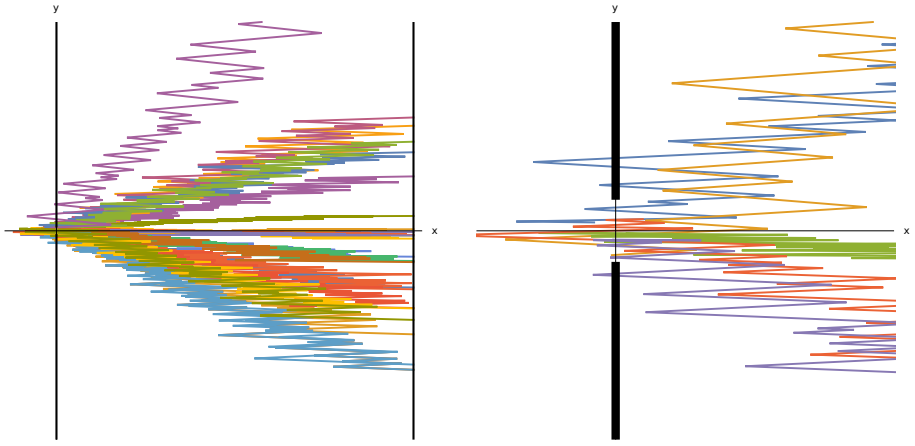

(b) $\hat{\mathbf{s}} = \hat{\mathbf{x}}$

Figure 3.4: Single slit trajectories with random initial positions distributed according to the Born rule for the initial wave function (3.10) with the boxcar function (3.16) in the y-direction. Pictured on the left and the right are respectively the far-field and near-field behaviors.

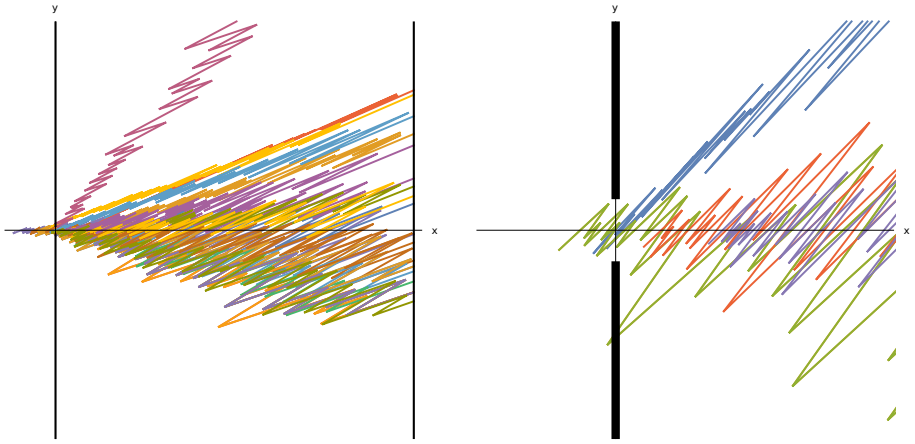

(c) $\hat{\mathbf{s}} = (\hat{\mathbf{x}} + \hat{\mathbf{y}} + \hat{\mathbf{z}})/\sqrt{3}$

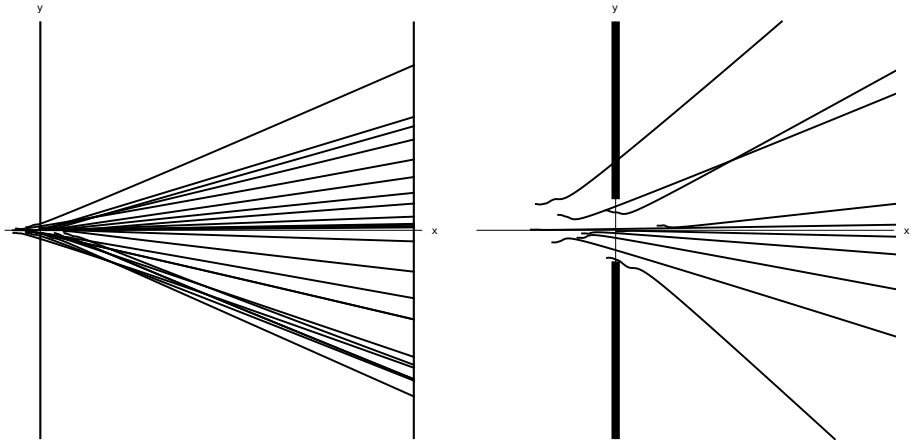

(d) Trajectories without the curling and tumbling (keeping only the first term in (3.7)).

Figure 3.4: (continued)

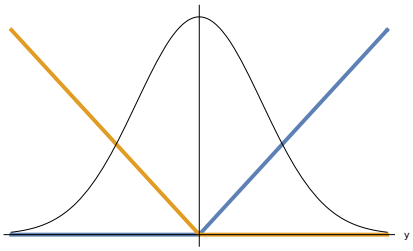

(a) The tumbling rate for a single slit Gaussian wave function is linear in y.

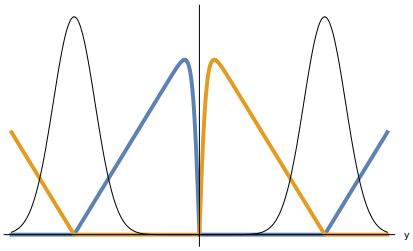

(b) Right after exiting the double slits.

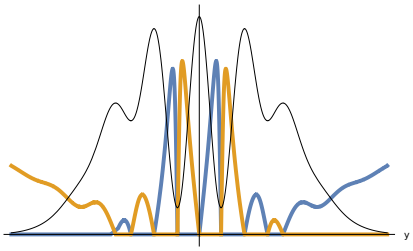

(c) During formation of interference pattern.

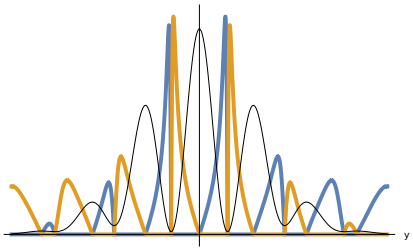

(d) After the pattern has formed.

Figure 3.5: The y-dependence of the tumbling rates when $\hat{\mathbf{s}} = \hat{\mathbf{y}}$. The blue curve corresponds to the tumbling rate from + to − chirality, and vice versa for the orange curve. In black is shown $|\psi|^2$. For a single slit, the profile is linear as shown in (a). For two slits, (b)-(d), oscillations appear as the wave function starts to show more peaks farther away from the wall.

towards higher y- and z-coordinates. The origin of that asymmetry are particles hitting the screen whilst on an excursion in the direction of the spin vector, away from the bulk of the wave packet. That, in other words, is an effect due to the electron's spin direction, here visualized explicitly.

3.4.2 Double slit interference

Moving on to the double slit experiment, b denotes half the distance between the centers of the slits, $b = 6\sigma_y = 120\hbar/mc$, and the height of the slits is

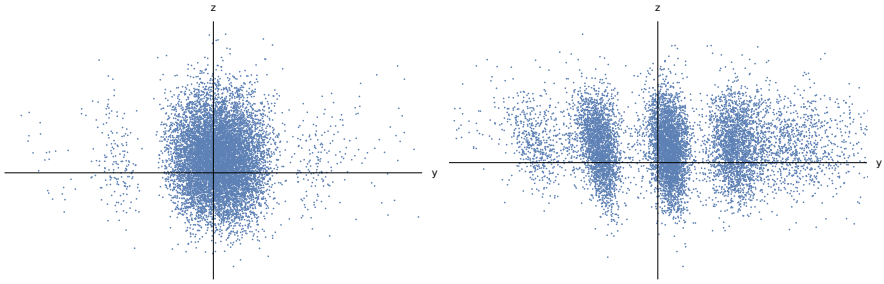

(a) The two-dimensional pattern as it appears on the screen, corresponding to the y- and z-coordinates of the particle.

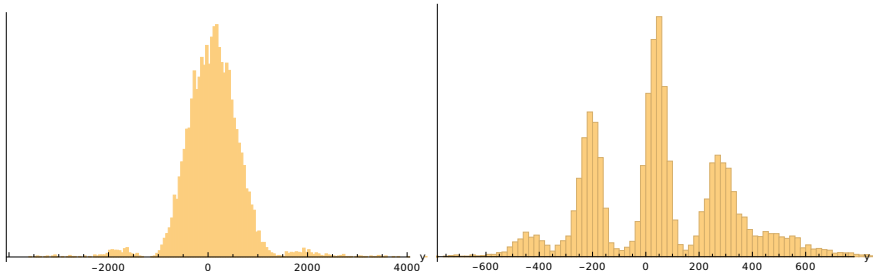

(b) Distribution of the y-coordinate of the particle impacts on the screen.

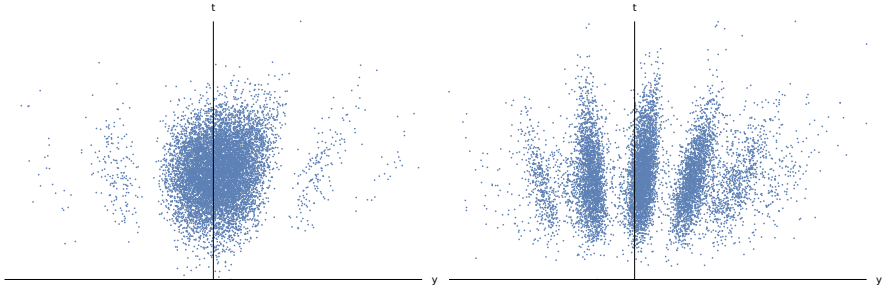

(c) Distribution of the y-coordinate of the particle impacts in function of the arrival time.

Figure 3.6: Patterns on the screen, for $\hat{\mathbf{s}} = (\hat{\mathbf{x}} + \hat{\mathbf{y}} + \hat{\mathbf{z}})/\sqrt{3}$. The single slit is on the left and the double slit is on the right.

$\sigma_z = 5\sigma_y$. As the focus now lies on the interference effects (and not diffraction[4]), for simplicity we use a superposition of single Gaussians for the y-component ψ^S in (3.10):

$$\psi^S(t,y) = \frac{1}{\sqrt{2}}\psi_y(t,y-b) + \frac{1}{\sqrt{2}}\psi_y(t,y+b) \tag{3.17}$$

The x- and z-components are unchanged from the previous section, and in particular, it is mainly the de Broglie wavelength $\hbar/mv_0$ that determines the shape of the interference pattern.
For understanding the tumbling, we need e.g. the logarithmic derivative, entering (3.7),

$$\frac{1}{\psi^G}\frac{\partial\psi^G}{\partial y} = \frac{1}{2\sigma_y^2(1+i\gamma t)}\left(-y + b\tanh\frac{by}{2\sigma_y^2(1+i\gamma t)}\right) \tag{3.18}$$

where $\gamma = \hbar/2m\sigma_y^2$. The nonzero distance between the slits adds a term proportional to b. As is clear from (3.9), that is important in the tumbling rate when the spin $\hat{\mathbf{s}}$ has a component in the y-direction. For large times t, deviations from the linear behavior of the rate function will be most noticeable near the minima of the interference pattern, as shown in Fig. 3.5. Notice how the rate function right after the slits, shown in Fig. 3.5b, approximates a piecewise linear function, with zeroes near the local maxima. As the interference pattern forms, the rate function takes on a more complicated shape, peaking where the wave function is small, and approximating a linear function where the wave function is approximately Gaussian.

Investigating the patterns that appear on the screen, we again fix $\hat{\mathbf{s}} = (\hat{\mathbf{x}} + \hat{\mathbf{y}} + \hat{\mathbf{z}})/\sqrt{3}$. As was the case with diffraction, even though interference fringes are clearly visible, cf. Fig. 3.6, they are not directly related to $|\psi|^2$; see similar (and also experimental) results and considerations in [101, 95]. Fig. 3.6c on the right strikingly resembles experimental results in [101].

The trajectories for various directions of the spin are plotted in Fig. 3.7. A comparison can now be made of the different dynamics, obtained by the various contributions in the velocity field (3.7). For the double slit experiment, trajectories without the curling and tumbling were pioneered in [131] and without tumbling in [82]. See Fig. 3.8 for the view of the trajectories in the (xy)-plane and Fig. 3.9 for three-dimensional views. Contrary to Fig. 3.7 we do not adhere to the Born rule here, constraining the particles to start at $x = 0$ and $z = 0$, with the same initial positions in each figure. Without the curling and tumbling, there is a symmetry around the x-axis, cf. Fig. 3.8a. This symmetry

[4]There are of course also diffraction gratings that involve many slits, and interference underlies diffraction phenomena. The terminology of this paper wants foremost to distinguish between single and double slits.

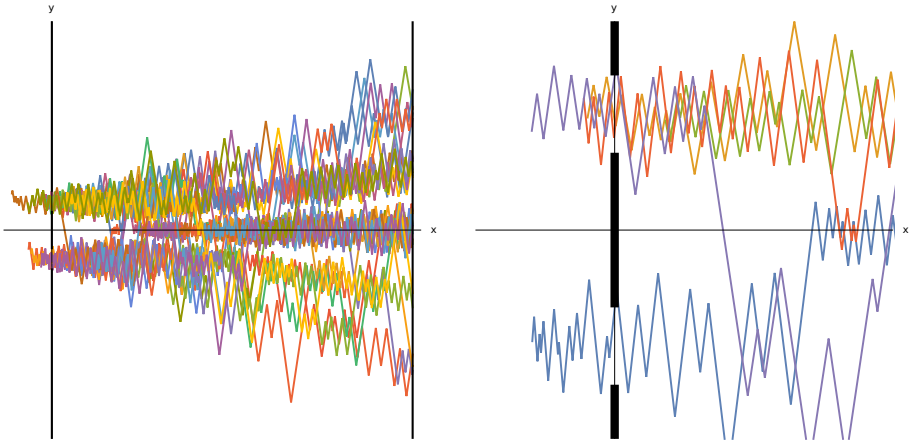

(a) $\hat{\mathbf{s}} = \hat{\mathbf{y}}$

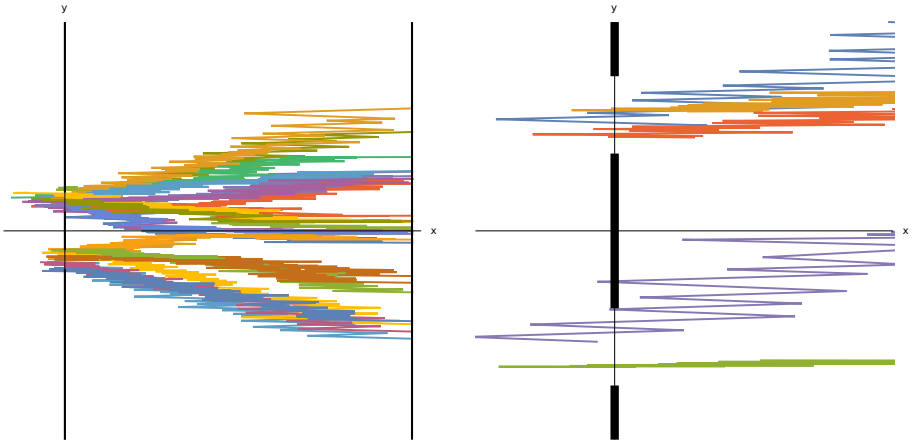

(b) $\hat{\mathbf{s}} = \hat{\mathbf{x}}$

Figure 3.7: Double slit trajectories with random initial positions distributed according to the Born rule for the initial wave function (3.10) with the Gaussian superposition (3.17) in the y-direction. Pictured on the left and the right are respectively the far-field and near-field behaviors.

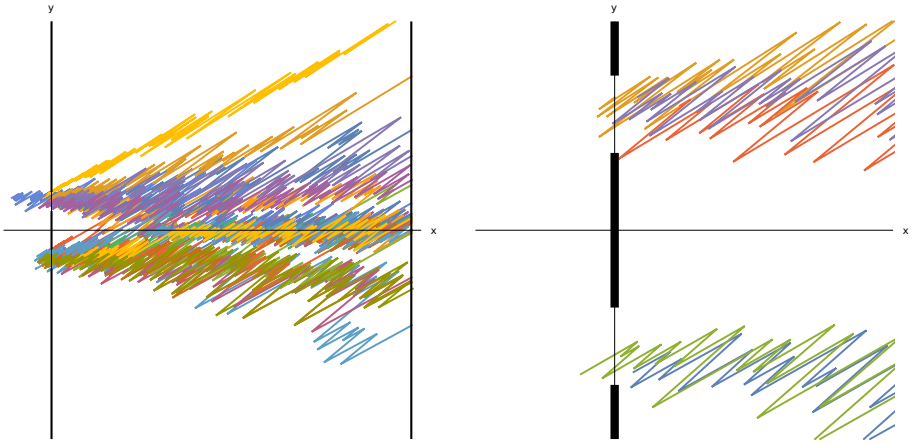

(c) $\hat{\mathbf{s}} = (\hat{\mathbf{x}} + \hat{\mathbf{y}} + \hat{\mathbf{z}})/\sqrt{3}$

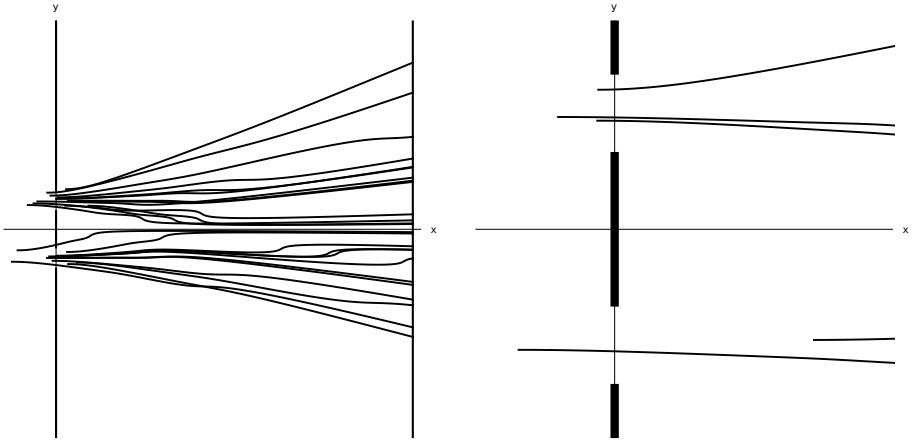

(d) Trajectories without curling and tumbling (only keeping the first term in (3.7)).

Figure 3.7: (continued)

is slightly spoiled when curling is introduced, cf. Fig. 3.8b (as was already noted in [82]), and even more so when the tumbling is included, cf. Fig. 3.8c. In the latter case, the tumbling also causes the particle to occasionally strays back to the other side of the wall. As the interference pattern develops, the probability distribution forms channels and the particle tends to get stuck in one of those channels. As mentioned before when we discussed diffraction, this is because the jump rate is such that the probability of reflection increases when the particle moves to a low density region.

As we scale up the physical parameters of the simulation, the zig-zag completely dominates the motion, as shown in Fig. 3.10. In Fig. 3.10a, the distance between the wall and the screen is $3 \times 10^9 \hbar/mc \approx 1\,\text{mm}$, with slits that are about 15 nm wide and spaced 100 nm apart. In Fig. 3.10b, the distance between the wall and the screen is $3 \times 10^{12} \hbar/mc \approx 1\,\text{m}$, with slits that are about 500 nm wide, spaced 3 µm apart. On their way to the screen, the particles undergo respectively about 200 000 and 5 600 000 tumbles. In contrast to the behavior on the smaller scales, the particle now explores the full width of the packet in the y-direction in both cases. While channels of probability are still formed by the $|\psi|^2$-distribution, trapping the particle for a certain amount of time, there is always a non-zero probability it will transition to another channel.

3.5 Arrival times

An implication concerns the possibility for measuring arrival times. Predicting or even defining arrival times for quantum particles are subject of on ongoing discussion, see [120, 48, 50] and references therein. Arrival times can however straightforwardly be determined in terms of the trajectories, here just by considering the time the particle first hits the screen. We consider a simple example as an initial exploration.[120]

While the electron moves at the speed of light between any two tumblings, the observed speed is less when dividing the distance between slits and screen by the time traveled. It is in that sense that tumbling (caused by the electron mass) "decelerates" the electron. However, this implies the electron's measured velocity will have a stochastic component, or rather, the time of its arrival at the screen will. Such a phenomenon is always present if the spin has a non-zero component in the direction of movement. As an illustration, we consider the Gaussian wave function (3.11) in the x-direction and take the spin to lie in the x-direction. Since the dynamics in this direction decouples from that in the other directions, we can ignore the y- and z-components of the motion. The dynamics is then given by (3.13). The initial positions of the particles are taken

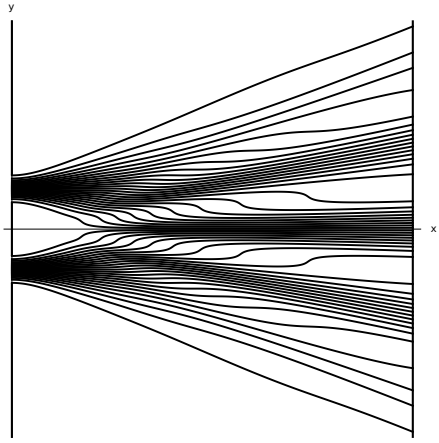

(a) Trajectories without curling and tumbling (keeping only the first term in (3.7)).

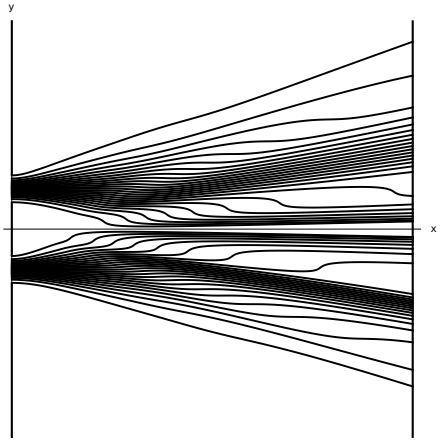

(b) Trajectories with curling but without tumbling (without the third term in (3.7)).

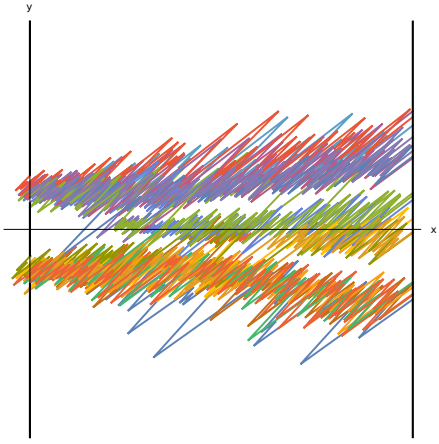

(c) Trajectories with curling and tumbling.

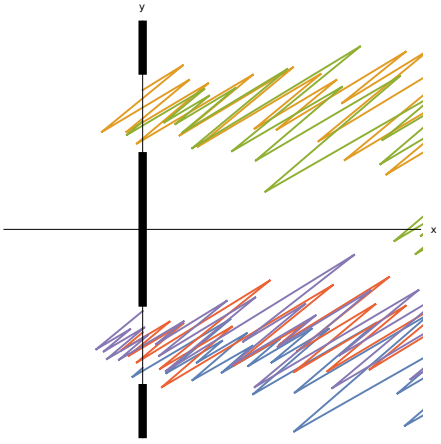

(d) Near-field behavior of (c).

Figure 3.8: Double slit trajectories for particles starting at $x = 0$ and $z = 0$, with the same initial positions in (a)-(c), and $\hat{\mathbf{s}} = (\hat{\mathbf{x}} + \hat{\mathbf{y}} + \hat{\mathbf{z}})/\sqrt{3}$. Comparison of the different dynamics.

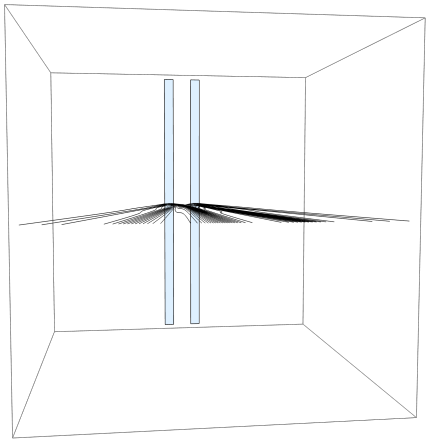

(a) Without tumbling and curling.

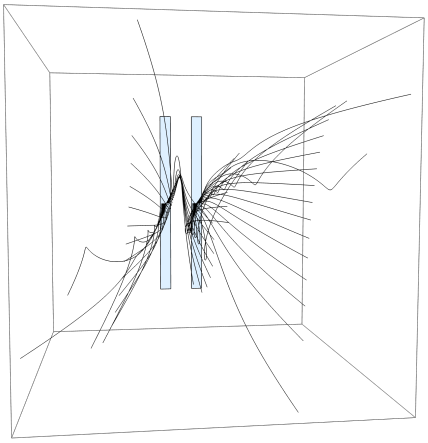

(b) With curling but without tumbling, $\hat{\mathbf{s}} = \hat{\mathbf{x}}$.

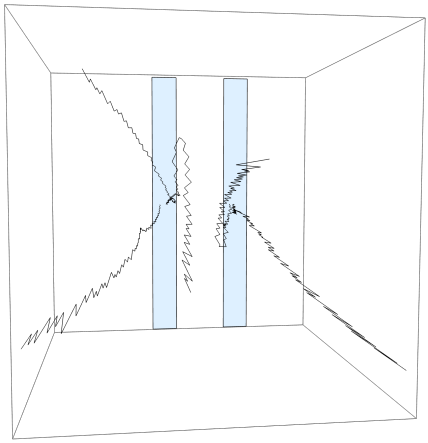

(c) With curling and tumbling, $\hat{\mathbf{s}} = \hat{\mathbf{x}}$.

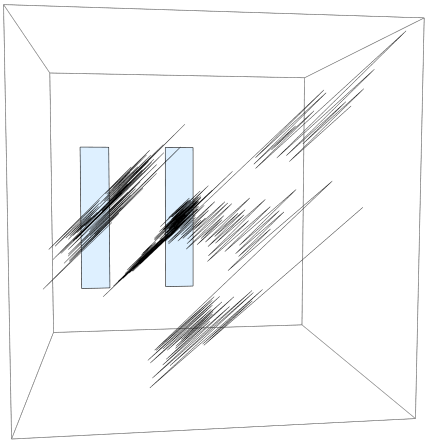

(d) With curling and tumbling, $\hat{\mathbf{s}} = (\hat{\mathbf{x}} + \hat{\mathbf{y}} + \hat{\mathbf{z}})/\sqrt{3}$.

Figure 3.9: Three-dimensional views towards wall. Particles start from $x = 0$ and $z = 0$.

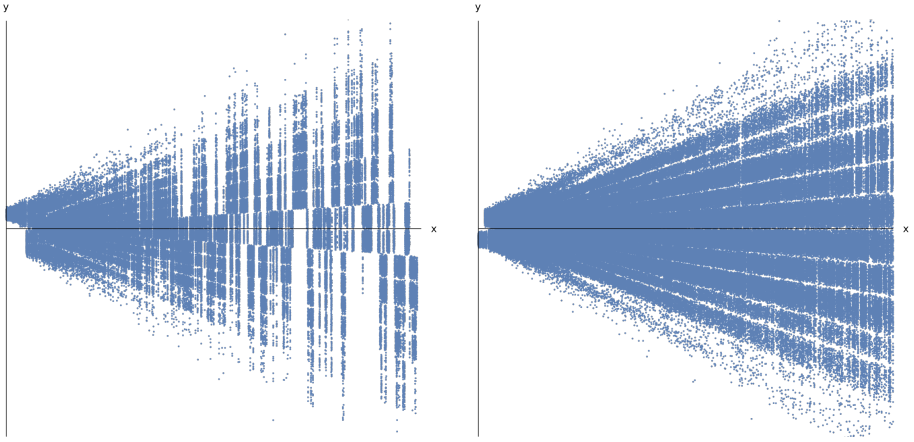

(a) Wall-screen distance is ca. 1 mm. The vertical extension measures ca. 1 µm.

(b) Wall-screen distance is ca. 1 m. The vertical extension measures ca. 40 µm.

Figure 3.10: Trajectory of a single particle with $\hat{\mathbf{s}} = \hat{\mathbf{y}}$ traversing the given distance. Unlike in the other figures, we only plot a point where a tumble happens, and not the (mostly straight) parts of the trajectories in between, as this would completely wash out the image.

according to the Born rule. In Fig. 3.11 we compare the zig-zag trajectories to one without zig-zag (only first term in (3.7)), and we take a look at the distribution of the arrival times of 10 000 particles. The overwhelming majority of particles arrive much earlier than would be the case when the curling and tumbling are omitted in (3.7).

It might seem puzzling that differences arise in the arrival time distributions depending on whether or not curling and tumbling are included in the dynamics. Namely, in each case, the ensemble position distribution is given by $|\psi|^2$. Therefore these theories agree on the distributions of positions of things, including e.g. the positions of the hands of a clock. The reason that we get different arrival times stems from the fact that we are dealing with a simplified analysis, which does not take into account the details of the measurement set-up, i.e., the details of how the particles get detected on the screen. It is striking that these effects seem to be important for time measurements, since they do not seem to matter for position measurements. In any case, including the details of the detection process in the analysis seems as yet not practically feasible, therefore it is worthwhile investigating approximative approaches like the one considered here, which ignore these details. Experiments should determine

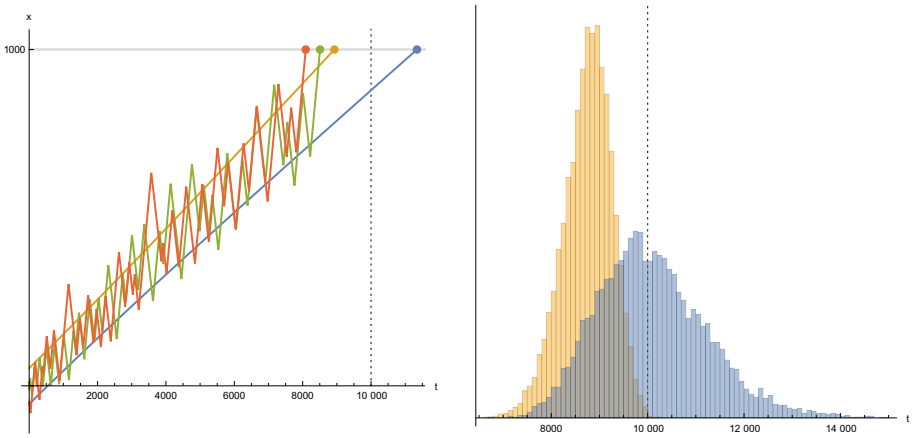

(a) Two zig-zag trajectories (red, green) compared to two trajectories without curling and tumbling (blue, orange). The horizontal grey line indicates the position of the screen.

(b) Comparison of the distribution of the arrival times of zig-zag trajectories (orange) with that in case of the dynamics without curling and tumbling (blue).

Figure 3.11: Arrival times in the case of a single Gaussian wave function (3.11) and $\hat{\mathbf{s}} = \hat{\mathbf{x}}$. In both plots, the dotted vertical line indicates the time at which the center of the wave packet reaches the screen.

which one of the approximation methods is more successful. It would therefore be interesting to consider realistic setups as e.g. described in [49], to see how the arrival time distributions for the zig-zag motion compare with those when tumbling or curling are ignored.

3.6 Back to classical run-and-tumbling

In the above, the trajectories realize the motion of a quantum particle, with its wave function guiding it. The result was a stochastic dynamics caused by the flipping of chiralities.
If we leave the strict quantum prescriptions (3.6) for velocity and tumbling fields, we remain with run-and-tumble particles as described in Section 3.2. In particular, we can use versions of tumbling rates which qualitatively reproduce the tumbling field Fig. 3.5. For example, we consider a one-dimensional model

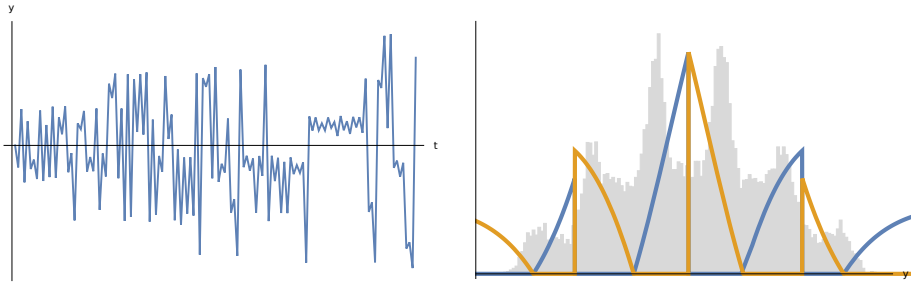

(a) One-dimensional trajectory: y-position versus time for a run-and-tumble particle moving at constant speed and tumbling according to the oscillatory curve in (b).

(b) Distribution of final positions, and associated tumbling rates (3.19).

Figure 3.12: Leaving quantum mechanics: the tumbling rates are given by (3.19) and not derived from a wave function.

where the rates are as in (3.8) but given by the positive and negative parts of

$$\tau(t,y) = \frac{y}{40} + 8\left(\frac{y}{12} - \left\lfloor \frac{y}{12} \right\rfloor - \frac{1}{2}\right) \tanh\left(\frac{t}{1000}\right) \operatorname{sech}\left(\frac{y}{15}\right) \tag{3.19}$$

That rate function has a linear part to keep particles from running away to infinity, on which we superimpose a slowly growing sawtooth, modulated by a hyperbolic secant envelope. We use a run-and-tumble particle moving in the y-direction, at constant speed $\pm c$. In Fig. 3.12a we plot the (one-dimensional) trajectory of a run-and-tumble particle which, by locally increased tumbling, gets trapped (more) in certain y-canals. The tumbling rate as plotted in Fig. 3.12b follows only approximately the behavior of the tumbling rates for the quantum mechanical case of Fig. 3.5, but there is no wave function now. Therefore, the interference of fermions can be embedded in a larger class of stochastic particle dynamics showing these wave effects. See also [106, 28] for similar points. From the point of view of soft condensed matter, it remains perhaps surprising that run-and-tumble particles, in a classical simulation of trajectories, may show an interference pattern.

3.7 Conclusions

The Standard Model of particle physics suggests that electrons be viewed as run-and-tumble particles. Adopting that view in the context of the Dirac theory,

analytic results for the wave function evolution can be used to determine the velocity fields and tumbling rates of the particle dynamics. We applied that to the case of diffraction and interference, visualizing the details of the run-and-tumble process, detailing the effects of spin, while recovering the usual patterns on the screen. Comparing in Fig. 3.8–Fig. 3.9 with the usual trajectories for the Schrödinger equation (keeping only the first term on the right-hand side of (3.7) and no tumbling), which lack the zig-zag dynamics, our new trajectories are markedly different. We observe that particles in their zig-zag motion explore the probability space available to them, however as the interference of the wave function takes place, the particles tend to get trapped for longer in "interference canals" of high probability. That can be simulated (literally now) by *pure* run-and-tumble particles (no quantum mechanics) as was shown in Fig. 3.12.

We have also started exploring arrival-time distributions, readily obtained in terms of the simulated trajectories. Interesting effects appear and it needs to be seen how these results compare to experiment.

Part II

Photon stochastic processes

Приятно, когда удаётся найти нечто новое в вытоптанной области.

Александр Соломонович Компанеец

4

On the derivation of the Kompaneets equation

Abstract

The relaxation of a photon bath to thermal equilibrium via Compton scattering with electrons is described in the Kompaneets equation (1956). The equation is mostly known from studies of astrophysical plasmas, for its convergence to the Planck distribution and for possible corrections to that Planck law in the cosmic microwave background, most notably from the Sunyaev-Zeldovich effect. We revisit its derivation emphasizing its structure as a Kramers-Moyal diffusion approximation to the quantum Boltzmann equation or Master equation with stimulated emission. We do not assume that the Planck law is stationary in performing the continuum approximation but we emphasize the necessity of the flux or Møller factor to arrive at a continuity equation. On the other hand, the structure allows more general assumptions than originally envisioned by Kompaneets.

This chapter was first published in [73], together with G.E. Freire Oliveira and C. Maes. The author of this thesis contributed to the calculations and the writing of the manuscript.

4.1 Introduction

The interaction between matter and radiation is a standard topic in plasma physics and cosmology. In low-density plasmas, Compton scattering is the dominant mechanism enabling energy exchange [15, 180]. Essentially, this process describes elastic collisions of photons and charged particles (which we assume to consist solely of electrons), preserving photon number. The time evolution of the radiation spectrum subject to Compton scattering on a plasma of nonrelativistic Maxwellian electrons was first obtained by A.S. Kompaneets in 1956 [99]. This arose from his theoretical research as part of the Soviet hydrogen bomb program in 1949. When the eponymous relaxation equation turned out to be useless for weapons research, the results were declassified and published by Kompaneets in 1956 [129, 107]. The Kompaneets equation later found new life in quantitatively describing the Sunyaev-Zeldovich effect, which is a distortion of the cosmic microwave background radiation by Compton scattering of hot electrons during its passage through clusters of galaxies [164, 165, 30].

For a nonrelativistic electron bath at temperature T, with $k_B T \ll m_e c^2$ for electron mass m_e, the Kompaneets equation

$$\omega^2 \frac{\partial n}{\partial t}(\omega, t) = \frac{n_e \sigma_T c}{m_e c^2} \frac{\partial}{\partial \omega} \omega^4 \left\{ k_B T \frac{\partial n}{\partial \omega}(\omega, t) + \hbar \left[1 + n(\omega, t)\right] n(\omega, t) \right\} \tag{4.1}$$

shows how a photon gas under conditions of spatial homogeneity and isotropy relaxes to thermal equilibrium from Compton scattering. It is a continuity equation for the (dimensionless) photon number $n(\omega, t)$ occupying frequency ω at time t. The spectral energy density is proportional to $\hbar(\omega/c)^3\, n(\omega, t)$ [154]. The range of frequencies is assumed to have a photon energy $\hbar\omega \sim k_B T \ll m_e c^2$. In (4.1), $\sigma_T \approx 0.66\,\mathrm{b}$ is the total Thomson cross section and n_e is the electron density, which together determine the photon mean free path $\ell = (n_e \sigma_T)^{-1}$ and the average time between collisions $\tau = \ell/c$.

The current in frequency space is given by

$$\frac{\partial n}{\partial t}(\omega, t) = \frac{1}{\omega^2} \frac{\partial}{\partial \omega} \big(\omega^2\, j_t(\omega) \big)$$

$$j_t(\omega) = \frac{n_e \sigma_T c}{m_e c^2} \omega^2 \left\{ k_B T \frac{\partial n}{\partial \omega}(\omega, t) + \hbar \left[1 + n(\omega, t)\right] n(\omega, t) \right\} \tag{4.2}$$

That current (4.2) vanishes when the photon number $n(\omega, t)$ is given by the Bose-Einstein expression,

$$n_{\mathrm{BE}}(\omega) = \frac{1}{e^{\beta(\hbar\omega - \mu)} - 1}, \qquad \mu \le 0, \tag{4.3}$$

at inverse temperature $\beta = 1/k_B T$, with a single free parameter, the photon chemical potential $\mu \leq 0$. The temperature T here refers to the temperature of the electron bath under the assumption that it is in thermal equilibrium, but this can be made more general as shown in Section 4.6. The relaxation behavior of (4.1) is obviously an interesting question in itself, but not the subject of the present paper; see e.g. [137, 29] for a numerical code. It suffices to note in addition that depending on the initial number of photons, the limiting photons as $t \uparrow \infty$ will have a Bose-Einstein distribution component ($n_{\rm eq}(\omega)$), as well as a condensate (for $\omega = 0$). That condensate appears when the initial number of photons is larger than the equilibrium number of photons $n_{\rm eq}$ at the given inverse temperature β. The excess photons cannot disappear, forming a Bose-Einstein condensate at $\omega = 0$, as the Kompaneets equation is photon-number preserving. For this interesting feature we refer to [59, 102] for a more detailed discussion.

Kompaneets himself only derived the exact form of the first term between the brackets in (4.1), which is purely a diffusive term due to Doppler shift experienced by the photons in the reference frame of the electrons. The (second) drift term, describing stimulated emission and the Compton recoil, were instead derived from the assumption that in thermal equilibrium the stationary distribution ought to be the Planck distribution. The so-called Comptonization, i.e., the redistribution of photon energies scattered by electrons consists of two terms indeed, both suppressed by the same factor of $m_e c^2$, the diffusion because the electron is moving so slowly (depending on $k_B T/m_e c^2$) that the Doppler shift is almost negligible, and the drift is divided by the reduced Compton frequency $\omega_c = m_e c^2/\hbar \approx 7.76 \times 10^{20}$ Hz so that there is barely any recoil.

The derivation of the Kompaneets equation has been called "distinctly non-trivial" [107], and many authors have presented or repeated their best derivation. However, we could not find any reference which carries a full derivation in the same spirit that Kompaneets originally proposed, using the correct relativistic expression of the kinetic (Boltzmann) equation. For example, it is worth making precise when in fact the diffusion approximation of the Boltzmann equation, the standard way of deriving (4.1), cannot yield a continuity equation. We found that such features are not fully explored in the existing literature. We believe that a "more didactical" derivation may also be useful to highlight physical limitations and possible extensions.

Kompaneets in 1956 is not explicit about the form of the kinetic equation used as starting point[1]. He proposes to carry an expansion up to second order in the

[1] In his *original* paper [99], Kompaneets mentions in a footnote that his work had already been published as Report No. 336 at the Institute of Chemical Physics, Academy of Sciences,

photon transferred energy, using the Thomson scattering cross section

$$\frac{\mathrm{d}\sigma^{\mathrm{Th}}}{\mathrm{d}\Omega_{\mathrm{rest}}} = \frac{3\sigma_T}{16\pi}\left(1+\cos^2\theta_{\mathrm{rest}}\right) \tag{4.4}$$

where $\mathrm{d}\Omega_{\mathrm{rest}}$ is the scattering solid angle measured in the electron rest frame. In 1963 Dreicer [55] more carefully describes the Fokker-Planck approximation to the Boltzmann equation for an electron-photon gas. However, he does not give an expression for the time evolution of the photon number. In 1965 Weymann [179] uses Dreicer's formalism to derive an equation identical to the one by Kompaneets, although not displaying the details of the calculation. Somewhat remarkably, although Dreicer's and Weymann's papers are published after Kompaneets' paper, they do not cite the latter. Nevertheless, those as well as many other references [144, 181, 93, 105] follow Kompaneets' recipe, also using the Thomson cross section. We highlight that it is not possible to find the Kompaneets equation by that approach while performing the diffusion approximation as proposed by Kompaneets; rather we must use the full relativistic expression with the Klein-Nishina cross section including the Møller velocity factor (see Section 4.4) in order to correct for the flux of electrons in the kinetic equation (4.27). In fact, this factor appears naturally while carefully deriving the relativistic Boltzmann equation; see for example [35, 174, 175].

What follows is split in two parts. Sections 4.2–4.3 make the first part, where general considerations explain how and why the Planck law is obtained from a Master equation for the bosonic occupation in reciprocal space. By performing a Kramers-Moyal (or diffusion) expansion on the Master equation of a discrete random walk in reciprocal space with suitably chosen transition rates, we show that the Kompaneets equation (and its extensions) can be obtained. That offers a quite different perspective which is especially simple and general. In particular, we believe that this approach is more adapted to carry nonequilibrium extensions on the Kompaneets equation.

The second part starts with Section 4.4 where we connect with the standard setup for deriving the Kompaneets equation. That centers around the diffusion approximation to the Boltzmann equation with the electron gas as stationary background. It becomes clear then in Section 4.5 what are the main steps and what is the nature of the approximation.

Apart from talking with history and reviewing part of the existing literature on the derivation of the Kompaneets equation, we are motivated by exploring possible extensions. Our motivation for a better understanding of the Kompaneets physics is based on [6] where the fascinating hypothesis was

USSR. We exhaustively searched the literature but we could not find this report. Interestingly, Peebles mentions as well that he could not find it either [129].

formulated of a nonequilibrium effect modifying the Planck spectrum in the cosmic background radiation. We do not quite continue that search in the present paper, but in Section 4.6 we give generalizations and some possible nonequilibrium extensions of the Kompaneets equation.

There exist many derivations of the Kompaneets equation, witnessing of its fundamental interest in problems of light-matter interaction. Revisiting some of them is useful we believe for clarifying subtleties (and even inconsistencies) that are rarely mentioned (and that a careful reader would stumble upon) even in textbook references. Together with the first part of this paper, a more comprehensive understanding of this famous equation, which is much less known in the statistical mechanics community, pays respect to all these efforts while it may possibly open new avenues to introduce nonequilibrum features in the physics of the Early Universe.

4.2 Detailed balance with stimulated emission

Pauli was probably the first to dynamically characterize thermal equilibrium for photons in an electron bath, identifying in 1923 the condition of detailed balance in the Master equation describing scattering and recovering the Planck law for its stationary distribution [127].
Transition rates for a jump process arising within a quantum many-particle system are derived from one-particle Green's functions [92]. Here we take a photonic set up with a symmetrized Fock space taking the tensor product over three-dimensional harmonic oscillators with wave vector $\mathbf{k}$ corresponding to frequency ω. An elementary transition is the annihilation of a photon with wave vector $\mathbf{k}$ while creating a photon with wave vector $\mathbf{k}'$. When the photons are in weak contact with a thermal bath at inverse temperature β, each transition creates a flux in reciprocal space with an expectation given by

$$j(\mathbf{k} \to \mathbf{k}') = \alpha(\mathbf{k}, \mathbf{k}')\, e^{\beta(\hbar\omega - \hbar\omega')/2} \left| \langle \mathrm{f} | a^\dagger_{\mathbf{k}'} a_{\mathbf{k}} | \mathrm{i} \rangle \right|^2 \tag{4.5}$$

where $\alpha(\mathbf{k}, \mathbf{k}') = \alpha(\mathbf{k}', \mathbf{k})$ is symmetric and left unspecified for the moment as a parameter of dynamical activity. We have taken that to lowest order the matrix element will contain a single term annihilating and creating a photon $a^\dagger_{\mathbf{k}'} a_{\mathbf{k}}$. Writing $n(\mathbf{k})$ for the occupation/level at wave vector $\mathbf{k}$, we put

$$|\mathrm{i}\rangle = |\ldots n(\mathbf{k}) \ldots n(\mathbf{k}') \ldots\rangle$$

for the initial state. The only non-zero matrix element will between that initial $|i\rangle$ and the final state

$$|\mathrm{f}\rangle = |\ldots n(\mathbf{k}) - 1 \ldots n(\mathbf{k}') + 1 \ldots\rangle$$

Since on each of the Hilbert spaces $a|n\rangle = \sqrt{n}\,|n-1\rangle$ and $a^\dagger|n\rangle = \sqrt{n+1}\,|n+1\rangle$, we find that

$$\left|\langle \mathrm{f}\,|a^\dagger_{\mathbf{k}'} a_{\mathbf{k}}|\mathrm{i}\rangle\right|^2 = (1+n(\mathbf{k}'))\,n(\mathbf{k})$$

Therefore (4.5) becomes

$$j(\mathbf{k}\to\mathbf{k}') = \alpha(\mathbf{k},\mathbf{k}')\,w(\mathbf{k},\mathbf{k}')\,n(\mathbf{k}) \tag{4.6}$$

$$w(\mathbf{k},\mathbf{k}') = e^{\beta(\hbar\omega-\hbar\omega')/2}\,(1+n(\mathbf{k}'))$$

In classic texts on Markov processes, (4.6) makes the sink term into $\mathbf{k}'$ from $\mathbf{k}$ and one would write a Master equation for the probability of occupying the various wave vectors. The source term is $j(\mathbf{k}'\to\mathbf{k})$. Ignoring however correlations between the occupations at different wave vectors, we can write the Master equation directly for the (now expected) occupation numbers

$$\frac{\partial}{\partial t} n_t(\mathbf{k}) = \sum_{\mathbf{k}'} \alpha(\mathbf{k},\mathbf{k}')\,\big[e^{\beta(\hbar\omega-\hbar\omega')/2}\,(1+n_t(\mathbf{k}'))n_t(\mathbf{k}) - e^{\beta(\hbar\omega'-\hbar\omega)/2}\,(1+n_t(\mathbf{k}))n_t(\mathbf{k}')\big] \tag{4.7}$$

As such, the evolution equation (4.7) does not need to be photon number-preserving, i.e., it does not follow for free that

$$\sum_{\mathbf{k}} \frac{\partial}{\partial t} n_t(\mathbf{k}) = \sum_{\mathbf{k},\mathbf{k}'} \alpha(\mathbf{k},\mathbf{k}')[w(\mathbf{k}',\mathbf{k})n_t(\mathbf{k}') - w(\mathbf{k},\mathbf{k}')n_t(\mathbf{k})] = 0 \tag{4.8}$$

unless $\alpha(\mathbf{k},\mathbf{k}') = \alpha(\mathbf{k}',\mathbf{k})$ is indeed symmetric. Only then, (4.7) is a continuity equation.
Secondly, detailed balance requires that $j(\mathbf{k}\to\mathbf{k}') - j(\mathbf{k}'\to\mathbf{k}) = 0$ for all $\mathbf{k},\mathbf{k}'$, or (for symmetric $\alpha(\mathbf{k},\mathbf{k}')$ always)

$$w(\mathbf{k},\mathbf{k}')\,n(\mathbf{k}) = w(\mathbf{k}',\mathbf{k})\,n(\mathbf{k}') \quad \text{or}$$

$$e^{\beta(\hbar\omega-\hbar\omega')/2}\,(1+n(\mathbf{k}'))\,n(\mathbf{k}) = e^{\beta(\hbar\omega'-\hbar\omega)/2}\,(1+n(\mathbf{k}))\,n(\mathbf{k}')$$

$$\Longrightarrow\; e^{\beta\hbar\omega}\,\frac{n(\mathbf{k})}{1+n(\mathbf{k})} = \text{ constant } = e^{\beta\mu} \tag{4.9}$$

which implies that

$$n(\mathbf{k}) = \frac{1}{e^{\beta\hbar\omega}-1}$$

by assuming that the chemical potential equals zero, $\mu = 0$. Note that we have only used (4.6) for an environment in thermal equilibrium where the

temperature may refer to an electron gas or anything else. The "anything else" would solely show in the prefactor $\alpha(\mathbf{k}, \mathbf{k}')$ for the kinetics (4.7). In that sense the evolution given by (4.7) represents a general Kompaneets equation, before any diffusion approximation.

4.3 Kramers-Moyal expansion

The previous section considers jumps in the space of wave vectors $\mathbf{k}$. We associate in the present section an energy $U(\mathbf{k})$ to the system and we expand the Master equation (4.7) for small energy changes $\mathbf{k} \to \mathbf{k}'$. That is more generally known as a Kramers-Moyal or diffusion approximation.
Let us start in one dimension, where we consider a lattice mesh $\delta > 0$ for $x \in \delta\mathbb{Z}$. Note we are in reciprocal space, so δ is an inverse length. The $x = k_1$ stands for the first component of the (rescaled) wave vector. We imagine a walker hopping on that lattice of wave vectors, to nearest neighbor sites with transition rates

$$w(x, x \pm \delta) = (1 + n(x \pm \delta))B\left(x \pm \frac{\delta}{2}\right) \times \exp\left\{-\frac{\beta}{2}\left(U(x \pm \delta) - U(x)\right)\right\} \exp\left\{\frac{\pm\beta\delta}{2} f\left(x \pm \frac{\delta}{2}\right)\right\} \quad (4.10)$$

Here, n is the instantaneous number of walkers; its presence in the rates represents the stimulated emission. The function $B > 0$ is an inhomogeneous activity rate and β is the inverse temperature of a medium enabling the hopping. There is also a driving force f and a potential U which are added following the condition of local detailed balance at fixed environment inverse temperature $\beta = 1/k_B T$ [108]. We do not for the moment dwell on the physical meaning of the driving f and we do not restrict us to photons but to bosonic systems more generally; see also Section 4.6. The rate (4.6) is a special case of (4.10), where $f \equiv 0$ and the photon energy $U = \hbar\omega$. Abusing notation, we also incorporate the symmetric activity $\alpha(\mathbf{k}, \mathbf{k}')$ in the rates as the prefactor B.

For fixed δ the Master equation as in (4.7) becomes

$$\frac{\partial n_t}{\partial t}(x) + j_t(x, x + \delta) - j_t(x - \delta, x) = 0 \quad \text{for} \quad (4.11)$$

$$j_t(x, x + \delta) = n_t(x)w(x, x + \delta) - n_t(x + \delta)w(x + \delta, x)$$

$$j_t(x - \delta, x) = n_t(x - \delta)w(x - \delta, x) - n_t(x)w(x, x - \delta)$$

We expand this last equation to second order in δ; see Appendix 4.A. The result is

$$\frac{\partial}{\partial t} n_t = \delta^2 \Big\{ \left(\beta B g' + \beta B' g\right)(1+n)n + \left(\beta B g + B'\right) n' + 2\beta B g n n' + B n'' \Big\} \tag{4.12}$$

with $g(x) = U'(x) - f(x)$. That can be written more explicitly as a continuity equation,

$$\frac{\partial n_t}{\partial t}(x) = \delta^2 \frac{\partial}{\partial x} \left\{ B(x) \left(\frac{\partial n_t}{\partial x}(x) + \beta g(x) \big(1 + n_t(x)\big) n_t(x) \right) \right\} \tag{4.13}$$

in which we recognize the structural elements of the Kompaneets equation (4.1).

We can indeed redo that in three dimensions, on $\delta\mathbb{Z} \times \delta\mathbb{Z} \times \delta\mathbb{Z}$. Taking the same rates in all directions as before with 3-dimensional "force" f, the diffusion approximation now reads

$$\partial_t n_t = \delta^2 \, \boldsymbol{\nabla} \cdot \mathbf{j} \tag{4.14}$$

with in Cartesian coordinates $(x_\ell, \ell = 1, 2, 3)$ for $\mathbf{j} = \sum_\ell j_\ell \hat{\mathbf{x}}_\ell$,

$$j_\ell = B \left(\frac{\partial n}{\partial x_\ell} + \beta g_\ell \, (1+n) n \right) \tag{4.15}$$

for $g_\ell = \frac{\partial U}{\partial x_\ell} - f_\ell$.
Moving finally to the setup for the Kompaneets equation we enter frequency space by assuming that $n_t = n(\omega, t), g = g(\omega), D = D(\omega)$ with frequency $\omega = c\sqrt{\sum_\ell x_\ell^2}$ for speed of light c. It means to rewrite (4.14) in spherical coordinates, with ω as radial variable:

$$\omega^2 \frac{\partial n}{\partial t}(\omega, t) = c\,\delta^2 \, \frac{\partial}{\partial \omega} \left\{ \omega^2 B(\omega) \left(c \, \frac{\partial n}{\partial \omega}(\omega, t) + \beta \, g(\omega) \big(1 + n(\omega, t)\big) n(\omega, t) \right) \right\} \tag{4.16}$$

That is an extended Kompaneets equation, to be compared with (4.1), where the energy change and the driving combine into $g(\omega) = c\frac{\partial U}{\partial \omega}(\omega) - f(\omega)$.
Making the choices

$$c^2 \delta^2 \, B(\omega) = \frac{k_B T}{m_e c^2} n_e \sigma_T \, c \; \omega^2, \qquad g(\omega) = \hbar \, c \tag{4.17}$$

the above equation (4.16) becomes exactly the one of Kompaneets (4.1). Note that $n_e \sigma_T c = \tau^{-1}$ is the average collision rate, as before. That shows that the full structure of the Kompaneets equation is obtained as the diffusion

approximation to a Master equation with stimulated emission, and this holds whenever the limiting activity and drift obey (4.17). Justifications for the choices (4.17) come from the physical nature of the process considered in the Kompaneets equation. The photon energy is there $U(\omega) = \hbar\omega$ and there is no driving $f \equiv 0$, making indeed $g = c\frac{\partial U}{\partial \omega} = \hbar c$. For understanding the first equality in (4.17), we note that $c^2\delta^2\, B(\omega)$ appears as the diffusion constant $D(\omega)$ in (4.16). The shift in frequency for a photon undergoing Compton scattering determines that diffusion constant as the conditional average squared shift

$$D(\omega) = \left\langle \frac{(\omega' - \omega)^2}{2\tau} \,\middle|\, \omega \right\rangle \tag{4.18}$$

The shift follows from the well-known Compton scattering formula [107]

$$\omega' - \omega = \frac{c\mathbf{p}\cdot(\hat{\mathbf{n}}' - \hat{\mathbf{n}}) - \hbar\omega(1 - \hat{\mathbf{n}}\cdot\hat{\mathbf{n}}')}{\gamma m_e c^2\,[1 - \mathbf{p}\cdot\hat{\mathbf{n}}'/\gamma m_e c + (\hbar\omega/\gamma m_e c^2)(1 - \hat{\mathbf{n}}\cdot\hat{\mathbf{n}}')]}\,\omega \tag{4.19}$$

where the electron momentum is $\mathbf{p}$, γ is the relativistic factor and $\hat{\mathbf{n}}' - \hat{\mathbf{n}}$ is the scattering vector. In the low-temperature regime where Compton scattering is relevant, under the assumption that the electrons and the photons are of comparable energy much less than $m_e c^2$, most of the momentum is carried by the electrons, meaning $|\mathbf{p}| \gg \omega/c$. Hence we can replace the term between the brackets in the denominator by unity, and only retain the first term in the numerator in (4.19)

$$\omega' - \omega \approx \frac{\mathbf{p}\cdot(\hat{\mathbf{n}}' - \hat{\mathbf{n}})}{m_e c}\omega \tag{4.20}$$

We can assume the square of projection of the scattering vector $\hat{\mathbf{n}}' - \hat{\mathbf{n}}$ on the momentum vector $\mathbf{p}$ to average out to a constant of magnitude 1, which we will hereafter ignore. Continuing then the calculation for (4.18) yields

$$D \propto \left\langle \frac{|\mathbf{p}|^2}{2m_e^2 c^2}\frac{\omega^2}{\tau} \right\rangle = \frac{1}{m_e c^2}\left\langle \frac{|\mathbf{p}|^2}{2m_e} \right\rangle \frac{\omega^2}{\tau} \propto \frac{k_B T}{m_e c^2}\frac{\omega^2}{\tau} \tag{4.21}$$

where the temperature T gives the average kinetic energy of the electron distribution. We thus recover the first equality in (4.17).

For better understanding and comparison, we add here the heuristics of the opposite situation where we consider an electron in a photon bath (in contact with other matter at temperature T). Since the electronic density of states goes as the square root of the energy E, we must have an equation for the number $\mathcal{N}(\mathcal{E}, \sqcup)$ of electrons of the form

$$\frac{\partial \mathcal{N}}{\partial t}(E,t) = \frac{1}{E^{1/2}}\frac{\partial}{\partial E}E^{1/2}\, j_t(E) \tag{4.22}$$

to be compared with (4.2). To determine the current $j_t(E)$ we remember that a crucial property of the Doppler effect, used to compute (4.18) and to arrive at (4.17), is that the shift in frequency is linear in the frequency itself, as seen in (4.20). Here however, because the shift in the electron's energy equals the same expression, the average squared energy shift is proportional to the square of the momentum instead, hence only linear in the energy. That allows us to write down the electronic version of the Kompaneets equation immediately

$$E^{1/2}\,\frac{\partial \mathcal{N}}{\partial t}(E,t) = b\,\frac{\partial}{\partial E}E^{3/2}\left\{k_B T\frac{\partial \mathcal{N}}{\partial E}(E,t) + \mathcal{N}(E,t)\right\} \tag{4.23}$$

for some rate $b \propto c\sigma_T \frac{U_\gamma}{m_e c^2}$, where U_γ is the energy density of the photon gas. Note finally that we neglect the fermionic nature of the electron, since we presume non-degeneracy of the electron gas (not having thus the fermionic version of stimulated emission). For verification, a derivation of this equation can be found in [86]. For applications to highly dense states of fermionic matter, the Pauli exclusion is significant and departures from (4.23) are expected. In such a regime however, the long-range Coulomb interactions become relevant and an extra term must be added to the Boltzmann equation (4.23) anyway.

4.4 The Boltzmann-Master equation

The Master equation (4.7) only involves the photon occupation and the electron bath is integrated out and remains present only via the bath temperature. Similarly, the dynamics (4.10) effectively treats the electron bath via temperature, mobility and possible driving f. To go back one (finer) level of description, we must introduce the integration step. Here we start from a Master equation jointly for electrons and photons. Formally, it has the general structure[2],

$$\frac{\partial n}{\partial t}(\mathbf{p},\mathbf{k};t) = \int \mathrm{d}^3\mathbf{p}'\;\mathrm{d}^3\mathbf{k}'\;\{n(\mathbf{p}',\mathbf{k}';t)w(p',k'\to p,k)(1+n(\mathbf{k},t)) \\ -n(\mathbf{p},\mathbf{k};t)w(p,k\to p',k')(1+n(\mathbf{k}',t))\} \tag{4.24}$$

for the joint occupation $n(\mathbf{p},\mathbf{k};t)$ at time t of electron momentum $\mathbf{p}$ and photon wave vector $\mathbf{k}$. The four-momenta participating in the transition are, of course, given by

$$p^{(\prime)} = \left(\frac{E}{c}^{(\prime)}, \mathbf{p}^{(\prime)}\right) \quad \text{and} \quad k^{(\prime)} = \left(\frac{\hbar\omega}{c}^{(\prime)}, \mathbf{k}^{(\prime)}\right)$$

[2]From here we make a distinction between the vectors $\mathbf{p}$ etc. and the four-vectors p.

We added the stimulated emission in terms of the photon occupation $n(\mathbf{k}', t)$, but include no such factor for the electrons, assuming them to be nondegenerate (dilute). The transition rates should be obtained from the microscopic process of interaction, here Compton scattering, but we write generally

$$w(p, k \to p', k') \, \mathrm{d}^3\mathbf{p}' \, \mathrm{d}^3\mathbf{k}' = \frac{\mathrm{d}\sigma}{\mathrm{d}\Omega}(\mathbf{p}, \mathbf{k}) \, \mathrm{d}\Omega \, c \left(1 - \frac{\mathbf{v}}{c} \cdot \hat{\mathbf{n}}\right) \tag{4.25}$$

for a differential cross section $\frac{\mathrm{d}\sigma}{\mathrm{d}\Omega}$, where the equality holds in the sense of distributions. The factor $c(1-\mathbf{v}/c\cdot\hat{\mathbf{n}})$ is commonly called the *Møller velocity* and it is necessary for a consistent microscopic description [35, 31, 175]. Neglecting that factor is a common inaccuracy in the literature, e.g. [86, 38, 170]. Viewed nonrelativistically it corresponds to the relative velocity between the electrons and the photons, but even with a proper relativistic treatment, where the relative velocity is of course c in every frame, this exact factor will show in the colliding flux density [167].

We want (4.24) to correspond to a Boltzmann equation where the total number of electrons and photons is conserved. It suffices here to invoke dynamical reversibility in the form

$$w(p, k \to p', k') = w(p', k' \to p, k) \tag{4.26}$$

which means that the rate function[3] is symmetric. Moreover, if we assume that the electron gas evolves on much shorter time-scales than the photons, we can suppose to two distributions are uncorrelated, allowing us to write

$$n(\mathbf{p}, \mathbf{k}; t) = \mathcal{N}(\mathbf{p}) \, n(\mathbf{k}, t),$$

where $\mathcal{N}(\mathbf{p})$ is the momentum distribution of the electrons, which need not necessarily be in thermal equilibrium. We also assume isotropy so that the above leads to the writing of the Boltzmann-type equation:

$$\frac{\partial n}{\partial t}(\omega) = \int \mathrm{d}^3\mathbf{p} \, \mathrm{d}w \, [n(\omega')\mathcal{N}(\mathbf{p}')(1 + n(\omega)) - n(\omega)\mathcal{N}(\mathbf{p})(1 + n(\omega'))] \tag{4.27}$$

where $\mathrm{d}w = \mathrm{d}\sigma \, c(1 - \mathbf{v}/c \cdot \hat{\mathbf{n}}), \mathrm{d}\sigma = \frac{\mathrm{d}\sigma}{\mathrm{d}\Omega} \, \mathrm{d}\Omega$ stands for the (unspecified for the moment) scattering cross section multiplied with the incoming flux of electrons. The scattering is subject to conservation of energy-momentum corresponding to the collision scheme

$$(p \, , \, k) \rightleftharpoons (p' \, , \, k')$$

[3]To be consistent with literature, we note here that $w(p, k \to p', k')$ defined as such is called the *non-covariant transition rate*. The *covariant transition rate* $W(p, k \to p', k')$ is defined such that $w(p, k \to p', k') = \frac{W(p, k \to p', k')}{E E' \hbar\omega \hbar\omega'}$

which means a transition of wave vectors and corresponding frequencies

$$\mathbf{k} \rightleftharpoons \mathbf{k}^{'}, \quad \omega = c|\mathbf{k}| \rightleftharpoons \omega' = c|\mathbf{k}'| \tag{4.28}$$

for the photon. The first term on the right-hand side of (4.27) is the source term where photons with frequency ω are created from collisions with electrons with momentum $\mathbf{p}'$, and the second term is the sink term where photons with frequency ω collide with electrons of momentum $\mathbf{p}$. In that case, the equation (4.27) is rewritable indeed as a Master (rate) equation and is really the more precise version of Eq. 1 in [99].

We can integrate out the electron bath to find the rates involving only the photons

$$w(k' \to k) = \int \mathrm{d}^3\mathbf{p}\ \mathrm{d}^3\mathbf{p}'\, w(p', k' \to p, k)\mathcal{N}(\mathbf{p}'). \tag{4.29}$$

Invoking the reversibility (4.26) of the rates, $w(p', k' \to p, k) = w(p, k \to p', k')$, we continue by writing down the inverse rates

$$w(k \to k') = \int \mathrm{d}^3\mathbf{p}\ \mathrm{d}^3\mathbf{p}'\, w(p', k' \to p, k)\mathcal{N}(\mathbf{p}')\frac{\mathcal{N}(\mathbf{p})}{\mathcal{N}(\mathbf{p}')} \tag{4.30}$$

To connect this to the setup in Section 4.2, we have to further include the assumption that the electrons are in thermal equilibrium with inverse temperature $\beta = 1/k_B T$, which implies that

$$\frac{\mathcal{N}(\mathbf{p})}{\mathcal{N}(\mathbf{p}')} = e^{-\beta(E-E')} = e^{-\beta(\hbar\omega' - \hbar\omega)}, \tag{4.31}$$

where the last equality follows from conservation of energy in the collisions. Inserting (4.31) into (4.30) yields the detailed balance relation for the photon transition rates (4.29),

$$\frac{w(k' \to k)}{w(k \to k')} = e^{-\beta(\hbar\omega - \hbar\omega')}.$$

4.5 Diffusion approximation to the Boltzmann Equation

The previous section shows how the kinetic equation which correctly introduces the Compton scattering between the electrons (making the steady thermal bath) and the photons gives rise to a Master equation as treated in Section 4.2.

From there, as shown in Section 4.3, the Kompaneets equation can be obtained. In the present section, we take the two steps together and directly apply the diffusion approximation to the Boltzmann equation. It is much closer to the published approaches and it gives us the opportunity to clarify a number of points which traditionally are left to the reader. In particular, our framework is more direct than [99, 144, 55, 179] because we do not *use* (in the derivation itself) that the Planck distribution is the stationary solution of (4.27). Under certain conditions on the possible cross sections, Escobedo and Mischler [59] rigorously prove the diffusion approximation to the Boltzmann equation in the context of an electron-photon gas. However, they do not explicitly link these conditions to the Thomson/Klein-Nishina cross section nor do they address the same problems we treat here.

We begin with (4.27) where $\mathrm{d}w = \mathrm{d}\Omega\, c\left(1 - \frac{\mathbf{v}}{c}\cdot\hat{\mathbf{n}}\right)\frac{\mathrm{d}\sigma}{\mathrm{d}\Omega}(\mathbf{p},\hat{\mathbf{n}},\Omega)$ and

$$\begin{aligned}\frac{\mathrm{d}\sigma}{\mathrm{d}\Omega}(\mathbf{p},\hat{\mathbf{n}},\Omega) =& \frac{3\sigma_T}{16\pi}\frac{1}{\gamma^2\left(1-\mathbf{p}\cdot\hat{\mathbf{n}}'/\gamma m_e c + \frac{\hbar\omega}{\gamma m_e c^2}(1-\hat{\mathbf{n}}\cdot\hat{\mathbf{n}}')\right)^2}\times \\ & \left\{1 + \frac{(\frac{\hbar\omega}{\gamma m_e c^2}(1-\hat{\mathbf{n}}\cdot\hat{\mathbf{n}}'))^2}{(1-\mathbf{p}\cdot\hat{\mathbf{n}}'/\gamma m_e c)(1-\mathbf{p}\cdot\hat{\mathbf{n}}'/\gamma m_e c + \frac{\hbar\omega}{\gamma m_e c^2}(1-\hat{\mathbf{n}}\cdot\hat{\mathbf{n}}'))}\right. \\ & \left. + \left(1 - \frac{(1-\hat{\mathbf{n}}\cdot\hat{\mathbf{n}}')}{\gamma^2(1-\mathbf{p}\cdot\hat{\mathbf{n}}/\gamma m_e c)(1-\mathbf{p}\cdot\hat{\mathbf{n}}'/\gamma m_e c))}\right)^2\right\} \quad (4.32)\end{aligned}$$

as the (correct) Klein-Nishina expression for the cross section. This expression appears in [8], but a derivation is not shown there. Jauch and Rohrlich [88] give a detailed derivation, but only express the differential cross section in terms of the scattering matrix. As we could not find any reference which contains the exact frame-independent expression for the Klein-Nishina cross section given above we will devote Appendix 4.B to this discussion. However, we also note here that once established the correct (and not so enlightening) expression above, we only need the first few orders of its expansion. As before, we keep in mind the collision scheme

$$\mathbf{p} + \frac{\hbar\omega}{c}\hat{\mathbf{n}} \rightleftharpoons \mathbf{p}' + \frac{\hbar\omega'}{c}\hat{\mathbf{n}}'$$

where we now express the wave vector as $\mathbf{k} = \frac{\hbar\omega}{c}\hat{\mathbf{n}}$, defining the scattering angle $\cos\theta = \hat{\mathbf{n}}\cdot\hat{\mathbf{n}}'$.

We follow the usual steps, assuming that: (i) the electrons are in thermal equilibrium at temperature T; (ii) the photons are soft, meaning that their

energy is very small compared to the rest energy of the electron ($\hbar\omega \ll m_e c^2$), but of same order of the electron bath energy ($\hbar\omega \sim k_B T$) ; (iii) electrons are nonrelativistic ($|\mathbf{p}| \ll m_e c$ or $k_B T \ll m_e c^2$). By combining (ii) and (iii) we conclude also that energy is transferred in small amounts only, permitting the continuum (or diffusion) approximation (and in fact, the transfer of energy depends both on the incoming ω and $\mathbf{p}$ as dictated by the Compton formula and, to the lowest order, it is proportional to the product of both (4.20)).
Points (ii) and (iii) suggest an expansion in terms of the energy shift, as proposed originally by Kompaneets [99]. For this purpose we define

$$\Delta = \frac{\hbar(\omega' - \omega)}{k_B T}$$

By looking at the Compton shift (4.19), we have

$$\Delta(\omega, \mathbf{p}) = \frac{\hbar\omega}{k_B T} \frac{c\mathbf{p}\cdot(\hat{\mathbf{n}}' - \hat{\mathbf{n}}) - \hbar\omega(1 - \hat{\mathbf{n}}\cdot\hat{\mathbf{n}}')}{\gamma m_e c^2 \left[1 - \mathbf{p}\cdot\hat{\mathbf{n}}'/\gamma m_e c + (\hbar\omega/\gamma m_e c^2)(1 - \hat{\mathbf{n}}\cdot\hat{\mathbf{n}}')\right]} \tag{4.33}$$

We refer the reader to [88] for more discussion of expressions (4.32) and (4.33).

Let us now go back to (4.27) to make an expansion up to second order in $\Delta(\omega, \mathbf{p})$, mimicking the Kramers-Moyal expansion of Section 4.3. We make the natural change of variables

$$\omega \to x = \frac{\hbar\omega}{k_B T}$$

$$\omega' \to x' = \frac{\hbar\omega'}{k_B T}$$

to write the photon numbers up to second order as

$$n(x', t)(1 + n(x, t)) =$$

$$n(x, t)(1 + n(x, t)) + (1 + n(x, t))\frac{\partial n}{\partial x}\,\Delta + (1 + n(x, t))\frac{\partial^2 n}{\partial x^2}\,\frac{\Delta^2}{2} \tag{4.34}$$

$$n(x, t)(1 + n(x', t)) =$$

$$n(x, t)(1 + n(x, t)) + n(x, t)\frac{\partial n}{\partial x}\,\Delta + n(x, t)\frac{\partial^2 n}{\partial x^2}\,\frac{\Delta^2}{2} \tag{4.35}$$

From (i) above, the electron distribution is Maxwellian at temperature T,

$$\mathcal{N}(\mathbf{p})\,\mathrm{d}^3\mathbf{p} = \mathcal{N}_{\mathrm{eq}}(|\mathbf{p}|)\,\mathrm{d}^3\mathbf{p} = n_e(2\pi m_e k_B T)^{-3/2}\exp\left(-\frac{p_x^2+p_y^2+p_z^2}{2m_e k_B T}\right)\mathrm{d}^3\mathbf{p} \tag{4.36}$$

where n_e is the electron density. Using conservation of energy

$$E' = E - \Delta\ k_B T$$

we get

$$\mathcal{N}_{\mathrm{eq}}(|\mathbf{p}'|) = \mathcal{N}_{\mathrm{eq}}(|\mathbf{p}|)\left(1+\Delta+\frac{\Delta^2}{2}\right) \tag{4.37}$$

By taking (4.34)–(4.35) and (4.37) in (4.27), we obtain

$$\frac{\partial n}{\partial t} = [\partial_x n + n(1+n)]\,I_1 + \left[\frac{1}{2}\partial_{xx} n + (1+n)\left(\frac{n}{2}+\partial_x n\right)\right] I_2 \tag{4.38}$$

where, with $\ell = 1, 2$,

$$I_\ell(x) = c\int \mathrm{d}^3\mathbf{p}\ \mathrm{d}\Omega\left(1-\frac{\mathbf{v}}{c}\cdot\hat{\mathbf{n}}\right)\frac{\mathrm{d}\sigma}{\mathrm{d}\Omega}(\mathbf{p},\hat{\mathbf{n}},\Omega)\,\mathcal{N}_{\mathrm{eq}}(|\mathbf{p}|)\Delta^\ell \tag{4.39}$$

The computation of the integrals $I_1(x)$ and $I_2(x)$ is presented in Appendices 4.C.1 and 4.C.2, with results

$$I_1(x) = \frac{n_e\sigma_T c\,k_B T}{m_e c^2}\ x(4-x) \tag{4.40}$$

$$I_2(x) = \frac{n_e\sigma_T c\,k_B T}{m_e c^2}\ 2x^2 \tag{4.41}$$

After standard manipulations, we end up with the Kompaneets equation

$$\frac{\partial n}{\partial t}(x,t) = \frac{n_e\sigma_T c\,k_B T}{m_e c^2}\frac{1}{x^2}\partial_x\left\{x^4(\partial_x n(x,t) + n(x,t)(1+n(x,t)))\right\} \tag{4.42}$$

which is (4.1).

As already mentioned, the common setup in the literature is to consider the Thomson cross section (4.4) *only*, without the Møller velocity factor

$$c\left(1-\frac{\mathbf{v}}{c}\cdot\hat{\mathbf{n}}\right)$$

to compute $I_2(x)$; the value of $I_1(x)$ is then obtained from assuming that (4.38) must be a continuity equation, with the current vanishing in equilibrium for

the Planck distribution. However, when using the Thomson cross section *only* one finds (see Appendix 4.C.3 for the computation of the integrals in this case)

$$I_1^{\mathrm{Th}}(x) = \frac{n_e \sigma_T c\, k_B T}{m_e c^2} x(1-x) \tag{4.43}$$

instead of (4.40). To the best of our knowledge that first Kompaneets integral was never computed. As a matter of logic, as we have seen in the previous section, it is not possible with solely the Thomson cross section (which ultimately leads to (4.43)) to find (4.42). The Møller velocity factor must be included in the definition of the rates, otherwise consistency in the microscopic description of the collision term is lost. This term naturally appears when carefully deriving (4.27), see [35], or when going from the covariant description to the non-covariant one, [175]. As mentioned, this term is also needed to yield conservation of the photon number, but what is surprising perhaps, is that none of these effects are seen on $I_2(x)$, whence making it possible to employ the traditional indirect argument used traditionally (including in Kompaneets' original paper) to fix the value of $I_1(x)$.
It is possible in the derviation of the Kompaneets equation to use the Thomson cross section together with the Møller factor (of course) as it satisfies dynamical reversibility as well[4]. Note however that upon writing (4.4) we are fixing the electron rest frame and, thus, all quantities must be expressed in this frame of reference (including the distribution functions). The diffusion approximation and the integrals must also be performed in this frame. We can avoid this complication by expressing the cross section in a frame-independent manner, just as (4.32). In that way we have the freedom to work with the Boltzmann equation (4.27) in the most convenient frame of reference[5] (where the electron distribution is isotropic Maxwellian). We could not find in the literature any frame-independent version of the Thomson cross section, neither a mention of such features which are so important to yield a consistent diffusion approximation.

Traditionally, equation (4.27) is called the *non-covariant Boltzmann equation* and while a fully covariant Boltzmann equation does indeed exist, we have chosen to not express it here. However, we invite the reader to check, for example, [175, 25] for the covariant formalism. These two versions are equivalent to each other, provided that we use the rates (4.25) to connect them. On the other hand, once the link is established, we can regard the Kompaneets equation as the nonrelativistic limit of either Boltzmann equation, which here is concretely

[4] In fact, any cross section which is obtained from an unitary scattering matrix yields dynamical reversibility; see [175] for a proof.

[5] *Non-covariance* should not be confused with *frame-independence*. (4.27) is an example of a non-covariant equation which is written in a frame-independent way.

realized as the second-order expansion in the energy shift, as expressed in the integrals (4.40) and (4.41). In this more kinematic approach, the interpretation of both integrals above is clear as the average shift and shift-squared of the energy, while in covariant approaches[6] the interpretation is not always straightforward. Derivations of the Kompaneets equation which proceed in a covariant manner include [25, 84, 44]. The covariant derivation is simpler in the sense that the main ingredient is the microscopic reversibility of the rates, in the spirit of Sections 4.2–4.3. The problems we mention above are taken care of automatically then. For example, using the scattering matrix gives the Møller prefactor and consistency of the different reference frames (since the quantities are always expressed in a Lorentz invariant way). In [36], Challinor and Lasenby managed to identify the moments of the shift (as above) in a covariant approach, and that was repeated later in [84]. Yet, in the integrals, the moments are still multiplied by a Dirac delta, which leaves open the exact analytical computation.

4.6 Extending the Kompaneets equation

There are various well-known extensions of the Kompaneets equation compared to what was mainly discussed in the previous sections. For example, the condition that the photons are soft, *i.e.*, $\hbar\omega \sim k_B T$ may be relaxed provided that we treat the regime $\hbar\omega \gg k_B T$ (hard photons) explicitly in the diffusion approximation to the Boltzmann equation. An extra contribution is found then in (4.1), referred to as the "extended Kompaneets equation to down-Comptonization" [181, 105]. The regime of down-Comptonization first appeared in [140] in the so-called Ross-McCray equation, where radiative transfer of X-ray photons is treated. The equation derived in [140], however, does not yield the Bose-Einstein distribution as stationary solution and should be regarded only as an asymptotic limit of such extended Kompaneets equation.

There are more and different processes in astrophysical plasmas that change the photon occupation number. Beyond Compton scattering, contributions due to (for example) *Bremsstrahlung* (involving the ions as well) and radiative (or double) Compton scattering may be considered, [99, 83, 107, 144]. Due to the radiative nature of such processes it is not true any longer that the photon number is conserved and we cannot describe them by a Master-Boltzmann equation.

Relativistic extensions to the Kompaneets equation and calculations done in the covariant Boltzmann description include [25, 84, 85, 44, 122, 124, 123]. Barbosa

[6]For simplicity, we call any derivation of the Kompaneets equation starting from the covariant Boltzmann equation a *covariant approach/derivation*. Strictly speaking, the use of the word *covariant* is not entirely correct because when assuming isotropy to carry the diffusion approximation, one is fixing the reference frame, thus breaking covariance.

[8] also addresses relativistic extensions, but using a more kinematic approach to the Fokker-Planck approximation.
Pitrou [135] and Buet *et al* [27] both deal with anistropic extensions to the Kompaneets equation, where the assumption of isotropy in the distribution functions is no longer required. More general solutions to (4.1) can be found in [45, 118]. More recently, the diffusion approximation as proposed by Kompaneets is applied to a neutrino gas [166, 177].
For applying the Kompaneets equation in the context of cosmology, the contribution of the cosmic expansion (red shift) must be taken into consideration. In [83, 137, 29, 11], that contribution appears as a convective term in the Boltzmann equation (4.27). A turbulent Doppler shift (as an integrated Sachs-Wolfe effect for a random gravitational potential field) would give an additional diffusion in frequency but we have not seen that being worked out.

Let us now turn to less standard generalizations. Recall that we have already derived an extended Kompaneets equation in (4.16) for bosons with energy U and possibly driven by the "force" f. Here we continue with a modification and two extra constraints where the electron bath need not be in equilibrium. As already pointed out in [8, 25, 24, 129], Kompaneets equation can indeed be recovered for an electron bath which is not in equilibrium, provided that the distribution of the electrons is isotropic, *i.e.*, that the distribution can be written in terms of the energy. Although some references already considered this fact by using different approaches, including [8, 25], we could not find references which conclude the same while starting from the non-covariant kinetic equation (4.27). The details of such a derivation are given in Appendix 4.C.4. By assuming: (i) isotropy of the distribution of the electrons,

$$\mathcal{N}(\mathbf{p},t)\,\mathrm{d}^3\mathbf{p} = \mathcal{N}(|\mathbf{p}|,t)\,\mathrm{d}^3\mathbf{p} \tag{4.44}$$

and (ii) that $\mathcal{N}$ decays faster than $|\mathbf{p}|^3$, *i.e.*,

$$\lim_{|\mathbf{p}|\to\infty} |\mathbf{p}|^3\mathcal{N}(|\mathbf{p}|,t) = 0 \tag{4.45}$$

we find Kompaneets equation (4.42) with an effective temperature

$$T_{\text{eff}} = \frac{\langle|\mathbf{p}|^2\rangle}{3k_B m_e}$$

where

$$n_e\,\langle|\mathbf{p}|^2\rangle = \int \mathrm{d}^3\mathbf{p}\,|\mathbf{p}|^2\,\mathcal{N}(|\mathbf{p}|)$$

Note that it is not so strange to recover the equilibrium (relaxation to) Planck distribution in the diffusion approximation. It only means that nonequilibrium features hide in higher order approximations. As possible scenarios for generating

nonequilibrium effects, we may have in mind gravitational sources (still largely unspecified) or the possible presence of (turbulent) magnetic fields driving the electrons.

4.7 Conclusions and outlook

Relaxation to quantum equilibrium distributions is a topic of much current interest. In that spirit, the Kompaneets equation for the Comptonization of photons in an electron bath is one of the few examples where a diffusion approximation to the Boltzmann equation can be explicitly done, in such way that we found useful to revisit its derivation.

First, we connected the derivation with statistical mechanical setups, known for example as Kramers-Moyal expansion and clarified a number of points related to the importance of using the physically correct scattering cross sections together with an *ab initio* correct Boltzmann equation (4.27). We explored and stressed many features which are absent or commonly neglected in literature, such as the appearance of the Møller velocity in the Boltzmann collision term.

Secondly, the re-derivations in the present paper may serve as useful point of departure to understand modifications and nonequilibrium corrections to the Planck law. Indeed, one of the goals of the present paper has been to derive the Kompaneets equation without resorting to the Kompaneets' approach based on the current vanishing at equilibrium. We found that diffusion in frequency space, with drift determined by exchanges in energy and possibly nonconservative processes combined with stimulated emission, leads to an extension of the Kompaneets equation. Such extensions will be used in future work to motivate specific low-frequency modifications to the Planck law, following the scenario and motivation in [6].

4.A Expansion of the transition rates

The transition rates (4.10) can be expanded from

$$w(x, x \pm \delta) = \left(1 + n \pm \delta n' + \frac{\delta^2}{2} n''\right) \times \left(B \pm \frac{\delta}{2} B' + \frac{\delta^2}{8} B''\right) \exp\left\{-\frac{\beta}{2}\left(\pm\delta(U' - f) + \frac{\delta^2}{2}(U'' - f')\right)\right\}$$

$$w(x \pm \delta, x) = (1+n) \times$$

$$\left(B \pm \frac{\delta}{2}B' + \frac{\delta^2}{8}B''\right) \exp\left\{\frac{+\beta}{2}\left(\pm\delta(U'-f) + \frac{\delta^2}{2}(U''-f')\right)\right\}$$

An expansion up to second order in δ yields

$$w(x, x \pm \delta) = A(x) \pm \frac{\delta}{2}C(x) + \frac{\delta^2}{2}E(x) \tag{4.46}$$

$$w(x \pm \delta, x) = A(x) \pm \frac{\delta}{2}F(x) + \frac{\delta^2}{2}G(x) \tag{4.47}$$

with short-hands

$$A(x) = B(1+n)$$

$$C(x) = 2Bn' - (\beta Bg - B')(1+n)$$

$$E(x) = \left(\frac{1}{4}(\beta^2 Bg^2 + B'') - \frac{1}{2}(\beta g B' + \beta g' B)\right)(1+n) - (\beta Bg - B')n' + Bn''$$

$$F(x) = (\beta Bg + B')(1+n)$$

$$G(x) = \left(\frac{1}{4}(\beta^2 Bg^2 + B'') + \frac{1}{2}(\beta g B' + \beta g' B)\right)(1+n)$$

$$g(x) = U'(x) - f(x)$$

That gives to leading order in the Master equation

$$\partial_t n = \delta^2 \left\{(G(x) - E(x))n(x) + F(x)\partial_x n(x) + A(x)\partial_{xx} n(x)\right\} \tag{4.48}$$

Substituting the short-hands we get (4.12).

4.B Klein-Nishina differential cross section

As before, let us suppose a collision process given by

$$(p, k) \leftrightharpoons (p', k')$$

with four-momenta

$$p^{(\prime)} = \left(\frac{E}{c}^{(\prime)}, \mathbf{p}^{(\prime)}\right) \quad \text{and} \quad k^{(\prime)} = \left(\frac{\hbar\omega}{c}^{(\prime)}, \mathbf{k}^{(\prime)}\right)$$

we fix our metric tensor to diag$(-+++)$ and use the same notation as Jauch and Rohrlich [88]. For convenience, we will use natural units ($\hbar = c = 1$), which will be restored later in (4.32). The total Klein-Nishina cross section for Compton scattering is obtained directly from the trace of the scattering matrix (the scattering amplitude), which is given by

$$\sigma = \frac{1}{-p' \cdot k'} \frac{1}{E'\omega'} \frac{3\sigma_T}{16\pi} \int \mathrm{d}^3\mathbf{p}' \, \mathrm{d}\omega' \, \mathrm{d}\Omega \omega'^2 \delta^{(4)}(p' + k' - p - k) \overline{X} \tag{4.49}$$

where $\overline{X}$ is the scattering amplitude. For a proof of this relation we refer the reader to [88, 155, 119]. By differentiating with respect to the solid angle and using the Fundamental Theorem of Calculus we obtain the differential cross section

$$\frac{\mathrm{d}\sigma}{\mathrm{d}\Omega} = \frac{1}{-p' \cdot k'} \frac{1}{E'\omega'} \frac{3\sigma_T}{16\pi} \int \mathrm{d}^3\mathbf{p}' \, \mathrm{d}\omega' \omega'^2 \delta^{(4)}(p' + k' - p - k) \overline{X}$$

this is the frame-independent representation of the differential cross section, where the frame-independent representation of the scattering angle is given by $\cos\theta = \hat{\mathbf{n}} \cdot \hat{\mathbf{n}'}$. By evaluating the integrals we get the following expression for the Klein-Nishina differential cross section

$$\frac{\mathrm{d}\sigma}{\mathrm{d}\Omega} = \frac{3\sigma_T}{16\pi} \left(\frac{\omega'}{\omega}\right)^2 \frac{1}{\gamma^2(1 - \boldsymbol{\beta} \cdot \hat{\mathbf{n}})^2} \overline{X} \tag{4.50}$$

where $\boldsymbol{\beta} = \mathbf{v}/c$ (or $\mathbf{v}$ in natural units). The outgoing photon frequency ω' is dependent from the ingoing frequency by the Compton shift (4.19), which can be expressed in the following way

$$\frac{\omega'}{\omega} = \frac{1 - \boldsymbol{\beta} \cdot \hat{\mathbf{n}}}{1 - \boldsymbol{\beta} \cdot \hat{\mathbf{n}}' + \frac{\omega}{E}(1 - \hat{\mathbf{n}} \cdot \hat{\mathbf{n}}')} \tag{4.51}$$

The scattering amplitude is given by

$$\overline{X} = \frac{p \cdot k}{p \cdot k'} + \frac{p \cdot k'}{p \cdot k} + 2\left(\frac{m^2}{p \cdot k'} - \frac{m^2}{p \cdot k}\right) + \left(\frac{m^2}{p \cdot k'} - \frac{m^2}{p \cdot k}\right)^2 \tag{4.52}$$

Substitute (4.51) in (4.50) to yield

$$\frac{\mathrm{d}\sigma}{\mathrm{d}\Omega} = \frac{3\sigma_T}{16\pi} \left[\frac{1}{\gamma(1 - \boldsymbol{\beta} \cdot \hat{\mathbf{n}}' + \frac{\omega}{E}(1 - \hat{\mathbf{n}} \cdot \hat{\mathbf{n}'}))}\right]^2 \overline{X} \tag{4.53}$$

In (4.52), using $p \cdot k^{(\prime)} = -E\omega^{(\prime)}(1 - \boldsymbol{\beta} \cdot \hat{\mathbf{n}}^{(\prime)})$ we have

$$\frac{p \cdot k}{p \cdot k'} + \frac{p \cdot k'}{p \cdot k} = 1 + \frac{\omega(1 - \hat{\mathbf{n}} \cdot \hat{\mathbf{n}}')}{E(1 - \boldsymbol{\beta} \cdot \hat{\mathbf{n}'})} + \frac{1 - \boldsymbol{\beta} \cdot \hat{\mathbf{n}}'}{1 - \boldsymbol{\beta} \cdot \hat{\mathbf{n}} + \frac{\omega}{E}(1 - \hat{\mathbf{n}} \cdot \hat{\mathbf{n}}')}$$

$$\frac{m^2}{p \cdot k'} - \frac{m^2}{p \cdot k} = -\frac{1 - \hat{\mathbf{n}} \cdot \hat{\mathbf{n}}'}{\gamma^2(1 - \boldsymbol{\beta} \cdot \hat{\mathbf{n}})(1 - \boldsymbol{\beta} \cdot \hat{\mathbf{n}}')}$$

Substituting both expressions into (4.52) yields

$$\overline{X} = 1 + \left[1 - \frac{(1 - \hat{\mathbf{n}} \cdot \hat{\mathbf{n}}')}{\gamma^2(1 - \boldsymbol{\beta} \cdot \hat{\mathbf{n}})(1 - \boldsymbol{\beta} \cdot \hat{\mathbf{n}}')}\right]^2 + \frac{\omega^2(1 - \hat{\mathbf{n}} \cdot \hat{\mathbf{n}}')^2}{E^2(1 - \boldsymbol{\beta} \cdot \hat{\mathbf{n}}')(1 - \boldsymbol{\beta} \cdot \hat{\mathbf{n}}' + \frac{\omega}{E}(1 - \hat{\mathbf{n}} \cdot \hat{\mathbf{n}}'))} \quad (4.54)$$

Putting back (4.54) into (4.53) we use

$$\boldsymbol{\beta} = \frac{\mathbf{p}}{E}$$

to yield the frame-independent representation of the Klein-Nishina cross section (4.32).

4.C Computation of integrals

4.C.1 Integral I_1

We compute

$$I_1(x) = c \int \mathrm{d}^3\mathbf{p}\ \mathrm{d}\Omega \left(1 - \frac{\mathbf{v}}{c} \cdot \hat{\mathbf{n}}\right) \frac{\mathrm{d}\sigma}{\mathrm{d}\Omega}(\mathbf{p}, \hat{\mathbf{n}}, \Omega)\mathcal{N}_{\mathrm{eq}}(|\mathbf{p}|)\Delta \quad (4.55)$$

In what follows we omit the dependencies on the variables for simplicity. The leading order is the second on the electron momenta and the expansion yields

$$\frac{16\pi}{3\sigma_T}\left(1 - \frac{\mathbf{p} \cdot \hat{\mathbf{n}}}{\gamma m_e c}\right)\frac{\mathrm{d}\sigma}{\mathrm{d}\Omega}\Delta = \frac{x\mathbf{p} \cdot (\hat{\mathbf{n}}' - \hat{\mathbf{n}})}{m_e c}(1 + \cos^2\theta) - \frac{x^2 k_B T}{m_e c^2}(1 - \cos\theta)(1 + \cos^2\theta) + \frac{x}{(m_e c)^2}\Big\{(1 + 2\cos\theta - \cos^2\theta)(\mathbf{p} \cdot \hat{\mathbf{n}})^2 + (3 - 2\cos\theta + 5\cos^2\theta)(\mathbf{p} \cdot \hat{\mathbf{n}}')^2 - 4(\mathbf{p} \cdot \hat{\mathbf{n}})(\mathbf{p} \cdot \hat{\mathbf{n}}')(1 + \cos^2\theta)\Big\} \quad (4.56)$$

where we used that $\mathbf{p} = \gamma m_e\, \mathbf{v}$.

We first compute the integral over $\mathbf{p}$ in Cartesian coordinates, and then over the solid angle. Since the distribution is isotropic, the first part yields a zero contribution, *i.e.*,

$$\int \mathrm{d}^3\mathbf{p}\, \mathbf{p} \cdot (\hat{\mathbf{n}}' - \hat{\mathbf{n}})\mathcal{N}_{\mathrm{eq}}(|\mathbf{p}|) = 0 \quad (4.57)$$

The integral over the momentum in the second parcel is readily done, yielding

$$\int \mathrm{d}^3\mathbf{p}\,\mathcal{N}_{\mathrm{eq}}(|\mathbf{p}|) = n_e$$

where we used (4.36). Observe moreover

$$(\mathbf{p}\cdot\hat{\mathbf{n}})^2 = p_x^2 n_x^2 + p_y^2 n_y^2 + p_z^2 n_z^2 + \text{cross terms in coordinates (similarly for } \hat{\mathbf{n}}')$$

$$(\mathbf{p}\cdot\hat{\mathbf{n}})(\mathbf{p}\cdot\hat{\mathbf{n}}') = p_x^2 n_x n_x' + p_y^2 n_y n_y' + p_z^2 n_z n_z' + \text{similar to above}$$

Cross terms in the coordinates yield zero contribution for the same reason as (4.57). Squared terms give a similar contribution, being

$$\int \mathrm{d}^3\mathbf{p}\,(\mathbf{p}\cdot\hat{\mathbf{n}})^2\mathcal{N}_{\mathrm{eq}}(|\mathbf{p}|) = I\times\hat{\mathbf{n}}^2 = I$$

$$\int \mathrm{d}^3\mathbf{p}\,(\mathbf{p}\cdot\hat{\mathbf{n}}')^2\mathcal{N}_{\mathrm{eq}}(|\mathbf{p}|) = I\times\hat{\mathbf{n}'}^2 = I$$

$$\int \mathrm{d}^3\mathbf{p}\,(\mathbf{p}\cdot\hat{\mathbf{n}})(\mathbf{p}\cdot\hat{\mathbf{n}}')\mathcal{N}_{\mathrm{eq}}(|\mathbf{p}|) = I\times\hat{\mathbf{n}}\cdot\hat{\mathbf{n}}' = I\cos\theta$$

$$\text{with}\quad I = \int \mathrm{d}^3\mathbf{p}\,p_x^2\,\mathcal{N}_{\mathrm{eq}}(|\mathbf{p}|) = n_e m_e\,k_B T \tag{4.58}$$

Using all that in $I_1(x)$ gives

$$I_1(x) = c\frac{3\sigma_T}{16\pi}\frac{n_e k_B T}{m_e c^2}\left(-x^2+4x\right)\left\{2\pi\int_{-1}^{1} d\cos\theta(1-\cos\theta)(1+\cos^2\theta)\right\}$$

and since $\int_{-1}^{1} dy(1-y)(1+y^2) = 8/3$, we find as desired

$$I_1(x) = \frac{n_e\sigma_T c\,k_B T}{m_e c^2}\,x(4-x) \tag{4.59}$$

4.C.2 Integral I_2

We compute

$$I_2(x) = c\int \mathrm{d}^3\mathbf{p}\,\mathrm{d}\Omega\left(1-\frac{\mathbf{v}}{c}\cdot\hat{\mathbf{n}}\right)\frac{\mathrm{d}\sigma}{\mathrm{d}\Omega}(\mathbf{p},\hat{\mathbf{n}},\Omega)\mathcal{N}_{\mathrm{eq}}(|\mathbf{p}|)\Delta^2 \tag{4.60}$$

The expansion up to second order in the electron momentum yields

$$\frac{16\pi}{3\sigma_T}\left(1-\frac{\mathbf{p}}{\gamma m_e c}\cdot\hat{\mathbf{n}}\right)\frac{\mathrm{d}\sigma}{\mathrm{d}\Omega}\Delta^2 = \left(\frac{x}{m_e c}\right)^2(\mathbf{p}\cdot(\hat{\mathbf{n}}'-\hat{\mathbf{n}}))^2(1+\cos^2\theta) \tag{4.61}$$

Using the exact same strategy as before, we have

$$\int \mathrm{d}^3\mathbf{p}\,(\mathbf{p}\cdot(\hat{\mathbf{n}}'-\hat{\mathbf{n}}))^2\mathcal{N}_{\mathrm{eq}}(|\mathbf{p}|) = I\times(\hat{\mathbf{n}}'-\hat{\mathbf{n}})^2 = 2I(1-\cos\theta)$$

$$\text{with}\quad I=\int \mathrm{d}^3\mathbf{p}\,p_x^2\,\mathcal{N}_{\mathrm{eq}}(|\mathbf{p}|) = n_e m_e\,k_B T$$

This yields for $I_2(x)$

$$\begin{aligned} I_2(x) &= c\frac{3\sigma_T}{16\pi}\frac{n_e k_B T}{m_e c^2}2x^2\left\{2\pi\int_{-1}^{1} d\cos\theta(1-\cos\theta)(1+\cos^2\theta)\right\} \\ &= \frac{n_e\sigma_T c\,k_B T}{m_e c^2}2x^2 \end{aligned} \tag{4.62}$$

as desired.

4.C.3 The integrals and the Thomson cross section

We demonstrate here that the integrals computed using the Thomson cross section (4.4) solely (thus neglecting the Møller prefactor) cannot yield the Kompaneets equation.

We calculate

$$I_\ell^{\mathrm{Th}}(x) = c\int \mathrm{d}^3\mathbf{p}\;\;\mathrm{d}\Omega_{\mathrm{rest}}\frac{\mathrm{d}\sigma^{\mathrm{Th}}}{\mathrm{d}\Omega_{\mathrm{rest}}}\mathcal{N}_{\mathrm{eq}}(|\mathbf{p}|)\Delta^\ell \tag{4.63}$$

with $\ell = 1, 2$. The expansion up to second order in the electron momentum yields

$$\begin{aligned} \frac{16\pi}{3\sigma_T}\frac{\mathrm{d}\sigma^{\mathrm{Th}}}{\mathrm{d}\Omega_{\mathrm{rest}}}\mathcal{N}_{\mathrm{eq}}(|\mathbf{p}|)\Delta &= \frac{x\mathbf{p}\cdot(\hat{\mathbf{n}}'-\hat{\mathbf{n}})}{m_e c}(1+\cos^2\theta) - \frac{x^2 k_B T}{m_e c^2}(1-\cos\theta) \\ &\times(1+\cos^2\theta) + \frac{x}{(m_e c)^2}\Big\{(\mathbf{p}\cdot\hat{\mathbf{n}}')^2 - (\mathbf{p}\cdot\hat{\mathbf{n}})(\mathbf{p}\cdot\hat{\mathbf{n}}')\Big\}(1+\cos^2\theta) \end{aligned} \tag{4.64}$$

$$\frac{16\pi}{3\sigma_T}\frac{\mathrm{d}\sigma^{\mathrm{Th}}}{\mathrm{d}\Omega_{\mathrm{rest}}}\mathcal{N}_{\mathrm{eq}}(|\mathbf{p}|)\Delta^2 = \left(\frac{x}{m_e c}\right)^2(\mathbf{p}\cdot(\hat{\mathbf{n}}'-\hat{\mathbf{n}}))^2(1+\cos^2\theta) \tag{4.65}$$

where we have dropped the "rest" as subscript in the scattering angle.

We readily observe a change in the last term ($O\left(|\mathbf{p}|^2\right)$) of expression (4.64) when comparing to (4.56), while (4.65) matches (4.61). Computing the integrals

in the exact same way as before leads to

$$I_1^{\mathrm{Th}}(x) = \frac{n_e \sigma_T c\, k_B T}{m_e c^2}\, x(1-x) \tag{4.66}$$

$$I_2^{\mathrm{Th}}(x) = \frac{n_e \sigma_T c\, k_B T}{m_e c^2} 2x^2 \tag{4.67}$$

demonstrating (4.43), as desired. In particular, we observe that $I_2^{\mathrm{Th}}(x)$ remains unchanged, *i.e.*, it is insensitive to the use of the Møller prefactor and the frame-independent expression of Klein-Nishina cross section (4.32). Thus, the change lies on $I_1^{\mathrm{Th}}(x)$, where we fail to account for all terms up to $O\left(|\mathbf{p}|^2\right)$, as the structure of expansion (4.64) shows.

4.C.4 Nonequilibrium case

From now on, we denote $|\mathbf{p}| = p$. In the same spirit as before we define

$$x = \frac{\hbar\omega}{\epsilon}, \quad \Delta = \frac{\hbar(\omega' - \omega)}{\epsilon}$$

where ϵ is the characteristic energy of the electron bath, $\epsilon = \frac{\langle p^2 \rangle}{3m_e}$. We do the expansion of the photon distribution, which gives the same as (4.34). The expansion in the electron distribution, however, gives to the leading order

$$\mathcal{N}(p') = \mathcal{N}(p) - \frac{m_e \epsilon \mathcal{N}'(p)}{p}\Delta + \left(-\frac{(m_e\epsilon)^2 \mathcal{N}'(p)}{p^3} + \frac{(m_e\epsilon)^2 \mathcal{N}''(p)}{p^2} \right) \frac{\Delta^2}{2} \tag{4.68}$$

with $\mathcal{N}'(p) = \dfrac{\partial \mathcal{N}}{\partial p}$ and so on

where we use a first assumption, that the electron distribution is isotropic, $\mathcal{N}(\mathbf{p}) = \mathcal{N}(p)$, with normalization

$$\int \mathrm{d}^3\mathbf{p}\, \mathcal{N}(p,t) = n_e$$

For the equilibrium case we have, of course, $\epsilon = k_B T$ and $\mathcal{N}(p,t) = \mathcal{N}_{\mathrm{eq}}(p)$ as in (4.36). One checks that in this case

$$-\frac{m_e \epsilon \mathcal{N}'_{\mathrm{eq}}(p)}{p} = \mathcal{N}_{\mathrm{eq}}(p)$$

$$\frac{(m_e\epsilon)^2 \mathcal{N}''_{\mathrm{eq}}(p)}{p^2} - \frac{(m_e\epsilon)^2 \mathcal{N}'_{\mathrm{eq}}(p)}{p^3} = \mathcal{N}_{\mathrm{eq}}(p)$$

Plugging into (4.27) reads to the leading order

$$\begin{aligned}\partial_t n =& n' I_1\left(\Delta, \mathcal{N}\right) + \frac{n''}{2} I_2\left(\Delta^2, \mathcal{N}\right) + n(1+n) I_3\left(\Delta, \frac{\mathcal{N}'}{p}\right) \\ &+ n'(1+n) I_4\left(\Delta^2, \frac{\mathcal{N}'}{p}\right) + \frac{n(1+n)}{2}\left(I_5\left(\Delta^2, \frac{\mathcal{N}''}{p^2}\right) + I_6\left(\Delta^2, \frac{\mathcal{N}'}{p^3}\right)\right)\end{aligned} \tag{4.69}$$

where

$$I_1\left(\Delta, \mathcal{N}\right) = c \int \mathrm{d}^3\mathbf{p}\, \mathrm{d}\Omega \left(1 - \frac{\mathbf{v}}{c}\cdot\hat{\mathbf{n}}\right) \frac{\mathrm{d}\sigma}{\mathrm{d}\Omega} \Delta\mathcal{N}$$

$$I_2\left(\Delta^2, \mathcal{N}\right) = c \int \mathrm{d}^3\mathbf{p}\, \mathrm{d}\Omega \left(1 - \frac{\mathbf{v}}{c}\cdot\hat{\mathbf{n}}\right) \frac{\mathrm{d}\sigma}{\mathrm{d}\Omega} \Delta^2\mathcal{N}$$

$$I_3\left(\Delta, \frac{\mathcal{N}'}{p}\right) = -c(m\epsilon) \int \mathrm{d}^3\mathbf{p}\, \mathrm{d}\Omega \left(1 - \frac{\mathbf{v}}{c}\cdot\hat{\mathbf{n}}\right) \frac{\mathrm{d}\sigma}{\mathrm{d}\Omega} \Delta\frac{\mathcal{N}'}{p}$$

$$I_4\left(\Delta^2, \frac{\mathcal{N}'}{p}\right) = -c(m_e\epsilon) \int \mathrm{d}^3\mathbf{p}\, \mathrm{d}\Omega \left(1 - \frac{\mathbf{v}}{c}\cdot\hat{\mathbf{n}}\right) \frac{\mathrm{d}\sigma}{\mathrm{d}\Omega} \Delta^2\frac{\mathcal{N}'}{p}$$

$$I_5\left(\Delta^2, \frac{\mathcal{N}''}{p^2}\right) = c(m_e\epsilon)^2 \int \mathrm{d}^3\mathbf{p}\, \mathrm{d}\Omega \left(1 - \frac{\mathbf{v}}{c}\cdot\hat{\mathbf{n}}\right) \frac{\mathrm{d}\sigma}{\mathrm{d}\Omega} \Delta^2\frac{\mathcal{N}''}{p^2}$$

$$I_6\left(\Delta^2, \frac{\mathcal{N}'}{p^3}\right) = -c(m_e\epsilon)^2 \int \mathrm{d}^3\mathbf{p}\, \mathrm{d}\Omega \left(1 - \frac{\mathbf{v}}{c}\cdot\hat{\mathbf{n}}\right) \frac{\mathrm{d}\sigma}{\mathrm{d}\Omega} \Delta^2\frac{\mathcal{N}'}{p^3}$$

First and second integral are computed in the exact same way as before and gives

$$I_1\left(\Delta, \mathcal{N}\right) = \frac{n_e \sigma_T c}{(m_e c)^2} \frac{\langle p^2\rangle}{3} x(4-x) \tag{4.70}$$

$$I_2\left(\Delta^2, \mathcal{N}\right) = \frac{n_e \sigma_T c}{(m_e c)^2} \frac{\langle p^2\rangle}{3} 2x^2 \tag{4.71}$$

The other integrals are calculated by integration by parts and using the second assumption $\lim_{p\to\infty} p^3\mathcal{N}(p) = 0$.

To compute I_4 we move to spherical coordinates $\mathrm{d}^3\mathbf{p} = p^2\,\mathrm{d}p\,\mathrm{d}\Omega_p$. Using (4.61) the integral over the electron momentum becomes

$$\begin{aligned}\int (\mathbf{p}\cdot(\hat{\mathbf{n}}'-\hat{\mathbf{n}}))^2\frac{\mathcal{N}'}{p}\,\mathrm{d}^3\mathbf{p} &= \int \mathrm{d}\Omega_p|\hat{\mathbf{n}}'-\hat{\mathbf{n}}|^2\cos^2\alpha\int_0^\infty \frac{p^2\mathcal{N}'}{p}p^2\,\mathrm{d}p\\ &= \int \mathrm{d}\Omega_p|\hat{\mathbf{n}}'-\hat{\mathbf{n}}|^2\cos^2\alpha\left\{p^3\mathcal{N}\Big|_0^\infty - 3\int_0^\infty p^2\mathcal{N}\,\mathrm{d}p\right\}\\ &= -3\int\int_0^\infty \mathrm{d}\Omega_p\,\mathrm{d}p\,|\hat{\mathbf{n}}'-\hat{\mathbf{n}}|^2\cos^2\alpha\,p^2\mathcal{N}\\ &= -3\int \mathrm{d}^3\,\mathbf{p}\;(\hat{\mathbf{p}}\cdot(\hat{\mathbf{n}}'-\hat{\mathbf{n}}))^2\mathcal{N}\end{aligned}$$

where we used (4.45), α for the angle between $(\hat{\mathbf{n}}-\hat{\mathbf{n}}')$ and $\hat{\mathbf{p}} = \mathbf{p}/p$. The last integral is computed in the very same fashion as we did for the equilibrium case. We find

$$\int \mathrm{d}^3\,\mathbf{p}\;(\hat{\mathbf{p}}\cdot(\hat{\mathbf{n}}'-\hat{\mathbf{n}}))^2\mathcal{N} = 2n_e(1-\cos\theta)\frac{1}{3}$$

which after integrating the solid angle gives I_4,

$$I_4\left(\Delta^2,\frac{\mathcal{N}'}{p}\right) = c(m_e\epsilon)\left(\frac{x}{m_e c}\right)^2\sigma_T 2n_e \tag{4.72}$$

Looking at expressions (4.70), (4.71) and (4.72) motivates introducing

$$\epsilon = k_B T_{\text{eff}}$$

$$\langle p^2\rangle = 3m_e k_B T_{\text{eff}}$$

Observe that these definitions are compatible with the equilibrium case. We get now

$$I_1\left(\Delta,\mathcal{N}\right) = \frac{n_e\sigma_T c\,k_B T_{\text{eff}}}{m_e c^2}x(4-x)$$

$$I_2\left(\Delta^2,\mathcal{N}\right) = \frac{n_e\sigma_T c\,k_B T_{\text{eff}}}{m_e c^2}2x^2$$

$$I_4\left(\Delta^2,\frac{\mathcal{N}'}{p}\right) = \frac{n_e\sigma_T c\,k_B T_{\text{eff}}}{m_e c^2}2x^2$$

The other integrals are quite similar, to yield

$$I_3\left(\Delta, \frac{\mathcal{N}'}{p}\right) = \frac{n_e \sigma_T c\, k_B T_{\text{eff}}}{m_e c^2} x(4-x)$$

$$I_5\left(\Delta^2, \frac{\mathcal{N}''}{p^2}\right) + I_6\left(\Delta^2, \frac{\mathcal{N}'}{p^3}\right) = \frac{n_e \sigma_T c\, k_B T_{\text{eff}}}{m_e c^2} 2x^2$$

We substitute the values back in (4.69) to find

$$\omega^2 \frac{\partial n}{\partial t}(\omega, t) = \frac{n_e \sigma_T c}{m_e c^2} \frac{\partial}{\partial \omega} \omega^4 \left\{ k_B T_{\text{eff}} \frac{\partial n}{\partial \omega}(t, \omega) + \hbar \left[1 + n(t, \omega)\right] n(t, \omega) \right\} \quad (4.73)$$

which is the Kompaneets equation but with an effective (kinetic) temperature

$$T_{\text{eff}} = \frac{\langle p^2 \rangle}{3 m_e k_B}$$

Le savant n'étudie pas la nature parce que cela est utile; il l'étudie parce qu'il y prend plaisir et il y prend plaisir parce qu'elle est belle.

Henri Poincaré

5

Photon frequency diffusion process

Abstract

We introduce a stochastic multi-photon dynamics on reciprocal space. Assuming isotropy, we derive the diffusion limit for a tagged photon to be a nonlinear Markov process on frequency. The nonlinearity stems from the stimulated emission. In the case of Compton scattering with thermal electrons, the limiting process describes the dynamical fluctuations around the Kompaneets equation. More generally, we construct a photon frequency diffusion process which enables to include nonequilibrium effects. Modifications of the Planck Law may thus be explored, where we focus on the low-frequency regime.

This chapter was first published as [74], together with G.E. Freire Oliveira and C. Maes. The author of this thesis coded the simulations and contributed to the calculations and the writing of the manuscript.

5.1 Introduction

Time-dependent and nonequilibrium dynamics of photons are of increasing interest in a wide range of subjects. Quantum electromagnetic fields can be manipulated to produce photonic lattices (spatial network of coupled photon modes) where time-dependent driving leads to a breaking of time-reversal

invariance (synthetic magnetic field) [97, 65, 141]. Same thing for wave guides where the input field may be driven by either a laser or microwave generator, imposing a nonequilibrium boundary condition on the propagating photons [136, 142]. In quantum optomechanical studies photon gases may be enclosed in cavities with time-dependent geometry such as from vibrating walls, [5]. In another domain and since much longer, plasma physics has dealt with the problem of understanding the origin of suprathermal tails [52, 7] and high-energy cosmic radiation as a result of the scattering of electrons with turbulent electromagnetic fields [66, 163, 173]. Finally, in Early Universe cosmology, the dynamical origin of the main features of the cosmic background radiation (CMB) remains of central importance, especially to understand (possible) deviations from homogeneity [26] or from the Planck Law [68, 152, 39, 6].
As understood from the pioneering days of statistical mechanics and in analogy with Brownian motion, we may expect that the studies mentioned above benefit from modeling fluctuations, *i.e.*, to identify the random motion in photon frequency space. For example, considering a mesoscopic level of description, we become able to insert nonequilibrium effects on the single-photon level allowing to discover meaningful modifications of the Planck Law.

In the present paper we derive a (stochastic) diffusion process for a tagged photon, that can be seen as the diffusion limit of a multi-photon hopping dynamics in reciprocal space. Stimulated emission results in the nonlinearity of the Markov diffusion process.
We first apply our construction to build a Kompaneets process, *i.e.*, the stochastic (single-photon) dynamics that has the well-known Kompaneets equation as its nonlinear Fokker-Planck equation. That new fluctuation dynamics is the counterpart to the analysis of Kompaneets in [99] and makes our first main result: the derivation of the frequency diffusion process for a tagged photon in a plasma dominated by Compton scattering. Similarly, many other processes such as double Compton and *Bremsstrahlung* can be considered, and thanks to our setup, are easily added to the dynamics, turning it into a fully nonlinear reaction-diffusion dynamics. Not only does that process complement (in some precise sense) the Kompaneets equation, it allows also to see beyond, leading to our second main contribution. A possible avenue indeed that gets opened, is the implementation and exploration of nonequilibrium effects modifying the Planck law, via physically motivated interventions on the single-photon level. Our work explores how changing drift and adding diffusion may change the low-frequency distribution, where the relaxation times in the Kompaneets process are largest, hence most vulnerable to nonequilibrium amendments.
As a final remark, it should be noted in all these cases that we start from a multi-photon diffusion process in frequency space. It means to include the stimulated emission in the reactivities. That presents a nontrivial aspect in

both the theoretical and computational analysis, leading finally to important nonlinearities in the corresponding Fokker-Planck equation. However, our results indicate that the processes simulate indeed the Kompaneets equation and its extensions, in the sense that the empirical density of photons follows these equations.

In the next section we describe the Kompaneets equation for relaxation to the Planck law via Compton scattering. In Section 5.3 we introduce the Kompaneets *process*, describing the hopping of photons in reciprocal space. Its diffusion limit for a tagged photon gives a nonlinear Markov process, described in Eq. (5.21). That simulation is explained in Section 5.4, where the results are shown in terms of the time-dependence of the spectral density. We confirm the validity of the simulation scheme by verifying relaxation to the Planck law along the Kompaneets equation. There, we also show the appearance of a condensate when the number of photons is taken to be large enough, an effect already observed in [102]. Other non photon-number preserving radiation processes are added in Section 5.5. Bremsstrahlung and double Compton scattering are described there as low-frequency corrections. These are reactive mechanisms to control photon-number that can be handled and taken effectively in the simulation. Section 5.6 discusses more general photon-number processes, extending the Kompaneets process to implement two types of low-frequency modifications, either in the drift or in the diffusion. They are nonequilibrium features in the photon dynamics, effectively implementable on the single-photon level that we simulate. Finally, in Section 5.7, we explain the simulation details for that extension (including reactive mechanisms). That illustrates in great detail how nonequilibrium features change the stationary solution to enhance low-frequency occupation (yielding there a higher effective temperature).

5.2 Kompaneets equation

The Compton effect is a quantum process in which photons scatter from free electrons. It eventually leads to the relaxation of the photon distribution to that of the Planck radiation law. The Kompaneets equation

$$\omega^2 \frac{\partial n}{\partial t}(t,\omega) = \frac{n_e \sigma_T c}{m_e c^2} \frac{\partial}{\partial \omega} \omega^4 \left\{ k_B T \frac{\partial n}{\partial \omega}(t,\omega) + \hbar \left[1 + n(t,\omega)\right] n(t,\omega) \right\} \qquad (5.1)$$

describes that relaxation towards equilibrium of a photon gas in contact with a nondegenerate, nonrelativistic electron bath in thermal equilibrium at temperature T. Here, $n(t,\omega)$ is the average occupation number at frequency ω of the photon gas at time t; stationarity is then achieved when $n(t,\omega)$ reaches

the Bose-Einstein distribution. Apart from the usual constants in (5.1), we recognize σ_T as the Thomson total cross section and n_e, m_e as the density and mass of the electrons, respectively. The induced Compton scattering [103, 14] leads to the nonlinearity (in the second term) appearing in the Kompaneets equation (5.1). 5.5 In 1957 Kompaneets [99] gave a mesoscopic derivation of (5.1), starting from a semi-classical Boltzmann equation. It remains essential for the understanding of the CMB spectrum and related phenomena such as the Sunyaev-Zeldovich effect [164, 165]. The understanding of the Kompaneets equation has been evolving over the years and excellent reviews include [154, 72, 180]. We emphasize that many extensions to the equation exist. For example, the isotropy condition for the distribution has been relaxed in [27, 135], while nonrelativistic extensions can be found in [8, 25, 84, 85, 44, 122, 124, 123]. More recently in [73] we addressed some consistency problems in Kompaneets' original framework [99].

For simplicity it is convenient to use the dimensionless counterpart of (5.1) in order to introduce (in the next Section) the Kompaneets *process*, which describes the hopping of photons in reciprocal space.
The dynamics of the average photon occupation number $n(t, x)$ at dimensionless frequency $x = \hbar\omega/k_B T$ in a thermal environment with temperature T, is obtained from equation (5.1) as

$$x^2 \frac{\partial n}{\partial t}(y, x) = \frac{\partial}{\partial x} x^4 \left\{ \frac{\partial n}{\partial x}(y, x) + [1 + n(y, x)]\, n(y, x) \right\} \tag{5.2}$$

where we have defined the dimensionless Compton optical depth

$$y = \frac{k_B T}{m_e c^2} n_e \sigma_T c\, t = \frac{t}{\tau_C}.$$

Here, τ_C is the characteristic time in which photons change their frequency due to Compton scattering with thermal electrons,

$$\left\langle \frac{1}{2\tau} \left(\frac{\Delta\omega}{\omega} \right)^2 \right\rangle \approx \frac{k_B T}{m_e c^2}\, \frac{1}{\tau} = \frac{1}{\tau_C} \tag{5.3}$$

where $\tau = l/c$ is the average collision rate, related to the mean free path of photons $l = (n_e \sigma_T)^{-1}$. For simplicity, we will take our units such that $\tau_C = 1$, identifing y with t.
Note that the

$$n_\mu(x) = \frac{1}{e^{x-\mu} - 1}, \qquad \mu \leq 0 \tag{5.4}$$

are stationary solutions of (5.2): $\frac{\mathrm{d}n_\mu}{\mathrm{d}x}(x) + [1 + n_\mu(x)]\, n_\mu(x) = 0$.

Central for our purposes to simulate the Compton scattering on a mesoscopic level is to write the Kompaneets equation (5.1)–(5.2) in terms of the photon density. Assuming that photons are confined to a box of volume V with periodic boundary conditions, the density of states is

$$g(\mathbf{k})\,\mathrm{d}^3\mathbf{k} = \frac{2V}{(2\pi)^3}\,\mathrm{d}^3\mathbf{k} = \frac{2V}{(2\pi)^3}4\pi k^2\,\mathrm{d}k$$

where $\mathbf{k}$ is the wave vector. It is useful here to assume isotropy: in function of the dimensionless $x = \hbar\omega/k_BT$, the density of states is

$$g(x)\,\mathrm{d}x = \frac{2V}{(2\pi)^3}\left(\frac{k_BT}{\hbar c}\right)^3 4\pi x^2\,\mathrm{d}x$$

From here we can integrate the photon occupation number to get the total number of photons

$$N_t = \int_0^\infty \mathrm{d}x g(x) n(t,x)$$

That allows to write the spectral probability density

$$\rho(t,x) = \frac{V}{N_t}\frac{1}{\pi^2}\left(\frac{k_BT}{\hbar c}\right)^3 x^2 n(t,x) = \frac{x^2 n(t,x)}{2\zeta(3)Z_t}, \tag{5.5}$$

where $2\zeta(3) = \int_0^\infty \mathrm{d}x\, x^2/(e^x-1) \simeq 2.404$. By using the normalization of the spectral probability density while integrating (5.5) over x, we can write

$$Z_t = \frac{1}{2\zeta(3)}\int_0^\infty \mathrm{d}x\, x^2 n(t,x) \propto \frac{N_t}{V}\left(\frac{\hbar c}{k_BT}\right)^3 \tag{5.6}$$

which is a possibly time-dependent parameter, depending on the temperature and proportional to the number of photons per volume. Since the Kompaneets equation (still without reaction mechanism) is photon-number preserving, $Z_t = Z$ is time-independent and yields for the stationary n_μ in (5.4),

$$Z = \frac{\mathrm{Li}_3(e^\mu)}{\zeta(3)}$$

with Li_3 the polylogarithm of order 3. In that notation, the Kompaneets equation (5.2) becomes

$$\frac{\partial\rho}{\partial t}(t,x) = -\frac{\partial}{\partial x}\left[\left(4x - x^2\left(1 + 2\zeta(3)Z\,\frac{\rho(t,x)}{x^2}\right)\right)\rho(t,x)\right] + \frac{\partial^2}{\partial x^2}\left[x^2\rho(t,x)\right] \tag{5.7}$$

Observe still that Z can be interpreted as the ratio of the actual photon spectral density to that of the Planck distribution corresponding to the same temperature.

For the Bose-Einstein distribution $n(t,x) = n_{\rm BE}(x) = n_0(x) = 1/(e^x - 1)$, the photon number equals

$$N_{\rm BE} = 2\zeta(3)\frac{V}{\pi^2}\left(\frac{k_B T}{\hbar c}\right)^3$$

corresponding to a spectral probability density with $Z = 1$:

$$\rho_{\rm BE}(x) = \frac{x^2 n_{BE}(x)}{2\zeta(3)} \tag{5.8}$$

We make a "hot" Planck spectral density by changing $x \to x/2$ (doubling the temperature), taking $n(x) = n_{\rm BE}(x/2)$, leading to

$$\rho_{\rm BE}^{\rm hot}(x) = \frac{x^2 n_{\rm BE}(x/2)}{16\zeta(3)} \tag{5.9}$$

in which case $Z = 8$. On the other hand, as Z goes to zero, we recover the Wien expression $\rho_{\rm Wien}(x) = x^2 e^{-x}/2$ to be the stationary spectral probability density for equation (5.7) which becomes linear at $Z = 0$.

As a final comment we note that the Kompaneets equation is positivity preserving [94]. That is important because any solution of the equation will retain its sign, suggesting indeed to interpret this equation as of Fokker-Planck type.

5.3 Mesoscopics of Compton scattering: Kompaneets stochastic process

When considering a single Compton scattering event, the transition rates are fully determined by the incident electron and photon momenta together with energy-momentum conservation. However, in the presence of repeated scattering, treating the electron as a classical particle and the photon as a boson, the transition rates must account for stimulated emission, *i.e.*, transitions are enhanced if photons are present in the final state. Mathematically, we work on a symmetrized Fock space [92], where transition rates (between incoming $|\mathrm{i}\rangle$ and final states $|\mathrm{f}\rangle$) have an additional term coming from the matrix element

$$\left|\langle \mathrm{f}\,|a^\dagger_{\mathbf{k}'} a_{\mathbf{k}}|\mathrm{i}\rangle\right|^2 = (1 + n(\mathbf{k}'))\, n(\mathbf{k}) \tag{5.10}$$

where $a_{\mathbf{k}}^{(\dagger)}$ are the annihilation (creation) operators in the Fock space related to the photon momentum $\mathbf{k}$, and $n(\mathbf{k})$ are occupation numbers. That is the only "interaction" between the photons that we take into account so far.

5.3.1 Jump process in reciprocal space

As introduced in [73], we start from a random walk of bosons in reciprocal space. Here we consider a bath of a large number N of photons, confined to a cube of sidelength ℓ with periodic boundary conditions. We will end up working in the thermodynamic limit for fixed density N/ℓ^3. For now however the modes are quantized, at a fixed distance $\delta = 2\pi/\ell$. We designate each photon by its wave vector $\mathbf{k}_i$ so that the full state of the bath is described by $\mathbf{K} = (\mathbf{k}_1, \ldots, \mathbf{k}_N)$. Yet, we must treat the photons indistinguishably, and soon we will work with occupation numbers.
Transitions $\mathbf{K} \to \mathbf{K}'$ between states are restricted to these for which only one photon jumps to another wave vector, *i.e.*, to transitions

$$\mathbf{K} = (\mathbf{k}_1, \ldots, \mathbf{k}_i, \ldots, \mathbf{k}_N) \longrightarrow \mathbf{K}' = (\mathbf{k}_1, \ldots, \mathbf{k}_i + \mathbf{a}\delta, \ldots, \mathbf{k}_N)$$

where $\mathbf{a}$ is one of the six unit vectors. The corresponding rate of such a transition is of the form

$$w_i(\mathbf{K}, \mathbf{a}\delta) = w(\mathbf{k}_i, \mathbf{a}\delta)\,(1 + n_{\mathbf{k}_i + \mathbf{a}\delta}(\mathbf{K}))$$

where

$$n_{\mathbf{k}}(\mathbf{K}) = \sum_i \delta_{\mathbf{k},\mathbf{k}_i}$$

(with the Kronecker delta) counts the number of photons at $\mathbf{k}$. It realizes the stimulated emission in the process. The rest of the rates is taken as usual,

$$w(\mathbf{k}, \mathbf{a}\delta) = D\left(\mathbf{k} + \frac{\mathbf{a}\delta}{2}\right) \exp\left\{-\frac{\beta}{2}\left(U(\mathbf{k} + \mathbf{a}\delta) - U(\mathbf{k})\right)\right\}$$

to satisfy detailed balance with energy function U at inverse temperature β. We also added a (time-symmetric) reactivity D, also to be specified below in the case of Compton scattering.

The thus defined process $\mathbf{K}(t)$ is Markovian and has backward generator L_δ, to be applied to observables $F(\mathbf{K})$, given by

$$L_\delta F(\mathbf{K}) = \sum_{i,\mathbf{a}} w_i(\mathbf{K}, \mathbf{a}\delta)\,(F(\mathbf{K}') - F(\mathbf{K})) \tag{5.11}$$

where $\mathbf{k}'_j = \mathbf{k}_j$ for $j \neq i$ and $\mathbf{k}'_i = \mathbf{k}_i + \mathbf{a}\delta$. So far, the process can be seen as a generalized zero range process [16]. That generalization is sometimes referred to as a "misanthrope process", motivated by the convenience of monotonicity; see [41, 153]. Here that name is less appropriate as the dependence on the target configuration is one of "stimulation".

We are not staying with the multiparticle dynamics generated by (5.11), as we wish to find the dynamics for a single tagged photon. To have a rigorous understanding of the dynamics of a tagged particle in a "misanthrope" (or stimulated) zero range process is far from trivial; see also [87]. Our approach will therefore be more heuristic.

To start, we find the time evolution of the expected occupation numbers by applying the above rule to the observables $n_{\mathbf{k}}$ and by noting that

$$n_{\mathbf{k}}(\mathbf{K}') - n_{\mathbf{k}}(\mathbf{K}) = \delta_{\mathbf{k},\mathbf{k}_i+\mathbf{a}\delta} - \delta_{\mathbf{k},\mathbf{k}_i}$$

Hence,

$$\begin{aligned} L_\delta n_{\mathbf{k}}(\mathbf{K}) &= \sum_{i,\mathbf{a}} w(\mathbf{k}_i, \mathbf{a}\delta)\,(1 + n_{\mathbf{k}_i+\mathbf{a}\delta}(\mathbf{K}))\,(\delta_{\mathbf{k},\mathbf{k}_i+\mathbf{a}\delta} - \delta_{\mathbf{k},\mathbf{k}_i}) \\ &= \sum_{\mathbf{a}} w(\mathbf{k}-\mathbf{a}\delta, \mathbf{a}\delta)\,(1 + n_{\mathbf{k}}(\mathbf{K}))\left(\sum_i \delta_{\mathbf{k},\mathbf{k}_i+\mathbf{a}\delta}\right) \\ &\qquad - w(\mathbf{k}, \mathbf{a}\delta)\,(1 + n_{\mathbf{k}+\mathbf{a}\delta}(\mathbf{K}))\left(\sum_i \delta_{\mathbf{k},\mathbf{k}_i}\right) \\ &= \sum_{\mathbf{a}} w(\mathbf{k}-\mathbf{a}\delta, \mathbf{a}\delta)\,(1 + n_{\mathbf{k}}(\mathbf{K}))\,n_{\mathbf{k}-\mathbf{a}\delta}(\mathbf{K}) \\ &\qquad - w(\mathbf{k}, \mathbf{a}\delta)\,(1 + n_{\mathbf{k}+\mathbf{a}\delta}(\mathbf{K}))\,n_{\mathbf{k}}(\mathbf{K}) \end{aligned} \tag{5.12}$$

Continuing with (5.12) and writing $n(t,\mathbf{k}) = \langle n_{\mathbf{k}}(\mathbf{K}(t))\rangle$ for the expectation value over the process at time t, we thus get

$$\frac{\partial n}{\partial t}(t,\mathbf{k}) = \sum_{\mathbf{a}} w(\mathbf{k}-\mathbf{a}\delta, \mathbf{a}\delta)\,\langle(1 + n_{\mathbf{k}})n_{\mathbf{k}-\mathbf{a}\delta}\rangle - w(\mathbf{k}, \mathbf{a}\delta)\,\langle(1 + n_{\mathbf{k}+\mathbf{a}\delta})n_{\mathbf{k}}\rangle$$

Next we assume that the correlations between occupations factorize. That is not only part of standard kinetic theory; it originates mainly in the extremely weak interaction between photons. We end up then with

$$\begin{aligned} \frac{\partial n}{\partial t}(t,\mathbf{k}) = \sum_{\mathbf{a}} & w(\mathbf{k}-\mathbf{a}\delta, \mathbf{a}\delta)(1 + n(t,\mathbf{k}))n(t,\mathbf{k}-\mathbf{a}\delta) \\ & - w(\mathbf{k}, \mathbf{a}\delta)(1 + n(t,\mathbf{k}+\mathbf{a}\delta))n(t,\mathbf{k}) \end{aligned} \tag{5.13}$$

which has the form of a nonlinear Master equation. We already note the resemblance with the Kompaneets equation (5.1) but that can be made more complete by taking the diffusion limit.

5.3.2 Diffusion limit

The process above can be considered in the limit $\delta \downarrow 0$ while rescaling time. To obtain the limiting diffusion process we calculate the limiting backward generator $L = L_\delta/\delta^2$ on permutation-invariant functions F which are piecewise constant on cubes of side 2δ around $\mathbf{K} \in (\delta\mathbb{Z})^{3N}$. We remember from (5.11) that

$$L_\delta F(\mathbf{K}) = \sum_{i,a} D\left(\mathbf{k}_i + \frac{\mathbf{a}\delta}{2}\right) \exp\left\{-\frac{\beta}{2}\left(U(\mathbf{k}_i + \mathbf{a}\delta) - U(\mathbf{k}_i)\right)\right\}$$

$$\times \left(1 + n_{\mathbf{k}_i + \mathbf{a}\delta}(\mathbf{K})\right)\left(F(\mathbf{K}') - F(\mathbf{K})\right) \quad (5.14)$$

For expanding that to order δ^2 we must take into account

$$w(\mathbf{k}, \mathbf{a}\delta) = \left(D(\mathbf{k}) + \frac{\delta}{2}\mathbf{a}\cdot\nabla_{\mathbf{k}} D(\mathbf{k})\right)\left(1 - \frac{\beta\delta}{2}\mathbf{a}\cdot\nabla_{\mathbf{k}} U(\mathbf{k})\right)$$

$$n_{\mathbf{k}+\mathbf{a}\delta} = n_{\mathbf{k}} + \delta\,\mathbf{a}\cdot\nabla_{\mathbf{k}} n$$

Whence, to nonvanishing order,

$$\frac{1}{\delta^2} L_\delta F(\mathbf{K}) = \sum_i D(\mathbf{k}_i)(1 + n_{\mathbf{k}_i}(\mathbf{K}))\Delta_{\mathbf{k}_i} F(\mathbf{K}) + \sum_{i,\mathbf{a}} \left\{\left(\frac{1}{2}\mathbf{a}\cdot\nabla_{\mathbf{k}} D(\mathbf{k}_i)\right.\right.$$

$$\left.\left. - \frac{\beta}{2} D(\mathbf{k}_i)\mathbf{a}\cdot\nabla_{\mathbf{k}} U(\mathbf{k}_i)\right)(1 + n_{\mathbf{k}_i}(\mathbf{K})) + D(\mathbf{k}_i)\,\mathbf{a}\cdot\nabla_{\mathbf{k}} n\right\}\mathbf{a}\cdot\nabla_{\mathbf{k}_i} F(\mathbf{K}) \quad (5.15)$$

We should remember that F depends on $\mathbf{K}$ only through the occupations $n_{\mathbf{k}}(\mathbf{K})$. Moreover we are interested in the dynamics of a tagged photon, which amounts to a single-particle description. We take therefore functions $F(\mathbf{K}) = \int \mathrm{d}^3\mathbf{k} f(\mathbf{k}) n_{\mathbf{k}}(\mathbf{K})$ for the field $n_{\mathbf{k}}(\mathbf{K}) = \sum_j \delta(\mathbf{k}_j - \mathbf{k})$,

$$F(\mathbf{K}) = \sum_j \int \mathrm{d}^3\mathbf{k} f(\mathbf{k})\,\delta(\mathbf{k}_\mathbf{j} - \mathbf{k}) = \sum_j f(\mathbf{k}_j) \quad (5.16)$$

In that case, expression (5.15) can be rewritten line per line and per wave vector by using $\frac{1}{\delta^2} L_\delta F(\mathbf{K}) = \int \mathrm{d}^3\mathbf{k}\, n(\mathbf{k})\, \mathcal{L}f(\mathbf{k})$ for

$$\mathcal{L}f(\mathbf{k}) = D(\mathbf{k})(1+n_\mathbf{k})\Delta_\mathbf{k} f(\mathbf{k}) + \sum_\mathbf{a} \left\{ \frac{1}{2}\mathbf{a}\cdot\nabla_\mathbf{k} D(\mathbf{k})(1+n_\mathbf{k}) \right.$$
$$\left. - \frac{\beta}{2} D(\mathbf{k})\mathbf{a}\cdot\nabla_\mathbf{k} U(\mathbf{k})(1+n_\mathbf{k}) + D(\mathbf{k})\ \mathbf{a}\cdot\nabla_\mathbf{k} n \right\}\ \ \mathbf{a}\cdot\nabla_\mathbf{k} f(\mathbf{k}) \quad (5.17)$$

Note now that

$$\int \mathrm{d}^3\mathbf{k}\, n_\mathbf{k} \left\{ D(\mathbf{k})\, n_\mathbf{k} \Delta_\mathbf{k} f(\mathbf{k}) \right.$$
$$\left. + \sum_a \left[\frac{1}{2}\mathbf{a}\cdot\nabla_\mathbf{k} D(\mathbf{k})\, n_\mathbf{k} + D(\mathbf{k})\ \mathbf{a}\cdot\nabla_\mathbf{k} n \right] \mathbf{a}\cdot\nabla_\mathbf{k} f(\mathbf{k}) \right\} = 0 \quad (5.18)$$

by partial integration. We thus get

$$\int \mathrm{d}^3\mathbf{k}\, n(\mathbf{k})\, \mathcal{L}f(\mathbf{k}) = D(\mathbf{k})\, \Delta_\mathbf{k} f(\mathbf{k})$$
$$+ \sum_a \left\{ \frac{1}{2}\mathbf{a}\cdot\nabla_\mathbf{k} D(\mathbf{k}) - \frac{\beta}{2} D(\mathbf{k})\mathbf{a}\cdot\nabla_\mathbf{k} U(\mathbf{k})(1+n_\mathbf{k}) \right\}\ \mathbf{a}\cdot\nabla_\mathbf{k} f(\mathbf{k}) \quad (5.19)$$

Remember that we interpret $n_\mathbf{k}$ as a given continuum field. As a consequence, the limiting diffusion of the tagged photon is given by

$$\dot{\mathbf{k}}_t = \nabla_\mathbf{k} D(\mathbf{k}_t) - \beta D(\mathbf{k}_t)\, \nabla_\mathbf{k} U(\mathbf{k}_t)(1+n_{\mathbf{k}_t}) + \sqrt{2D(\mathbf{k}_t)}\, \boldsymbol{\Xi}_t \quad (5.20)$$

where $\boldsymbol{\Xi}_t$ is a standard white noise on $\mathbb{R}^3$ and Itô-convention must be applied. The derivation of (5.20) from (5.19) is not trivial. It would follow standard practice without the nonlinearity (stimulated emission) by understanding the backward generator $\mathcal{L}$ as the generator of the time-evolution of the walk in reciprocal space. Yet, full rigor is not attempted here and the precise derivation of the tagged photon dynamics remains mathematically challenging; see also [71] for more details. Numerical checks will follow below.

5.3.3 Tagged photon nonlinear Markov process

We get to our main result. Assume that the process is isotropic to suppose that D and U only depend on the radial component x with $\mathbf{k} = x/(\beta\hbar c)\hat{\mathbf{x}}$. We keep

referring to $x = \beta\hbar\omega$ as the dimensionless frequency.
We apply Itô's lemma to (5.20), with calculation in Appendix 5.A, to end up with

$$\dot{x} = 2\frac{D(x)}{x} + \partial_x D(x) - D(x)\partial_x U(x)(1 + n(t,x)) + \sqrt{2D(x)}\,\xi_t \qquad (5.21)$$

where ξ_t is again standard white noise. That Itô-stochastic process (5.21) is what we call the Kompaneets process, and its construction and simulation (in the next Section) is our first main result. It is the (nonlinear) Langevin dynamics associated to the Kompaneets equation (5.7) in the case where

$$U(x) = x, \qquad D(x) = x^2. \qquad (5.22)$$

Note the dependence on the photon occupation field $n(t,x)$. What we have here is a mean-field nonlinear Markov process for the tagged photon, where the field $n(t,x)$ represents the empirical occupations [98, 70]; see also [76]. It realizes the Kompaneets equation as a nonlinear Fokker-Planck equation. That follows the spirit of the McKean-Vlasov equation [114], where the mean-field interaction leads to the nonlinearity in a multi-particle limit. Our derivation has been "theoretical" but confirmation of the soundness of our approach is obtained in the next section. One difficulty we ignore here is the singularity in the modulus of the vector $\mathbf{k}$. It also implies that the white noise can lead to negative values of x. Yet, in the simulations when starting with a particle number less than or equal to the value corresponding to the Planck distribution ($Z \leq 1$), even without an explicit boundary condition, there is no probability flux through the origin, that is, no negative frequencies are observed. For a sufficiently small time step in the simulation, no particle ever reaches $x = 0$.

5.4 Simulation of the Kompaneets process

Suppose the following Itô stochastic differential equation for $X_t \in \mathbb{R}$,

$$\dot{X}_t = B(X_t) + \sqrt{2D(X_t)}\,\xi_t, \qquad t \geq 0 \qquad (5.23)$$

with standard white noise ξ_t. Then, the Euler-Maruyama algorithm reads

$$X_{t_{i+1}} = X_{t_i} + B(X_{t_i})\Delta t + \sqrt{2D(X_{t_i})}\,\Delta W_i + O(\Delta t^{3/2})$$

in which $\Delta t = t_{i+1} - t_i$ is the timestep and ΔW_i is a Gaussian random variable with mean 0 and variance Δt at iteration i.
If $B = B(X_t, \rho_t)$ depends also on the distribution function ρ_t at time t, we need

to consider an ensemble of processes. Here we take N_E independent Kompaneets processes, and approximate the probability density ρ_t with the empirical density ρ_t^E, which follows from a histogram of the frequencies of the ensemble. We expect in the limit $\rho_t^E \to \rho_t$ (large N_E) that the implementation of stimulated emission is exact. Furthermore, a initial value for Z is chosen, see (5.6), which can be interpreted as the ratio of the total number of photons to the number of photons which would be present in the same volume if the occupation number were to follow a Bose-Einstein distribution. We can then at any point in time invert (5.5) yielding the empirical occupation number

$$n_t^E(x) = 2\zeta(3) Z \frac{\rho_t^E(x)}{x^2}.$$

We simulate an ensemble of around $N_E \simeq 10^5$ particles, fixing the total time $\simeq 100$ and using a timestep of $\mathrm{d}t = 10^{-4}$. The timestep was chosen to be low enough that lowering it did not appreciably change the simulation. The histograms are binned with a step of $\mathrm{d}x = 0.05$ in frequency domain. As most of the distribution is concentrated between 0 and 10, this implies a bin will have on average about 500 particles.

The Euler-Maruyama algorithm for each particle reads at each iteration i

$$x_{t_{i+1}} = x_{t_i} + \left(4x_{t_i} - x_{t_i}^2 \left(1 + n_{t_i}^E(x_{t_i})\right)\right) \mathrm{d}t + x_{t_i} \sqrt{2\,\mathrm{d}t}\, u_i \tag{5.24}$$

The above equation corresponds to the choices

$$B(x, \rho_t) = 4x - x^2(1 + n_t(x)) \qquad \text{with} \qquad n_t(x) = 2\zeta(3) Z \frac{\rho_t(x)}{x^2} \tag{5.25}$$

$$D(x) = x^2 \tag{5.26}$$

for drift and diffusion in (5.23), respectively (equivalent of (5.22)). Note here that at low frequencies, $x \ll 1$, there is almost no activity when also $x^2 n_t(x) \ll 1$. At each iteration i, we update the frequency according to (5.24). Note that we check at each step the histogram at the frequency obtained in the previous time step. Then, after the Euler-Maruyama step, the histogram is updated accordingly. It is also important to mention here that we need to specify the initial occupation field $n_0(x)$, which determines the probability density $\rho_0(x)$ from which the initial x_0 is drawn. The step from n_0 to ρ_0 requires specifying Z in (5.5). In other words, there can be two different evolutions even when the initial ρ_0 are identical, if there is a different Z.

To validate the correctness of our (somewhat heuristic) derivation, we compare the empirical spectral probability density obtained by our process to a numerical

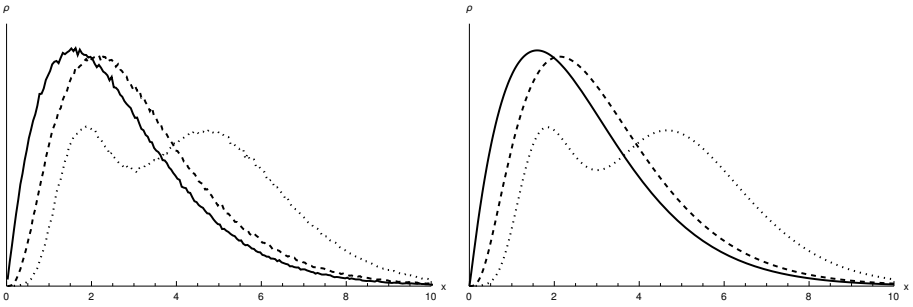

Figure 5.1: The spectral probability density ρ_t in function of the dimensionless frequency x with plots for $t = 0.05, 0.5$ and 5, respectively dotted, dashed and solid. We compare the Kompaneets process (5.21) on the left with a numerical solution of the Kompaneets equation on the right. The initial condition (not shown here) was taken to be a sum of two Gaussians centered around $x = 2$ and $x = 6$ with standard deviations of respectively 2 and 1, and weights of respectively 1/3 and 2/3.

integration of the Kompaneets process. The results are shown in fig. 5.1 and show a clear agreement between the two. The initial condition as described in the caption, a sum of two Gaussians, is not supposed to be physical but was purposefully chosen to better visually highlight the accordance.

To quantitatively check how much the obtained histogram deviates from the theoretical prediction, we can for every time t compute the excess $\rho_{\mathrm{NUM}}(t,x) - \rho_{\mathrm{BE}}(t,x)$, where $\rho_{\mathrm{NUM}}(t,x)$ is the numerical integration of the Kompaneets equations. Our simulations show that over the entire frequency range the results have a precision on the order of 10^{-3}.

If we lower Z to, say, 0.1, the frequency spectral density instead converges to something closely resembling the Wien distribution $\simeq x^2 e^{-x}$, as verified in Fig. 5.3. This corresponds to (5.4) with $\mu \simeq -2.13$. There is no further convergence to the Planck law here because there is particle conservation and because of the absence of low-frequency drift or diffusion for $x \ll 1$, making both (5.25) and (5.26) negligible since $n_t(x)$ is of order 1 there.

We conclude from these simulations that the constructed process (5.21) can be reliably simulated and indeed, for its deterministic behavior reproduces the time-evolution (5.7), and hence the Kompaneets equation (5.1). We have given examples of various initial conditions and we conclude that the Kompaneets process shows two different time-scales: one is a fast relaxation to the Planck

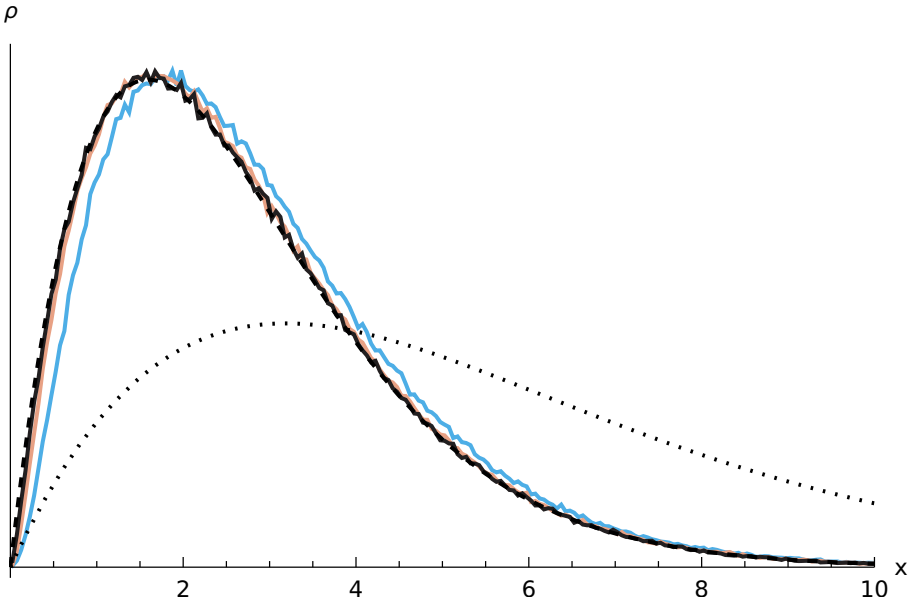

Figure 5.2: The spectral probability density ρ_t in function of the dimensionless frequency x for the Kompaneets process (5.21), with plots for $t = 1, 2, 3$ going from right to left. The dotted line indicates the initial "hot Planck" condition corresponding to the occupation field $n_0(x) = n_{\mathrm{BE}}(x/2)/8$ for which $Z = 1$. Notice the fast thermalization to a Wien-like tail, followed by a slow final thermalization at lower frequencies ($x < 6$).

shape, better at high frequencies, after which a slower relaxation occurs shifting the distribution at the correct temperature. Such a fast prethermalization followed by a slower adjustment is not uncommon in kinetic equations; it already happens in the classical Boltzmann equation where a local Maxwellian is rapidly established.

Finally, we note that when taking $Z > 1$, a condensate is expected to form [102]. Fig. 5.4 shows that condensate appearing for the simulated spectral density for $Z = 1.1$. In that case, we also find particles going out of bounds at $x = 0$, leading to unphysical negative energies. However, that may be remedied by non-particle-conserving processes (e.g. double Compton or Brehmsstrahlung), which absorb the condensate at the origin (though simulation results are not shown here).

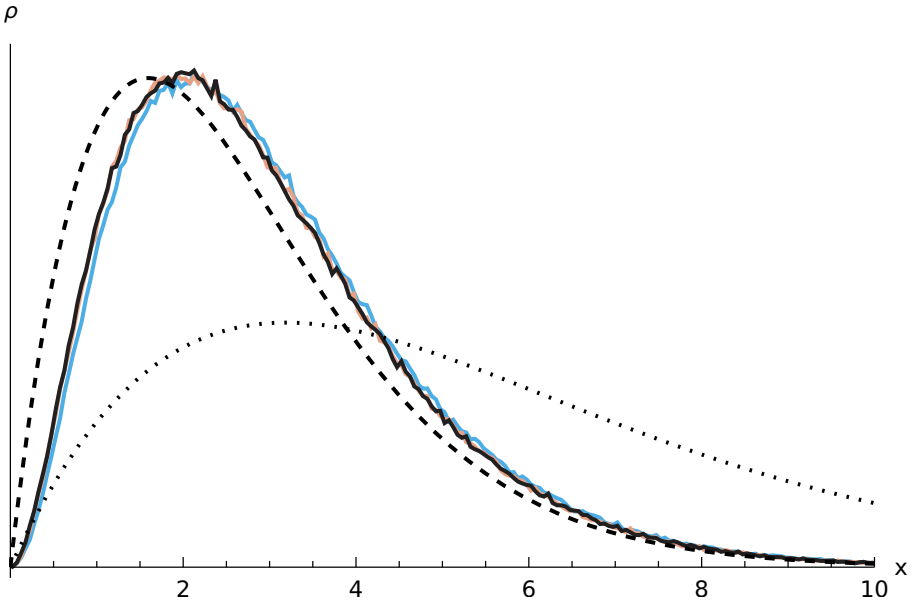

Figure 5.3: Similar to Fig. 5.2, but with $Z = 0.1$, *i.e.*, with the initial occupation field $n_0(x) = n_{\rm BE}(x/2)/80$. There is a marked difference (going like x^2 at low frequency) with the dashed line representing the Planck density, as there is particle conservation. There is only the fast thermalization to a(n almost) Wien density because of the absence of low-frequency activity, $x^2 n_t(x) \ll 1$ at low x.

5.5 Bremsstrahlung and double Compton scattering

Double Compton scattering and Bremsstrahlung are additional radiation processes, physically similar in controlling emission and absorption of photons. Since the number of photons is not conserved in this case, we can regard them as mechanisms to control the photon number density.
Both can be implemented as stochastic processes but we skip the derivations. We refer to [128, 107], where the analysis that leads to the master equation was first obtained by Kompaneets (Eq. (18) in [99]).

The Bremsstrahlung process resembles a chemical reaction, where photons are produced by electrons as they are deflected by nuclei. Here, we use the

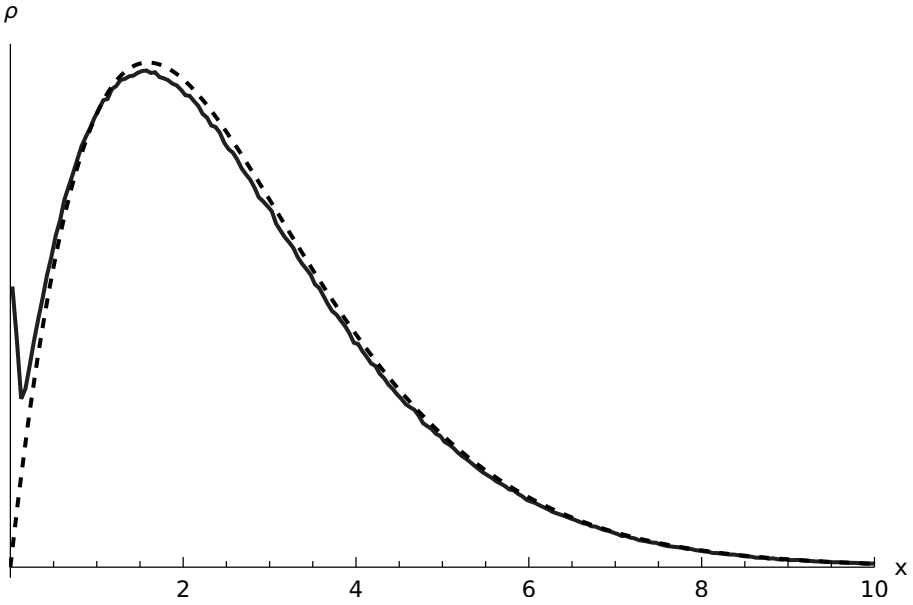

Figure 5.4: "Stationary" spectral density for $Z = 1.1$. The dashed line is the Planck density. Notice the formation of a condensate around the origin. In that case, there is also the appearance of non-physical negative frequencies. The condensate and the non-physical behavior may be remedied by considering radiative processes like Bremsstrahlung.

expression derived by Kompaneets to write in a slightly different manner

$$\left(\frac{\partial n}{\partial t}\right)_{\mathrm{B}} = \frac{\tau_C}{\tau_B(x)}\left(\frac{1}{e^x - 1} - n(t,x)\right) \tag{5.27}$$

where we have used τ_C, the characteristic Compton timescale of (5.3), to make the comparison with the frequency dependent timescale $\tau_B(x)$ of Bremsstrahlung. Notice how there is no diffusion or drift, Bremsstrahlung instead provides a pointwise convergence of the occupation numbers towards the Bose-Einstein distribution.
If we temporarily reinstate units, and assuming for a moment that all nuclei are single protons, which means their density matches that of the electrons, we find that

$$\frac{\tau_C}{\tau_B(x)} = \frac{9\alpha n_e}{8}\sqrt{\frac{\pi}{2}\left(\frac{m_e c^2}{k_B T}\right)^3}\left(\frac{\hbar c}{k_B T}\right)^3 \frac{\sinh(x/2)K_0(x/2)}{x^3} \tag{5.28}$$

where α is the fine structure constant and K_0 is a modified Bessel function of the second kind [125] (adapted to our notation from [99]). Given the x^{-3} dependence of the timescale, we see that Bremsstrahlung dominates the very lowest frequencies, but is negligible everywhere else. Qualitatively, they reproduce the above reactive processes.

Similarly, we can treat the double Compton mechanism, whose radiative nature makes the treatment parallel to Bremsstrahlung. We choose to not give the detailed expression for the timescale, but we follow [104] to note that double Compton scattering is faster in producing the Planck spectrum. In fact, both have nearly the same frequency dependence, but Bremsstrahlung is more relevant for rarefied photon gases and matter-dominated plasmas. Conversely, double Compton scattering becomes more important at higher electron-temperatures and for radiation-dominated plasmas [104].

Nevertheless, in our simulation of the extened Kompaneets process below, we do not need the detailed implementation of the processes. Using the fact that both radiative mechanisms have "nearly" the same frequency dependence, we control in the simulations the number of photons by hand. Both processes completely dominate the lower frequency ranges, but are negligible compared to Compton scattering for higher frequencies. In the simulations of the Kompaneets process we will simply add or remove particles under a certain cutoff such that their occupation numbers always exactly correspond to the Bose-Einstein distribution for a given volume and temperature.

5.6 Extension of the Kompaneets process

It is well known that the Boltzmann equation, the traditional point of departure to obtain (5.1), may wash out certain nonequilibrium degrees of freedom of the electron bath: any isotropic distribution [8, 25, 24, 129] for the bath (which respects a mild constraint on the decay rate towards zero at infinity)[73] yields the Kompaneets equation with a suitable redefinition of the temperature.
As proposed in [73], the Kompaneets equation can be extended to include more general diffusivities and a possible driving. In the present section we directly interfere with the Kompaneets process to add nonequilibrium features to the photon process, leaving aside for a moment the specific origin. There will in fact be two main directions of nonequilibrium, effectively introduced in a generalized Kompaneets equation.

On the level of the Kompaneets equation, the nonequilibrium extension is taken to be

$$\frac{\partial n}{\partial t} = \frac{1}{x^2}\frac{\partial}{\partial x}x^4\left\{\frac{\partial n}{\partial x}(t,x) + (1+bx^k)[1+n(t,x)]n(t,x)\right\} + \frac{c}{x^2}\frac{\partial}{\partial x}x\left\{\frac{\partial n}{\partial x}(t,x)\right\} \tag{5.29}$$

parametrized by positive constants b, c and k. As before, we have changed to dimensionless variables. That makes a special case of a more general extended Kompaneets equation

$$x^2\frac{\partial n}{\partial t}(t,x) = \frac{\partial}{\partial x}x^2 D(x)\left\{\frac{\partial n}{\partial x}(t,x) + g(x)[1+n(t,x)]n(t,x)\right\} \tag{5.30}$$

for

$$D(x) = x^2 + \frac{c}{x}, \qquad g(x) = \frac{1+bx^k}{1+cx^{-3}} \tag{5.31}$$

Obviously, the case $c = b = 0$ recovers the standard Kompaneets equation.

The change in the drift where to the energy function $U(\omega) = \hbar\omega$ (for the standard Kompaneets process) an extra potential $\sim \omega^{k+1}$ is added, is motivated by the search for higher order drivings where the force may depend on the frequency. One is to change the drift, where we imagine a driving that depends on the frequency instead of a constant "force" as in the Kompaneets process. Obviously, we do not assume photon-photon scattering, which is extremely weak in vacuum [46]. The drift can however be realized by employing strong light-matter coupling, resulting in strong effective energy exchanges (and dissipation) on single-photon level [143]. In other words, we change (5.22) (or (5.25)) and replace the constant U' with a frequency-dependent force g.

A second change is to add an extra diffusion (changing (5.26)) where the diffusion constant no longer has the features of Compton scattering, but gets modified at low frequencies. By making $c \neq 0$ an extra diffusion has been added in frequency space where the diffusivity decays with frequency, certainly unlike Compton-type processes. Obviously, the dependence c/x in (5.31) should not be taken literally all the way to $x \downarrow 0$ but an appropriate cutoff will be installed in the simulation (in the next section). In general, while interested in low-frequency effects, we are not interested in the very-low frequency-behavior $x \downarrow 0$. The extra diffusive term (the last term in (5.29)) was also introduced in [6], motivated by hints of low-frequency modifications in the Planck law, as observed from ARCADE 2 data [68, 152] and EDGES experiment [39]. The idea is to drastically increase the activity of low-frequency photons, which are otherwise largely untouched in Compton scattering. Or, in other words, to decrease the activity of high-energy photons. The latter was motivated by

a mechanism similar to stochastic turbulence. One should think here of the analogue of creating suprathermal tails in electron velocity distributions by their Rutherford scattering against turbulent fields [52, 7]. From the Coulomb interaction, high energy electrons are least scattered. Similarly, low-frequency photons are least affected by Compton scattering and that allows them to become abundant by nonequilibrium effects, breaking detailed balance with respect to the Planck law.

A rearrangement is in order to rewrite (5.30) in terms of the spectral density $\rho(t,x)$, defined in the exact same way as (5.5), yielding

$$\frac{\partial}{\partial t}\rho(t,x) = -\frac{\partial}{\partial x}\left[\left(2\frac{D(x)}{x} + \partial_x D(x) - D(x)g(x)\left(1+n(t,x)\right)\right)\rho(t,x)\right] + \frac{\partial^2}{\partial x^2}[D(x)\rho(t,x)] \quad (5.32)$$

Note the stimulated emission with the occupation number density $n(t,x)$; of course we can subsitute the spectral density from (5.5). Yet is numbers that matter, not probability.
Observe that (5.30) remains a continuity equation, photon-number preserving just like Kompaneets. It means that Z_t in (5.5) for the density of the nonequilibrium extension (5.30) is also a time-independent prefactor, depending only on the environment temperature and the (constant) number of photons per volume.
Interpreting similarly as before the above equation as a Fokker-Planck type equation, we find the associated Langevin equation in the Itô-interpretation

$$\dot{x} = 2\frac{D(x)}{x} + \partial_x D(x) - D(x)g(x)\left(1+n(t,x)\right) + \sqrt{2D(x)}\,\xi_t \quad (5.33)$$

where ξ_t is a standard white noise as before. According to (5.23), we have in this case

$$B(x,\rho_t) = 2\frac{D(x)}{x} + \partial_x D(x) - D(x)g(x)\left(1+n(t,x)\right) \quad (5.34)$$

with drift and diffusion given by expression (5.31), and $n(t,x)$ derived from $\rho(t,x)$ as before.

To be compared with (5.21), the above equation defines the *extended Kompaneets process* and makes our second main result: it is the fluctuating single-photon dynamics that takes into account physically interesting nonequilibrium features.

Note that a stationary solution to (5.29) can be found, of the form

$$n_{\rm st}(x;b,c;k) = \frac{1}{\exp\left(\int_{x_0}^{x} {\rm d}s\, \frac{1+bs^k}{1+cs^{-3}}\right) - 1} \tag{5.35}$$

where x_0 is the cutoff for the extra diffusion, as we expect for a realistic situation. That solution is only valid for $x > x_0$. For $x \leq x_0$ the details of the cutoff should enter in the exponent as to make $n_{\rm st}$ well defined. When adding radiative processes to (5.32) at low frequencies such as Bremsstrahlung (see Section 5.5), the stationary solution differs from (5.35) as well.

5.7 Simulation of the extended Kompaneets process

Simulations of these extended processes are straightforward, we repeat the algorithm of Section 5.4, but with different functions B and D. Furthermore, we perform an *ad hoc* implementation of Bremsstrahlung and double Compton scattering, by simply clamping the occupation numbers of the lowest frequencies to the Planck distribution, as explained in Section 5.5. Specifically, we look at the lowest 1% of the frequency range, which in our case consists of the lowest two bins, and compare the empirical occupation number with value expected from the Planck distribution. In case there is an excess, the surplus amount of particles are randomly chosen and removed from the simulation. On the other hand, if there is a deficit, particles are added, randomly distributed over the bin, to make up the difference.
Notice that as particles are being added to or removed from the ensemble, the value of Z will change, i.e, it becomes time-dependent $Z = Z_t$.
In the following subsections we separate the influence of b and c in (5.31); indeed we estimate it is interesting to study their influence separately and the physical mechanisms underlying their presence.

5.7.1 Adding low-frequency diffusion

We first take $c = 0.1$, leaving $b = 0$ in (5.31). A spurious difficulty arises for nonzero c, as the given diffusion and drift coefficients diverge near the origin. To remedy this, we implement a cutoff x_0 in the simulation, which we take to be 0.1 (i.e. 1% of the relevant frequency range), where the extra diffusion term is taken to go linearly to zero as x goes below this cutoff, as it is nonphysical for the activity to remain the same all the way to zero frequency anyway.

Simulating with initially 2×10^5 particles, Fig 5.5 shows the resulting frequency histogram of the simulation for a total time $\simeq 5$ with the black solid line

corresponding to (almost) stationarity. Deviations from the dashed Planckian distribution are evident, with an abundance of low-frequency photons, but keeping the Planck-shape at larger frequency. Together with the extra diffusivity, we implement reactive mechanisms. That makes the behavior below the cutoff frequency x_0 similar as if we were to turn off the extra diffusive term, i.e, to make $c = 0$ for $x < x_0$. With that in mind we define

$$h(x) = \int_0^x \mathrm{d}x' \begin{cases} \frac{1}{1+c/x'^3} & \text{for } x' > x_0 \\ 1 & \text{for } x' < x_0 \end{cases}.$$

Then, the stationary distribution appears very well described as

$$n_{\rm st}(x) = \frac{1}{\exp(h(x)) - 1} \tag{5.36}$$

as is tested in Fig. 5.5. That theoretical density would correspond to $Z = 1.82$, which is however not the value $Z \approx 1.73$ that is found in the simulation. This is not surprising since the addition of reactive processes should make the stationary distribution slightly different at low frequencies.

We define an effective temperature $T_{\rm eff}(x)$ as a function of the frequency, derived from the empirical occupation number at this frequency by inverting the Planck distribution,

$$n_{{\rm Pl},T_{\rm eff}}(x) = \frac{1}{\exp(x/T_{\rm eff}) - 1} \tag{5.37}$$

Because of our choice of units, this will be expressed as a ratio to the temperature of the background electron gas. Fig. 5.6 plots this effective temperature for the stationary distribution.

5.7.2 Adding frequency-dependent drift

Taking now a non-zero driving in (5.31), we set $b = 0.1$ and $k = 0.4$, keeping $c = 0$. A marked deviation from the Planck law becomes visible. It is also interesting to note a remarkable feature for $b \neq 0$, which is the formation of a condensate around $x = 0$. However, the low-frequency reaction mechanism (either double Compton or Bremssthralung) is able to absorb the condensate. In fact, the appearance of that condensate can be explained by looking at the stochastic equation (5.33), where the extra drift coming from $g(x)$ contributes in the stimulated emission term, making shifts towards negatives values of frequency more frequent.

Here, in contrast with the diffusive addition in Fig. 5.5, high frequencies get much more affected.

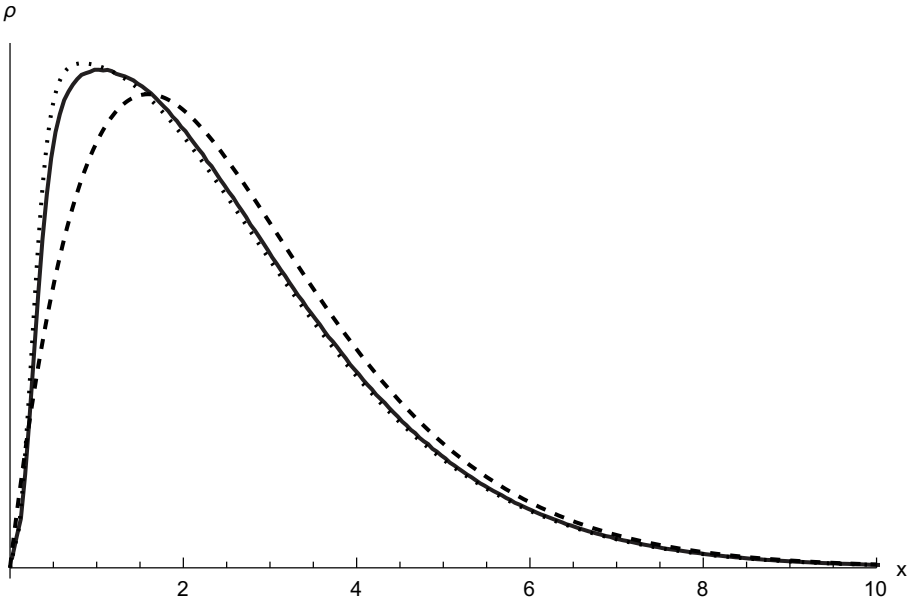

Figure 5.5: Solid line corresponds to the simulation of (5.33) using (5.31) for $c = 0.10, b = 0$. The dashed line is the Planck law. The dotted line depicts the supposed stationary distribution (5.36).

5.8 Conclusions

The present paper achieves to construct photon processes in frequency space dominated by Compton scattering. The stimulated emission produces the nonlinearities. From the single-photon stochastic process, we enter the realm of time-dependent fluctuation phenomena for photon dynamics. It implies we can start exploring nonequilibrium photon dynamics, much in the tradition of stochastic dynamics for open particle systems. We have explored the addition of nonequilibrium drift and diffusion terms which affect mostly the low-frequency part in a modified Planck spectrum.

Various applications can be envisaged, subject of future studies, while the present paper sets the mathematical and simulational structure of the photon diffusion process. Despite the appearance of nonlinearities, due to stimulated emission, which makes a nontrivial aspect, we simulate this process using traditional algorithms for stochastic equations and conclude that relaxation to the equilibrium Planck law can be reliable simulated, as seen in Fig. 5.2. The

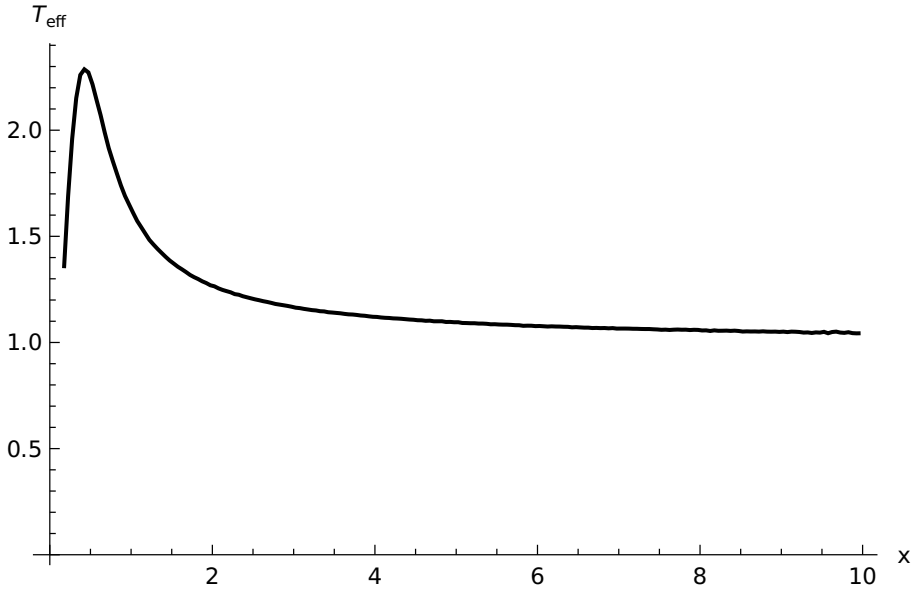

Figure 5.6: Profile of effective temperature corresponding to Fig. 5.5 and defined in (5.37). The very-low frequency regime is dominated by the *ad hoc* cutoff and procedures replacing Bremsstrahlung and double Compton scattering, as explained in the text. For low frequency $1 < x < 5$ the effective temperature is significantly higher than the Planck-value.

nonlinearity is satisfactorily dealt by considering an ensemble of processes while using histograms to construct the empirical spectral density of photons at each time step. Physical processes such as Bremsstrahlung and double Compton can also be easily included by an *ad hoc* procedure we describe in Section 5.5. It means to continuously set, below some cutoff frequency, the density of photons to its corresponding value in the Planck spectrum, under the argument that low-frequency photons rapidly thermalize via reactive mechanisms.

The Z parameter can be tuned as to make the stimulated emission weaker and convergence to a Wien-like spectrum is observed in the simulations; see Fig. 5.3. In fact, this would correspond to a rarefied photon gas, where stimulated emission is expected to become less important. On the other hand, detailed balance with respect to Planck's law is broken by considering the extension to the Kompaneets equation. There, nonequilibrium drift and diffusion make extra contributions to the standard equation for the single-photon process. The proposed extension (5.29) is parameterized by the values b, c and k, such that $b = c = 0$ corresponds

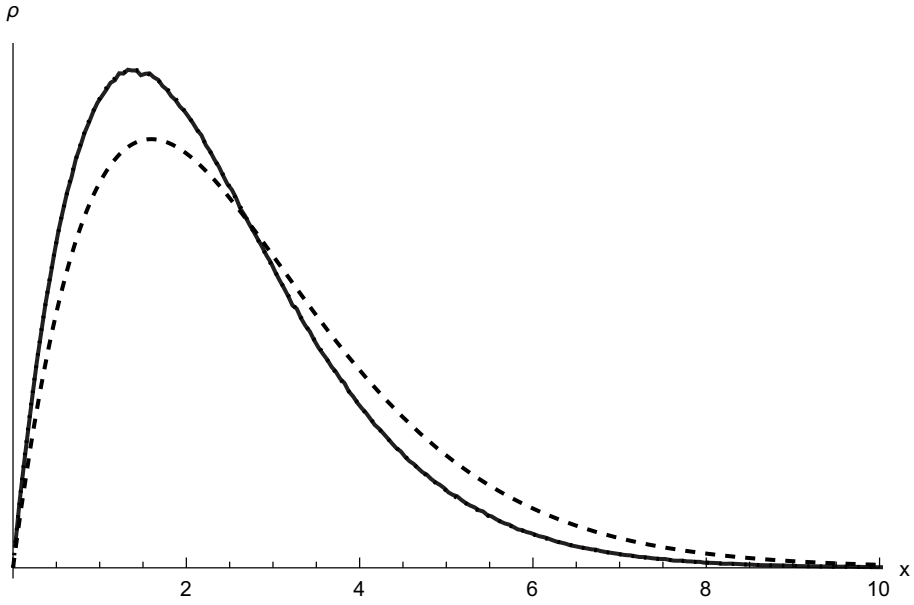

Figure 5.7: Stationary density profile when adding the frequency-dependent drift with $b = 0.1$ and $k = 0.4$, keeping $c = 0$ in (5.31). Again a deviation is seen from the Planck law (dashed line), with the simulation almost completely overlapping with the stationary solution.

to the standard Kompaneets process (5.21). The simulation results, Figs. 5.5 and 5.7, show that, for the values of parameters considered, modifications to the Planck law that ultimately lead to higher occupancy in the low-frequency part of the spectrum are seen. Those modifications match very well with the theoretical stationary solution (5.36), but slight deviations are expected due to the inclusion of reaction mechanisms.

From the mathematical point of view, the derivation of the Kompaneets process is interesting and challenging. It appears to open a new theme in the domain of nonlinear Markov diffusions [71].

Let us finish by emphasizing that the proposed mechanisms remain conjectural and that the theory is largely phenomenological. A follow-up can be found in [75], where a resetting mechanism is added to the Kompaneets process corresponding to random abrupt Doppler shifts to the low frequency regime.

5.A Itô's lemma and the Kompaneets process

Suppose we have a (possibly) time-dependent function of the random variable $\mathbf{X}_t$

$$f = f(t, \mathbf{X}_t)$$

then, f itself is a random variable. Suppose also that $\mathbf{X}_t$ follows the stochastic differential equation

$$\dot{\mathbf{X}}_t = \mathbf{B}(\mathbf{X}_t) + \mathbf{Q}_t(\mathbf{X}_t)\boldsymbol{\Xi}_t$$

where $\boldsymbol{\Xi}_t$ is a three-dimensional white noise as before.

Then, Itô's lemma states that f satisfies the stochastic differential equation

$$\dot{f}(t, \mathbf{X}_t) = \frac{\partial f}{\partial t} + (\nabla_{\mathbf{X}} f) \cdot \mathbf{B} + \frac{1}{2}\mathrm{Tr}\left[\mathbf{Q}_t^T \left(H_X f\right) \mathbf{Q}_t\right] + \left(\nabla_{\mathbf{X}} f\right)^T \mathbf{Q}_t \, \boldsymbol{\Xi}_t \quad (5.38)$$

where the positive $d \times d$ matrix $\mathbf{Q}_t$ is such that the diffusion tensor

$$\mathbf{D} = \frac{1}{2}\mathbf{Q}_t\mathbf{Q}_t^T$$

and H_X is the Hessian matrix with respect to $\mathbf{X}_t$.

We use that to show in more detail the derivation of equation (5.21). We begin with the i-th generator in (5.15)

$$\frac{1}{\delta^2} L_{i\delta} F(\mathbf{K}) = D(\mathbf{k}_i)(1 + n_{\mathbf{k}_i}(\mathbf{K}))\Delta_{\mathbf{k}_i} F(\mathbf{K}) + \sum_{\mathbf{a}} \Bigg\{ \Bigg(\frac{1}{2}\mathbf{a} \cdot \nabla_{\mathbf{k}} D(\mathbf{k}_i)$$

$$- \frac{\beta}{2} D(\mathbf{k}_i)\mathbf{a} \cdot \nabla_{\mathbf{k}} U(\mathbf{k}_i) \Bigg)(1 + n_{\mathbf{k}_i}(\mathbf{K})) + D(\mathbf{k}_i)\, \mathbf{a} \cdot \nabla_{\mathbf{k}} n \Bigg\} \mathbf{a} \cdot \nabla_{\mathbf{k}_i} F(\mathbf{K}) \quad (5.39)$$

which leads by applying the steps (5.16)–(5.19) to the Itô process for the i-th photon

$$\dot{\mathbf{k}}_{\mathbf{i}t} = \nabla_{\mathbf{k}} D(\mathbf{k}_{\mathbf{i}t}) - \beta D(\mathbf{k}_{\mathbf{i}t})\, \nabla_{\mathbf{k}} U(\mathbf{k}_{\mathbf{i}t})(1 + n_{\mathbf{k}_{\mathbf{i}t}}(\mathbf{K})) + \sqrt{2D(\mathbf{k}_{\mathbf{i}t})}\, \boldsymbol{\Xi}_t \quad (5.40)$$

In order to simplify notation, we will opt to not differentiate the quantities from their dimensionless counterpart, therefore, it should be noted that all quantities appearing here are dimensionless. In particular, we shall identify the photon energy with its dimensionless version

$$\beta U(\omega_i) \to U(x_i) = x_i$$

We apply Itô's lemma for

$$f(\mathbf{k_i}) = |\mathbf{k_i}|.$$

A simple calculation yields

$$\nabla_{\mathbf{k_i}} f = \frac{\mathbf{k_i}}{|\mathbf{k_i}|}$$

$$H_{\mathbf{k_i}} f = \begin{pmatrix} \frac{1}{|\mathbf{k_i}|} - \frac{{k_{ix}}^2}{|\mathbf{k_i}|^3} & & \\ & \frac{1}{|\mathbf{k_i}|} - \frac{{k_{iy}}^2}{|\mathbf{k_i}|^3} & \\ & & \frac{1}{|\mathbf{k_i}|} - \frac{{k_{iz}}^2}{|\mathbf{k_i}|^3} \end{pmatrix}$$

recall from (5.40) that

$$\mathbf{B}(\mathbf{k_i}) = \nabla_{\mathbf{k}} D(\mathbf{k_i}) - D(\mathbf{k_i}) \nabla_{\mathbf{k}} U(\mathbf{k_i})(1 + n_{\mathbf{k_i}}(\mathbf{K}))$$

$$\mathbf{Q}(\mathbf{k_i}) = \sqrt{2D(\mathbf{k_i})}\, \mathbf{I}_{3\times 3}$$

Therefore, we can easily find all terms in Itô's lemma (5.38)

$$\begin{cases} \partial_t f = 0 \\ (\nabla_{\mathbf{X}} f) \cdot \mathbf{B} = \frac{\mathbf{k_i}}{|\mathbf{k_i}|} \cdot (\nabla_{\mathbf{k}} D(\mathbf{k_i}) - D(\mathbf{k_i}) \nabla_{\mathbf{k}} U(\mathbf{k_i})(1 + n_{\mathbf{k_i}}(\mathbf{K}))) \\ \frac{1}{2} \mathrm{Tr}\left[\mathbf{Q}_t^T \left(H_X f\right) \mathbf{Q}_t\right] = 2 \frac{D(\mathbf{k_i})}{|\mathbf{k_i}|} \\ \left(\boldsymbol{\nabla}_{\boldsymbol{X}} f\right)^T \mathbf{Q}_t = \sqrt{2D(\mathbf{k_i})}\, \frac{\mathbf{k_i}}{|\mathbf{k_i}|} \end{cases}$$

we substitute back in (5.38) and write quantities in terms of the dimensionless frequency $\mathbf{k_i} = x_i\, \hat{\mathbf{x}}_\mathbf{i}$. Repeating the process for $i = 1, \ldots, N$, taking the sum and the continuum limit for the generator in frequency space similarly than done in steps (5.15)–(5.19) we find (5.21).
Applying directly Itô's lemma for a nonlinear Markov diffusion is not needed here, but is another mathematical question that is raised by the Kompaneets process.

5.B Data availability statement

The data and software that support the findings of this study are openly available on GitLab[115].

But know this, friend of mine.
Ya ever reset, I'll be swingin' by
again for a little chat with ya.

Mr. Resetti

6

Resetting photons

Abstract

Starting from a frequency diffusion process for a tagged photon which simulates relaxation to the Planck law, we introduce a resetting where photons lower their frequency at random times. We consider two versions, one where the resetting to low frequency is independent of the existing frequency and a second case where the reduction in frequency scales with the original frequency. The result is a nonlinear Markov process where the stationary distribution modifies the Planck law by abundance of low-frequency occupation. The physical relevance of such photon resetting processes can be found in explorations of nonequilibrium effects, e.g., via random expansions of a confined plasma or photon gas or via strongly inelastic scattering with matter.

This chapter was first published in [75], together with G.E. Freire Oliveira and C. Maes. The author of this thesis extended the simulations, drew the figures and contributed to the writing of the manuscript.

6.1 Introduction

Since its original conception in [169, 63, 61, 62], resetting has been introduced and added to diffusion processes for a variety of reasons. Typically, optimizing

search strategies has been the underlying motivation, but one can also imagine physical resettings. By the latter we mean the result of a time-dependent potential, for which there are random moments of confinement, or the random appearance in certain locations of attractors, or the random contraction/expansion of an enclosed volume. In the present paper, we investigate a new scenario where resetting is applied in frequency space of photons. In that way we explore physically motivated nonequilibrium effects on the Planck distribution, while also adding physical substance to the application of resetting for nonlinear diffusions, [37].

Resetting photons to a lower frequency refers to reducing the wave vector (in the reciprocal lattice), which, in real space, refers to an expansion. One physical mechanism we can imagine here is that of a confined plasma where the confinement is continually lifted at random moments. On the other hand, repeated inelastic scatterings of photons inside a cavity with the electrons in the wall can also provide a source for resetting behavior. We can picture that photons instantaneously lose their energy to electrons, which is rapidly dissipated to an external bath.

Mathematically, the photon frequency resetting may take various forms: we focus on a resetting in terms of a Doppler shift where the frequency gets divided $\omega \to \omega/d$ by some number d (divisor). We can imagine however (and we will introduce) other resetting procedures corresponding to different physical mechanisms, but they yield pretty much the same effects, as we will see. To avoid condensation of the photons at zero momentum, we apply a thermal push-back: when the tagged photon reaches zero frequency, it is redistributed following the Planck law. That may be due to other sources of black-body radiation but here is used only to conserve total photon number, creating a current in frequency space. The resetting is restricted to low-frequency values which is related to our major physics motivation; to explore possible deviations to the Planck law from random and abrupt expansion of a plasma or photon gas.
To incorporate that resetting of photon frequency ω, we use a nonlinear Markov process for a tagged photon in a plasma where the main mechanism is Compton scattering. (Other radiation processes are easily added but are not considered here.) The nonlinearity of the Markov process follows from the stimulated emission, a quantum feature, and the corresponding (nonlinear) Fokker-Planck equation is the well-known Kompaneets equation [99]. The latter describes relaxation to the Planck radiation law, $\propto \omega^3/(\exp[\hbar\omega/(k_BT)] - 1)$. In certain cases however, e.g. for photons inside optomechanical cavities, while resetting the frequency still makes sense, Compton scattering plays a minor role. Still we stick for convenience to the setup where the radiation relaxes to thermal

equilibrium within the context of the Kompaneets equation. For cosmological applications, e.g. in the primordial plasma, an erratic expansion of the universe has not been contemplated before (leading to a stochastic Doppler shift of photon frequency) but the Kompaneets equation is the standard tool there [129].

In the next section we recall the elements of the Kompaneets process (without resetting) in the context of elastic Compton scattering with thermal electrons. In Section 6.3 we introduce the resetting mechanisms and their physical motivation. The simulations are discussed in Section 6.4 and we obtain nonequilibrium photon distributions. The abundance at low frequencies is not surprising, but interesting for understanding possible scenarios of breaking the Planck distribution of the cosmic microwave background, while preserving almost perfectly the moderate to larger frequency regime of the Planck law. More (speculative) conclusions and possible applications are presented in the final Section 6.5.

6.2 The Kompaneets process

As reference process we consider a fluctuation dynamics which realizes the Kompaneets equation as its nonlinear Fokker-Planck equation. In fact, that process was recently introduced in [74], but here we briefly revisit the setup.

6.2.1 Kompaneets equation

Relaxation towards equilibrium of a photon gas in contact with a nondegenerate, nonrelativistic electron bath in thermal equilibrium at temperature T can be achieved via Compton scattering. Starting from the semi-classical Boltzmann-Uehling-Uhlenbeck equation for a dilute plasma, Kompaneets arrived at an equation for the (average) occupation number $n(\tau,\omega)$ at frequency ω of the photon gas at time τ, [99]:

$$\omega^2\frac{\partial n}{\partial \tau}(\tau,\omega)=\frac{n_e\sigma_T c}{m_e c^2}\frac{\partial}{\partial\omega}\omega^4\left\{k_BT\frac{\partial n}{\partial\omega}(\tau,\omega)+\hbar\left[1+n(\tau,\omega)\right]n(\tau,\omega)\right\} \qquad (6.1)$$

The constant σ_T is the Thomson total cross section, and n_e, m_e are the density and mass of the electrons, respectively. The mc^2/k_BT multiplier to the timescale expresses that electrons are slow-moving and so the average collision barely shifts a photon's frequency. That is what allowed Kompaneets to make a diffusion approximation to the Boltzmann-equation; see [73] for more details.

The ω^2- dependence (hidden in the ω^4) is due to the fact that the frequency shift is proportional to the frequency itself, implying that the variance on the shift goes like ω^2. The induced Compton scattering due to stimulated emission, [103, 14], is present in the nonlinearity of the drift term, which is the second term in (6.1). Its origin is that the photon carries momentum proportional to its frequency. A more statistical-mechanical perspective and microscopic derivation of (6.1) is presented in [73].

An important point is made by noting that the Kompaneets equation (6.1) implements only the Compton interaction to write the dynamics for $n(\tau, \omega)$. That has its own approximations and restrictions. As it is usually the case with differential evolution equations in physics, if we include other mechanisms, such as Bremsstrahlung or double Compton interaction, their contribution is independent of the Compton interaction and appears only additively in (6.1) (see e.g. [99, 104]). The same happens when adding resetting to low-enough frequencies, but we now think of Doppler shifts by metric or cavity expansion.

Stationarity is achieved when $n(\tau, \omega)$ becomes the Bose-Einstein distribution with chemical potential μ,

$$n_{\rm BE}(\omega) = \frac{1}{e^{\beta(\hbar\omega - \mu)} - 1}, \qquad \beta = \frac{1}{k_B T}$$

The Kompaneets equation yields a good understanding of the dynamical origin of the cosmic microwave background and of the related Sunyaev-Zeldovich effect [164, 165]. Excellent reviews include [154, 72, 180]. Extensions and generalizations are e.g. obtained in [27, 135, 8, 25, 84, 85, 44, 122, 124, 123, 73].

To have a dimensionless Kompaneets equation we use $x = \hbar\omega/k_B T$, to rewrite (6.1) as

$$x^2 \frac{\partial n}{\partial t}(t, x) = \frac{\partial}{\partial x} x^4 \left\{ \frac{\partial n}{\partial x}(t, x) + [1 + n(t, x)]\, n(t, x) \right\} \tag{6.2}$$

The time-variable τ has also changed into the dimensionless Compton optical depth

$$t = n_e\, \sigma_T\, c \frac{k_B T}{m_e c^2}\, \tau \;\coloneqq \frac{\tau}{\tau_C}$$

There, τ_C is related to the Doppler shift, having

$$\left\langle \frac{1}{2\tau_c} \left(\frac{\Delta\omega}{\omega} \right)^2 \right\rangle \approx \frac{k_B T}{m_e c^2} n_e \sigma_T c \coloneqq \frac{1}{\tau_C} \tag{6.3}$$

for its variance, where the collision time $\tau_c = \ell/c$ is obtained from the mean free path of photons $\ell = (n_e\sigma_T)^{-1}$. In the expression above, the average is taken with respect to the distribution of electrons.

As it stands written the Kompaneets equation(6.2) is expressed in function of the occupation number $n(t,x)$, which is a unitless quantity quite literally counting the average number of photons present in a given wave-mode. For our purposes, the equation must be written for the photon density $\rho(t,x)$ instead. This entails multiplying the occupation number by the density of states, followed by a normalization through division by the total number of photons N. The spectral probability density for photons in a box of volume V with periodic boundary conditions will then equal (see [74])

$$\rho(t,x) = \frac{V}{N}\frac{1}{\pi^2}\left(\frac{k_BT}{\hbar c}\right)^3 x^2 n(t,x). \tag{6.4}$$

In terms of the photon spectral density (6.4), the Kompaneets equation (6.2) becomes

$$\frac{\partial\rho}{\partial t}(t,x) = -\frac{\partial}{\partial x}\left[\left(4x - x^2\left(1 + 2\zeta(3)\,\frac{\rho(t,x)}{x^2}\right)\right)\rho(t,x)\right] + \frac{\partial^2}{\partial x^2}\left[x^2\rho(t,x)\right] \tag{6.5}$$

When $n(t,x) = n_{\mathrm{BE}}(x) = 1/(\exp(x)-1)$ (Planck law) the photon number N equals

$$N_{\mathrm{BE}} = 2\zeta(3)\frac{V}{\pi^2}\left(\frac{k_BT}{\hbar c}\right)^3$$

with $\zeta(3) = 1/2\int_0^\infty \mathrm{d}x\, x^2/(e^x-1) \simeq 1.202$, and the spectral probability density is $\rho_{\mathrm{BE}}(x) = \frac{x^2\, n_{\mathrm{BE}}(x)}{2\zeta(3)}$, the stationary equilibrium solution to (6.5).

6.2.2 Tagged photon stochastic process

The Kompaneets equation is positivity preserving, [94]. It allows therefore a probabilistic interpretation as nonlinear Fokker-Planck equation. That was explicitly realized in [74], and we refer to the corresponding stochastic dynamics of a tagged photon as the Kompaneets process.
A more general tagged photon diffusion process is, in Itô-convention,

$$\dot{x} = B(t,x,n_t) + \sqrt{2D(x)}\,\xi_t \tag{6.6}$$

where ξ_t is standard white noise and

$$B(t,x,n_t) = 2\frac{D(x)}{x} + D'(x) - \beta D(x)U'(x)(1+n(t,x))$$

is the drift term. Note, from the last term, that we need to know the particle number $n(t, x)$ to update the dimensionless frequency x following (6.6). The Itô–stochastic process (6.6) is our Kompaneets process in the case where

$$\beta U(x) = x, \qquad D(x) = x^2$$

Note also that $x \geq 0$. Even without explicit boundary conditions, there is however no probability flux through the origin $\omega = 0$, meaning that negative frequencies are not observed in the simulations. We therefore in the present work ignore the detailed implementation of radiative processes such as *Bremsstrahlung* or double Compton scattering that in real nature control the photon number density, picking up and absorbing photons with low-enough frequencies.

As an illustration of the soundness of the process, we reproduce here in Fig. 6.1 the results obtained from the simulation of the stochastic equation (6.5) using the Euler-Maruyama algorithm [172]. To implement stimulated emission, which makes a nontrivial aspect both in the simulation and theory, we consider an ensemble of N processes, using the empirical histogram of frequencies to update the drift term at each timestep accordingly. The details of the implementation including reactive mechanisms together with a more comprehensive discussion can be found in [74]. From Fig. 6.1 we see the relaxation towards the Planck law, confirming the validity of the implementation scheme.

6.3 Resetting the Kompaneets process

We start from the Kompaneets process (6.6) defined in the previous section and add Poissonian resetting with a constant rate. The resetting rate is denoted by $r > 0$. Three methods are introduced for resetting, the so-called "division" method, where the energy of the photon is divided by a constant factor d, the "uniform" method, where the photon's energy is reset to a random value uniformly distributed between 0 and a cutoff x_0, and finally the "exponential" method, where the new energy of the photon follows an exponential distribution with scale $1/\lambda_0$. Similar choices of resetting positions have been considered before; see for example [61, 21].

For a justification of introducing such a resetting of the photon frequency, we suggest two possibilities. A first one is imagining a discontinuous expansion of the Universe, on top of the usual and smooth expansion predicted by the highly symmetric Friedmann–Lemaître–Robertson–Walker (FLRW)–solution of the Einstein field equations. From the beginning of the lepton epoch (where

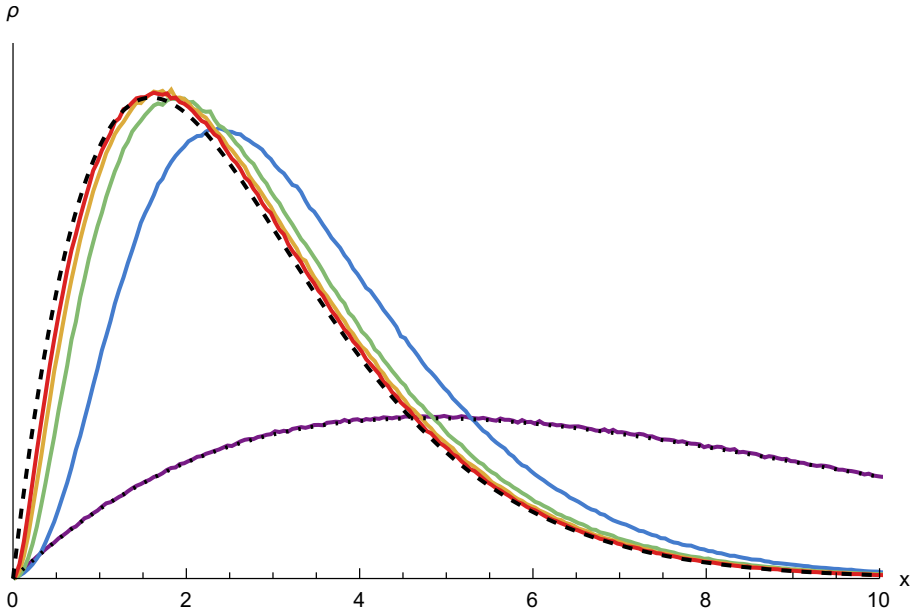

Figure 6.1: Frequency distribution for the Kompaneets process for $t = 0.0, 0.5, 1.0, 1.5$ and 2.0. The initial condition is a "hot Planck Law" at a temperature three times the temperature T used in the dynamics, corresponding to the rescale $x \to x/3$ of the dimensionless frequency. There is a fast pre-thermalization for the moderate and high frequencies, followed by a slower relaxation at the lower frequency scale. See more details in [74].

leptons dominated the mass of the Universe) to the time of recombination (when photons decoupled from matter), space has expanded a millionfold, and from recombination until now the scale factor has increased by another factor of one thousand. In the FLRW–solution, this scale factor has risen continuously and homogeneously. Moving away from this highly idealized FLRW–scenario, we can imagine indeed more localized, abrupt increases, applying only to a fraction of photons. As a photon's frequency is inversely proportional to the scale factor, that in effect is a division of photon frequencies by some large factor at random times. The process is reminiscent of the Doppler shift in frequency, and in fact mathematically and conceptually that is identical to that of Doppler shifts from expanding matter. The metric expansion of space and the Doppler effect amount to the same thing concerning frequency shift.
In this regard a second motivation exists, which might be experimentally feasible.

There we suggest to consider a cavity with randomly, quickly receding walls. Any photon catching up to these walls would again undergo a downwards shift in frequency. It would be interesting to see how the nonequilibrium frequency distribution starts to deviate from the Planck Law. Interestingly, Fermi in 1949, [66], considered the opposite scenario for understanding the origin of high-energy cosmic rays. He suggested that relativistic particles would accelerate by means of their collision with interstellar clouds that move randomly and act as 'magnetic mirrors'. The average energy gain is proportional there to $(v_c/v_p)^2$ where v_c is the speed of the cloud and v_p the speed of the particle. That is similar to the loss in energy of our photons due to the low-frequency resetting. Related to all that is our reason to reset to lower frequencies only; we look at abrupt expansion of the plasma or gas. Yet, as a matter of fact, if we were to reset the photons to larger frequencies, the average frequency could be much larger than k_BT, which disagrees with the assumptions needed for the derivation of the Kompaneets equation. That is not a problem in our case, since we reset photons to lower frequencies.

The above suggests that the frequency of the photon be updated by the following stochastic rules: in an infinitesimal interval $\mathrm{d}t$ we have

$$x(t+\mathrm{d}t) = x(t) + B(t,x,n_t)\,\mathrm{d}t + \sqrt{2D(x)\,\mathrm{d}t}\;\xi_t \tag{6.7}$$

with probability $1 - r\,\mathrm{d}t$, and

$$x(t+\mathrm{d}t) = \begin{cases} x(t)/d & \text{“division” method} \\ x \sim \mathrm{Uniform}(0,x_0) & \text{“uniform” method} \\ x \sim \mathrm{Exp}(\lambda_0) & \text{“exponential” method} \end{cases} \tag{6.8}$$

with probability $r\,\mathrm{d}t$.

The resetting protocol, therefore, requires the specification of two parameters: the resetting rate r, which controls the strength of resetting, i.e., larger r produces larger population of reset photons in the stationary distribution; and the protocol parameter $\{d, x_0, \lambda_0\}$, which controls the range in frequency space where the reset photon is placed. In that sense, the protocol parameter, acts similarly to a “cutoff”. It is natural to choose $r \leq 0.1$ as the Kompaneets process has itself a relaxation time of order one, which is one order faster then. It is also observed in the present work that the effects of resetting are negligible in the stationary distribution when $r \lessapprox 10^{-3}$ for the range of other parameters considered here.

We avoid condensation of photons at zero frequency by a thermal push-back. In other words, whenever the tagged photon reaches zero frequency, it is getting a

new frequency distributed according to the Planck law. In that way, we create a frequency current, where the resetting drives to lower frequency and the thermal push-back induces higher frequencies (when needed). As physical realization of that thermal push-back we may imagine other sources of black-body realization that supplement the photon gas to keep the same photon number and reach a stationary (nontrivial) distribution.

As a final remark, we emphasize that most studies of stochastic resetting consider linear diffusion processes as they allow analytic treatments. Our diffusion process is nonlinear as even the Fokker-Planck equation is nonlinear in the probability density, and on a fundamental level. So far, [37] is the only other reference in the literature. In our case the nonlinearity has a specific physical origin which is the (quantum feature of) stimulated emission (for photons). In the above, we have chosen for a fluctuation approach, allowing simulation. In principle, we could also consider a perturbative approach. In fact, the linearized Kompaneets equation considered as a regular Fokker-Planck equation has a kernel which is exactly known; see [121]. While that linear-Kompaneets scenario can be regarded as a valid regime when considering very low temperatures for the electron bath, we deal with a case where the nonlinearity is so strong that the perturbative approach would not be so relevant. At any rate, simulation is also giving a more robust method. After all, resetting is an idealization and as usual in physics and their experiments, validity and relevance are functions of energy, length- and time-scales, which, here and elsewhere, is important to realize in moving from theory to experiment.

6.4 Simulation results and discussion

To simulate these dynamics, we revisit the procedure from [74]. We consider an ensemble of 10^7 particles, which are binned in frequency space with a width of 10^{-3}. We run the simulation until $t = 10$, with a timestep Δt of 10^{-3}. Adding to this, at every timestep and for every particle, we perform the resetting step with a probability $r\Delta t$; see (6.7). The timestep Δt is chosen such that this product is much smaller than 1, making sure that the probability of two resets happening to the same particle in the same timestep remains negligible.

The results of such a simulation are shown in Fig. 6.2. With the average time between resets for a given photon being much smaller than the characteristic timescale of the Kompaneets process, it comes to no surprise that the deviations from the Planck law are mostly contained around the origin. After all, as we saw also in Fig. 6.1, relaxation to the Planck law takes a time of order 1, while

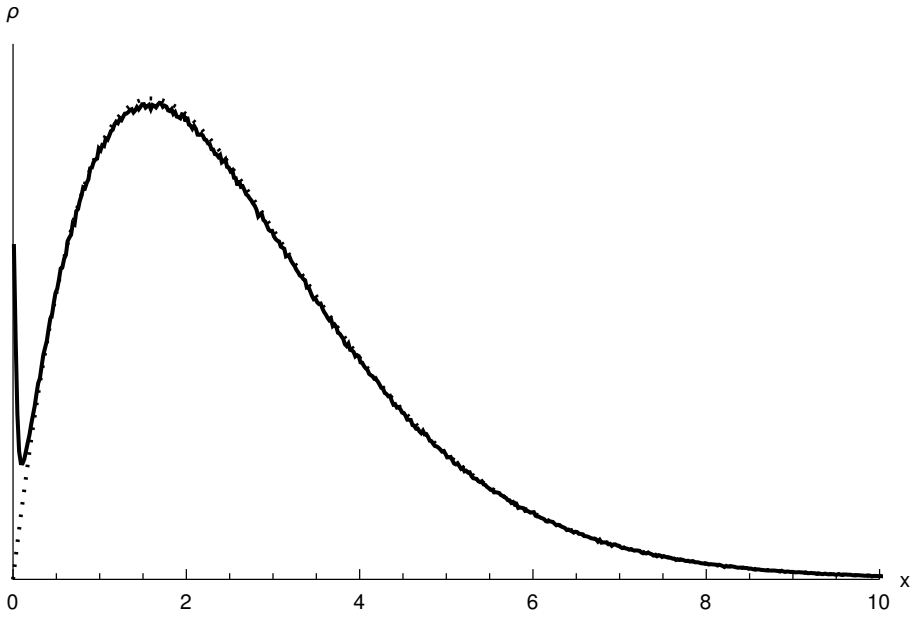

Figure 6.2: Stationary distribution for a resetting rate of $r = 10^{-2}$ and a divisor $d = 100$. For comparison, the dotted line gives the Planck distribution

the resetting rate $r \leq 0.1$. In Fig. 6.2 we see little or no difference between the resetting and no-resetting for reaching the Planck distribution at moderate to large frequencies. Therefore, in Fig. 6.4, we zoom in to the lower frequencies (where relaxation in the Kompaneets process is slowest), showing x only from 0 to 0.5 (which is about 5% of the full frequency range). From that figure, we clearly observe deviations from the Planck law in that frequency range due to resetting.

A first aspect to observe there, is that the different resetting procedures in (6.7) yield similar qualitative behavior by tuning properly the parameters $\{d, x_0, \lambda_0\}$. That happens already by simply tuning the average photon frequency under the resetting distribution to match for the different resetting protocols. According to our definitions for the "uniform" and "exponential" methods we have the following averages after many resetting events,

$$\langle x \rangle_{\rm Uni} = \frac{x_0}{2} \qquad \text{and} \qquad \langle x \rangle_{\rm Exp} = \frac{1}{\lambda_0}$$

while for the "division" protocol, because the timescale of resetting is smaller than the timescale of the relaxation towards the Planck law, we can to a high degree of accuracy assume the photon right before resetting to be distributed according to the Planck distribution, which gives it an average frequency of

$$\langle x\rangle_{\text{Planck}} = \int_0^\infty \mathrm{d}x\, x\rho_{\text{Planck}}(x) \approx 2.701$$

where the Planck distribution is $\rho_{\text{Planck}}(x) = \frac{1}{2\zeta(3)}\frac{1}{e^x-1}$. Then after many "division" resetting events, the expected photon frequency is

$$\langle x\rangle_{\text{Div}} = \frac{\langle x\rangle_{\text{Planck}}}{d}$$

If, for the same given rate, the parameters are tuned such that these first moments coincide, we may expect the different resetting protocols to produce the same behavior on average whenever

$$\langle x\rangle_{\text{Uni}} = \langle x\rangle_{\text{Exp}} = \langle x\rangle_{\text{Div}} \implies \frac{x_0}{2} = \frac{1}{\lambda_0} = \frac{\langle x\rangle_{\text{Planck}}}{d}$$

To verify that, we perform three simulations, one for each method, with a resetting rate of $r = 0.01$, and the parameters chosen such that $\langle x\rangle$ after resetting equals ≈ 0.014. We indeed observe a reasonable agreement between the simulations with those different resetting-mechanisms, as seen in Fig. 6.3.

That motivates using only one resetting protocol, which is taken to be the "division" (Doppler shift). In order to explore the effects of the various parameters, we take $r = 0.02, 0.05, 0.10, 0.20$, varying the divisor d from 25 to 400. Pictures of the frequency probability distribution at (very) low frequency are shown in Fig. 6.4.

Notice there the presence of a non-zero amount of photons at frequency zero, rejoining the Planck distribution either gradually or with a strong jump downwards first. To quantify the size of this condensate, we estimate the probability density at the origin by averaging over the 10 lowest bins (for comparison, this is 0.1% of the support of the Planck distribution). We plot the result for various rates and divisors in Fig 6.5 (log-log plots). The curves for different divisors overlap reasonably well with a power law having an exponent of 0.5.

Secondly, we observe that the intercept with the y-axis seems to be independent of the divisor d. To understand that, we calculate the Kompaneets flux $(2-x)x\rho(x) - x^2\rho'(x) - 2\zeta(3)\rho(x)^2$, to be $-2\zeta(3)\rho(0)^2$ near the origin. That has to match the resetting flux, which is simply r, implying that $\rho(0) \approx \sqrt{\frac{r}{2\zeta(3)}}$.

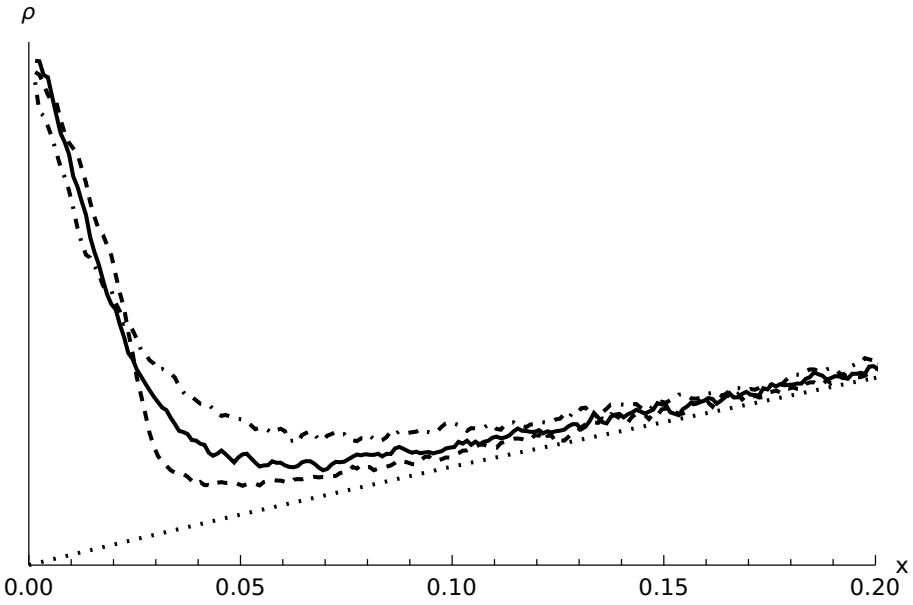

Figure 6.3: Comparison between three methods of resetting, overlaid on top of the Planck distribution (dotted straight line). The three simulations have the same resetting rate $r = 0.01$, while the resetting parameters are $d = 200$, $x_0 \approx 0.027$ and $\lambda_0 \approx 74$, all giving approximately equal first moment $\langle x \rangle \approx 0.014$.

That explains the exponent 0.5 in the curves of Fig. 6.5 and that prediction for the zero-frequency density is indeed also quantitatively close to what we observe, though it is not entirely accurate.

6.5 Conclusions

We have applied a frequency-resetting mechanism to a tagged photon undergoing Compton scattering from a thermal matter environment. The frequency is Doppler shifted at random moments by imagining a punctuated increase of the scale factor, e.g. in an FLRW-scenario with cosmic expansion "in fits and starts" applied to the primordial plasma before recombination. Alternatively, we may consider optomechanical setups where a cavity randomly and quickly expands. Strongly inelastic scattering with matter can also provide a source for resetting, but further studies on the exact mechanisms must be carried.

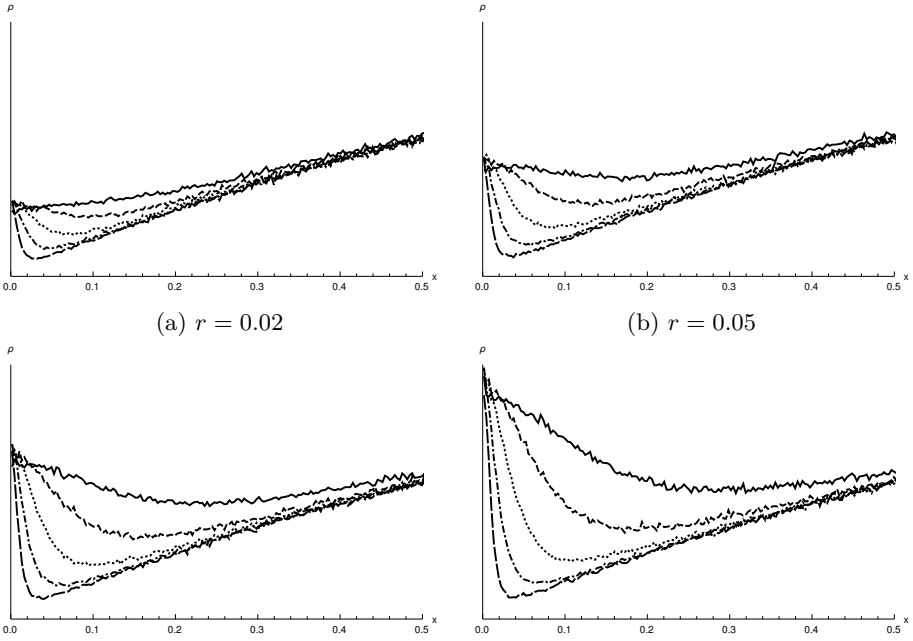

(a) $r = 0.02$ (b) $r = 0.05$

(c) $r = 0.10$ (d) $r = 0.20$

Figure 6.4: Stationary distributions at low frequencies for four resetting rates r. In each case, as the curves move down, the divisor $d = 25, 50, 100, 200, 400$.

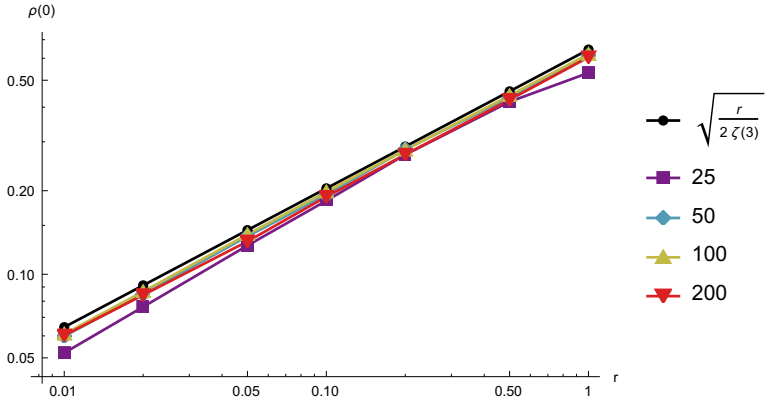

Figure 6.5: Spectral probability density at the origin in function of the rate r for various divisors d.

The result of this resetting is naturally felt mostly at low frequencies while the Planck law is almost perfectly preserved at moderate to high frequencies. It may be an observable effect for certain parameters and we feel particularly encouraged by the preliminary results of observation and analysis of the ARCADE-data; see [6, 68, 152, 39]. The jury is still out however whether deviations from the Planck law would be really there in the cosmic microwave background. Whether quantum optical experiments (in our labs on Earth) as well can reproduce the obtained predictions is an open question and exciting challenge.

Epilogue

Sometimes science is more art than science, Morty.
A lot of people don't get that.

Rick Sanchez

7

Conclusions and outlook

As we reach the final pages of this work, the time has come to gather our thoughts and reflect on what we have learned. Yet it also means to make peace with the inevitable reality that not all our expectations could have been fulfilled, and with the limitations which constrained our work. Though this can also be viewed as an opportunity to look forward to future research.

In this work we have presented a diverse range of novel advancements touching on the field of nonequilibrium statistical mechanics.

In the first Part, we start off with Chapter 2, in which we develop a quantum mechanical version of geometrodynamics through canonical quantization. For the matter sector we adopted non-relativistic uncharged point particles. The usual problem of time was obviated with the usage of de Broglie-Bohm mechanics. The final result is conceptually quite simple, presenting itself as a quantum extension of the Einstein equations, contained to a quantum contribution to the conserved energy-momentum tensor. One limitation of our research immediately presents itself, the fact that we constrain ourselves to non-relativistic particles. Furthermore, the mathematical machinery makes heavy use of functional calculus, which at our level is somewhat lacking in rigor, and is somewhat burdened by divergences. We hope that in future research these issues can be addressed. A prospective research opportunity could be to apply this model in a weak field or semi-classical approximation.

Thereafter, in Chapter 3 we investigate an unexpected link between quantum

mechanics and nonequilibrium statistical mechanics by making an analogy between the Dirac equation and active matter. Building on dynamics proposed in earlier work[158], simulations were performed to visualize the stochastic process implied by these dynamics for the first time. One particular interesting future research possibility concerns the arrival times of particles in single- and double-slit experiments[47].

Incorporating this part into our writing provides an opportunity to reflect on the title "Trajectories" of this doctoral thesis. This theme has consistently threaded through our work, to associate trajectories to particles, be they electrons or photons, deterministic or stochastic. Not only does this approach offer a means of visualization (what was called Anschaulichkeit by some physicists in the early 20th century), but it also presents didactic and methodological advantages when delving into fundamental questions of physics, including relativity and quantum mechanics. Moreover, it serves as an interesting tool for comprehending the nature of dynamical activity in nonequilibrium statistical mechanics. We think of questions related to arrival time distributions in quantum mechanics, the decomposition in massless Weyl electrons with chiral coupling (imparting mass to the Dirac electron), and even explore a quantum version of geometrodynamics in Chapter 2.

In the second Part, we discussed a novel look at a photon stochastic process, describing the relaxation towards equilibrium of a photon gas by Compton scattering with thermal electrons. Although we assumed the photons to be completely delocalized, this implies their wavelength is well-defined, and we could follow a tagged photon as it traverses its trajectory through reciprocal space.

We have presented a more justified derivation of the Kompaneets equation in Chapter 4 and presented it as a possible jumping-off point for adding nonequilibrium conditions. Subsequently in Chapter 5 we generalized the photon stochastic process to a broader framework, establishing a nonlinear Langevin dynamics of which the Kompaneets process is just one realization. These dynamics were simulated with added nonequilibrium conditions, investigating a possible resolution to the unexplained excess of the cosmic microwave background radiation at the lowest frequencies. Finally, the simulations were extended in Chapter 6 to investigate the application of stochastic resetting to photons.

Two limitations come to mind after discussing these results. For one, our approach towards radiative processes, which are especially relevant at the lower frequencies, was quite utilitarian, and their nature was not taken into account as rigorously as we would have liked. Perhaps of greater importance is the fact that we constrained ourselves to conditions characterized by plasma background, and the main mechanism of energy transfer involves Compton scattering. It

could be very interesting to take the walls of the cavity into account, with energy transfer happening either mechanically or thermally. We leave these questions open for future research.

It is our humble hope that these results can make some contribution to the understanding of nonequilibrium.

Bibliography

[1] C. Anastopoulos and B. L. Hu. A master equation for gravitational decoherence: probing the textures of spacetime. *Classical and Quantum Gravity*, 30(16):165007, July 2013. DOI: 10.1088/0264-9381/30/16/165007.

[2] C. Anastopoulos and B. L. Hu. Probing a gravitational cat state. *Classical and Quantum Gravity*, 32(16):165022, July 2015. DOI: 10.1088/0264-9381/32/16/165022.

[3] R. Arnowitt, S. Deser, and C. W. Misner. Republication of: the dynamics of general relativity. *General Relativity and Gravitation*, 40(9):1997–2027, Aug. 2008. DOI: 10.1007/s10714-008-0661-1.

[4] P. Aung and G. Puru. Non-equilibrium Thermodynamics of Glassy Systems. In *APS Ohio Sections Spring Meeting Abstracts*, APS Meeting Abstracts, P1.037, P1.037, Apr. 2011.

[5] A. Baev, P. N. Prasad, H. Ågren, M. Samoć, and M. Wegener. Metaphotonics: an emerging field with opportunities and challenges. *Physics Reports*, 594:1–60, 2015. ISSN: 0370-1573. DOI: https://doi.org/10.1016/j.physrep.2015.07.002. URL: https://www.sciencedirect.com/science/article/pii/S0370157315003361. Metaphotonics: An emerging field with opportunities and challenges.

[6] M. Baiesi, C. Burigana, L. Conti, G. Falasco, C. Maes, L. Rondoni, and T. Trombetti. Possible nonequilibrium imprint in the cosmic background at low frequencies. *Phys. Rev. Research*, 2:013210, 1, Feb. 2020. DOI: 10.1103/PhysRevResearch.2.013210.

[7] T. Banerjee, U. Basu, and C. Maes. Active velocity processes with suprathermal stationary distributions and long-time tails. *Phys. Rev. E*, 101:062130, 6, June 2020. DOI: 10.1103/PhysRevE.101.062130.

[8] D. Barbosa. A note on compton scattering. *The Astrophysical Journal*, 254:301–308, 1982.

[9] J. S. Bell. Beables for quantum field theory. In B. J. Hiley and D. Peat, editors, *Quantum Implications: Essays in Honour of David Bohm*, pages 227–234. Methuen, 1987.

[10] J. S. Bell and A. Aspect. *Speakable and Unspeakable in Quantum Mechanics*. Cambridge University Press, June 2004. DOI: 10.1017/cbo9780511815676.

[11] J. Bernstein. *Kinetic theory in the expanding universe*. Cambridge University Press, 2004.

[12] J. Bezanson, A. Edelman, S. Karpinski, and V. B. Shah. Julia: a fresh approach to numerical computing. *SIAM review*, 59(1):65–98, 2017.

[13] J. Bierkens and S. M. V. Lunel. Spectral analysis of the zigzag process. *Annales de l'Institut Henri Poincaré, Probabilités et Statistiques*, 58(2):827–860, 2022. DOI: 10.1214/21-AIHP1188.

[14] R. D. Blandford and E. T. Scharlemann. On induced Compton scattering by relativistic particles. *Astrophysics and Space Science*, 36(2):303–317, Sept. 1975. DOI: 10.1007/bf00645256.

[15] G. R. Blumenthal and R. J. Gould. Bremsstrahlung, synchrotron radiation, and compton scattering of high-energy electrons traversing dilute gases. *Rev. Mod. Phys.*, 42:237–270, 2, Apr. 1970. DOI: 10.1103/RevModPhys.42.237.

[16] R. A. Blythe and M. R. Evans. Nonequilibrium steady states of matrix-product form: a solver's guide. *Journal of Physics A: Mathematical and Theoretical*, 40(46):R333–R441, Oct. 2007. DOI: 10.1088/1751-8113/40/46/r01.

[17] D. Bohm and B. Hiley. *The Undivided Universe: An Ontological Interpretation of Quantum Theory*. Physics, philosophy. Routledge, 1993. ISBN: 9780415065887.

[18] D. Bohm. Comments on an Article of Takabayasi conserning the Formulation of Quantum Mechanics with Classical Pictures. *Progress of Theoretical Physics*, 9(3):273–287, Mar. 1953. ISSN: 0033-068X. DOI: 10.1143/ptp/9.3.273. eprint: https://academic.oup.com/ptp/article-pdf/9/3/273/5413208/9-3-273.pdf.

[19] M. Bojowald. *Canonical Gravity and Applications*. Cambridge University Press, Dec. 2010. DOI: 10.1017/cbo9780511921759.

[20] S. Bose, A. Mazumdar, G. W. Morley, H. Ulbricht, M. Toroš, M. Paternostro, A. A. Geraci, P. F. Barker, M. S. Kim, and G. Milburn. Spin entanglement witness for quantum gravity. *Phys. Rev. Lett.*, 119:240401, 24, Dec. 2017. DOI: 10.1103/PhysRevLett.119.240401.

[21] D. Boyer and C. Solis-Salas. Random walks with preferential relocations to places visited in the past and their application to biology. *Phys. Rev. Lett.*, 112:240601, 24, June 2014. DOI: 10.1103/PhysRevLett.112.240601.

[22] G. Breit. An interpretation of dirac's theory of the electron. *Proceedings of the National Academy of Sciences*, 14(7):553–559, July 1928. DOI: 10.1073/pnas.14.7.553.

[23] R. Brinzanik, P. Jensen, and K. Bennemann. Model study for the nonequilibrium magnetic domain structure during the growth of nanostructured ultrathin films. *Journal of Magnetism and Magnetic Materials*, 238(2):258–269, 2002. ISSN: 0304-8853. DOI: https://doi.org/10.1016/S0304-8853(01)00926-X. URL: https://www.sciencedirect.com/science/article/pii/S030488530100926X.

[24] L. S. Brown. Compton scattering in a plasma. *Annals of Physics*, 200(1):190–205, 1990.

[25] L. S. Brown and D. L. Preston. Leading relativistic corrections to the kompaneets equation. *Astroparticle Physics*, 35(11):742–748, 2012.

[26] T. Buchert. Dark Energy from structure: a status report. *General Relativity and Gravitation*, 40(2-3):467–527, Dec. 2007. DOI: 10.1007/s10714-007-0554-8.

[27] C. Buet, B. Després, and T. Leroy. Anisotropic models and angular moments methods for the Compton scattering. working paper or preprint, Feb. 2018. URL: https://hal.sorbonne-universite.fr/hal-01717173.

[28] P. S. Burada, R. Maity, and F. Jülicher. Hydrodynamics of chiral squirmers. *Physical Review E*, 105(2), Feb. 2022. DOI: 10.1103/physreve.105.024603.

[29] C. Burigana, P. Procopio, and A. De Rosa. On the solution of the kompaneets equation in cosmological context: a numerical code to predict the cmb spectrum under general conditions. *Proceedings of the International Astronomical Union*, 6(S274):361–364, 2010. DOI: 10.1017/S1743921311007277.

[30] C. Burigana. Sunyaev-zeldovich and cosmic microwave background. In *Proceedings of First MCCT-SKADS Training School — PoS(MCCT-SKADS)*. Sissa Medialab, Aug. 2008. DOI: 10.22323/1.059.0013.

[31] M. Cannoni. Lorentz invariant relative velocity and relativistic binary collisions. *International Journal of Modern Physics A*, 32(02n03):1730002, Jan. 2017. DOI: 10.1142/s0217751x17300022.

[32] S. Carlip. *General Relativity*. Oxford University Press, London, England, Jan. 2019.

[33] P. Cartier and C. DeWitt-Morette. *Functional integration: action and symmetries*. Cambridge University Press, 2006.

[34] J. R. Cash and A. H. Karp. A variable order runge-kutta method for initial value problems with rapidly varying right-hand sides. *ACM Transactions on Mathematical Software (TOMS)*, 16(3):201–222, 1990.

[35] C. Cercignani and G. M. Kremer. Relativistic boltzmann equation. In *The Relativistic Boltzmann Equation: Theory and Applications*, pages 31–63. Springer, 2002.

[36] A. Challinor and A. Lasenby. Relativistic corrections to the sunyaev-zeldovich effect. *The Astrophysical Journal*, 499(1):1, 1998.

[37] P. Chelminiak. Non-linear diffusion with stochastic resetting. *arXiv preprint arXiv:2107.14680*, 2021.

[38] J. Chen, J. You, and F. Cheng. Diffusion approximation in comptonization process of hard x-ray passing through a 'cold' plasma-a generalized kompaneets equation. *Journal of Physics A: Mathematical and General*, 27(8):2905–2914, Apr. 1994. DOI: 10.1088/0305-4470/27/8/026.

[39] K. Cheung, J.-L. Kuo, K.-W. Ng, and Y.-L. S. Tsai. The impact of EDGES 21-cm data on dark matter interactions. *Physics Letters B*, 789:137–144, 2019. ISSN: 0370-2693. DOI: https://doi.org/10.1016/j.physletb.2018.11.058. URL: https://www.sciencedirect.com/science/article/pii/S0370269318309419.

[40] T. Christodoulakis and J. Zanelli. Operator ordering in quantum mechanics and quantum gravity. *Il Nuovo Cimento B Series 11*, 93(1):1–21, May 1986. DOI: 10.1007/bf02728299.

[41] C. Cocozza-Thivent. Processus des misanthropes. *Zeitschrift für Wahrscheinlichkeitstheorie und Verwandte Gebiete*, 70(4):509–523, 1985. DOI: 10.1007/bf00531864.

[42] S. Colin and H. M. Wiseman. The zig-zag road to reality. *Journal of Physics A: Mathematical and Theoretical*, 44(34):345304, Aug. 2011. DOI: 10.1088/1751-8113/44/34/345304.

[43] S. Colin and W. Struyve. Quantum non-equilibrium and relaxation to equilibrium for a class of de broglie–bohm-type theories. *New Journal of Physics*, 12(4):043008, Apr. 2010. DOI: 10.1088/1367-2630/12/4/043008.

[44] G. Cooper. Compton fokker-planck equation for hot plasmas. *Physical Review D*, 3(10):2312, 1971.

[45] E. Cortés and M. Escobedo. On a boltzmann equation for compton scattering from non relativistic electrons at low density. *Journal of Statistical Physics*, 175(5):819–878, 2019.

[46] D. d'Enterria and G. G. da Silveira. Observing light-by-light scattering at the large hadron collider. *Physical Review Letters*, 111(8), 2013. DOI: 10.1103/physrevlett.111.080405.

[47] S. Das, D.-A. Deckert, L. Kellers, and W. Struyve. Double-slit experiment remastered, 2022. arXiv: 2211.13362 [quant-ph].

[48] S. Das and M. Nöth. Times of arrival and gauge invariance. *Proceedings of the Royal Society A: Mathematical, Physical and Engineering Sciences*, 477(2250):20210101, June 2021. DOI: 10.1098/rspa.2021.0101.

[49] S. Das, M. Nöth, and D. Dürr. Exotic bohmian arrival times of spin-1/2 particles: an analytical treatment. *Physical Review A*, 99(5), May 2019. DOI: 10.1103/physreva.99.052124.

[50] S. Das and W. Struyve. Questioning the adequacy of certain quantum arrival-time distributions. *Physical Review A*, 104(4), Oct. 2021. DOI: 10.1103/physreva.104.042214.

[51] G. F. de Angelis, G. Jona-Lasinio, M. Serva, and N. Zanghì. Stochastic mechanics of a dirac particle in two spacetime dimensions. *Journal of Physics A: Mathematical and General*, 19(6):865, Apr. 1986. DOI: 10.1088/0305-4470/19/6/017.

[52] T. Demaerel, W. De Roeck, and C. Maes. Producing suprathermal tails in the stationary velocity distribution. *Physica A: Statistical Mechanics and its Applications*, 552:122179, 2020. ISSN: 0378-4371. DOI: https://doi.org/10.1016/j.physa.2019.122179. URL: https://www.sciencedirect.com/science/article/pii/S0378437119312634. Tributes of Non-equilibrium Statistical Physics.

[53] T. Demaerel, C. Maes, and W. Struyve. Cosmic acceleration from quantum friedmann equations. *Classical and Quantum Gravity*, 37(8):085006, Mar. 2020. DOI: 10.1088/1361-6382/ab738b.

[54] T. Demaerel and W. Struyve. Elimination of cosmological singularities in quantum cosmology by suitable operator orderings. *Physical Review D*, 100(4), Aug. 2019. DOI: 10.1103/physrevd.100.046008.

[55] H. Dreicer. Kinetic theory of an electron-photon gas. *Physics of Fluids*, 7(5):735, 1964. DOI: 10.1063/1.1711276.

[56] D. Dürr, S. Goldstein, T. Norsen, W. Struyve, and N. Zanghì. Can bohmian mechanics be made relativistic? *Proceedings of the Royal Society A: Mathematical, Physical and Engineering Sciences*, 470(2162):20130699, Feb. 2014. DOI: 10.1098/rspa.2013.0699.

[57] D. Dürr, S. Goldstein, R. Tumulka, and N. Zanghì. Bell-type quantum field theories. *Journal of Physics A: Mathematical and General*, 38(4):R1–R43, Jan. 2005. DOI: 10.1088/0305-4470/38/4/r01.

[58] D. Dürr and W. Struyve. Quantum einstein equations. *Classical and Quantum Gravity*, 37(13):135002, June 2020. DOI: 10.1088/1361-6382/ab92ed.

[59] M. Escobedo and S. Mischler. On a quantum boltzmann equation for a gas of photons. *Journal de Mathématiques Pures et Appliquées*, 80(5):471–515, 2001. ISSN: 0021-7824. DOI: https://doi.org/10.1016/S0021-7824(00)01201-0. URL: https://www.sciencedirect.com/science/article/pii/S0021782400012010.

[60] M. Esfeld, M. Hubert, D. Lazarovici, and D. Dürr. The ontology of bohmian mechanics. *The British Journal for the Philosophy of Science*, 65(4):773–796, 2014. DOI: 10.1093/bjps/axt019.

[61] M. R. Evans and S. N. Majumdar. Diffusion with optimal resetting. *Journal of Physics A: Mathematical and Theoretical*, 44(43):435001, Oct. 2011. DOI: 10.1088/1751-8113/44/43/435001.

[62] M. R. Evans, S. N. Majumdar, and G. Schehr. Stochastic resetting and applications. *Journal of Physics A: Mathematical and Theoretical*, 53(19):193001, Apr. 2020. DOI: 10.1088/1751-8121/ab7cfe.

[63] M. R. Evans and S. N. Majumdar. Diffusion with stochastic resetting. *Phys. Rev. Lett.*, 106:160601, 16, Apr. 2011. DOI: 10.1103/PhysRevLett.106.160601.

[64] F. Falciano, N. Pinto-Neto, and W. Struyve. Wheeler-DeWitt quantization and singularities. *Physical Review D*, 91(4), Feb. 2015. DOI: 10.1103/physrevd.91.043524.

[65] K. Fang, Z. Yu, and S. Fan. Realizing effective magnetic field for photons by controlling the phase of dynamic modulation. *Nature Photonics*, 6(11):782–787, Nov. 2012. ISSN: 1749-4885. DOI: 10.1038/nphoton.2012.236.

[66] E. Fermi. On the origin of the cosmic radiation. *Phys. Rev.*, 75:1169–1174, 8, Apr. 1949. DOI: 10.1103/PhysRev.75.1169.

[67] R. P. Feynman, A. R. Hibbs, and D. F. Styer. *Quantum mechanics and path integrals*. Courier Corporation, 2010.

[68] D. J. Fixsen, A. Kogut, S. Levin, M. Limon, P. Lubin, P. Mirel, M. Seiffert, J. Singal, E. Wollack, T. Villela, and C. A. Wuensche. ARCADE 2 MEASUREMENT OF THE ABSOLUTE SKY BRIGHTNESS AT 3-90 GHz. *The Astrophysical Journal*, 734(1):5, May 2011. DOI: 10.1088/0004-637x/734/1/5.

[69] É. Fodor, R. L. Jack, and M. E. Cates. Irreversibility and biased ensembles in active matter: insights from stochastic thermodynamics. *Annual Review of Condensed Matter Physics*, 13(1):215–238, Mar. 2022. DOI: 10.1146/annurev-conmatphys-031720-032419.

[70] T. D. Frank. Strongly nonlinear stochastic processes in physics and the life sciences. *ISRN Mathematical Physics*, 2013:1–28, Mar. 2013. DOI: 10.1155/2013/149169.

[71] T. D. Frank. *Nonlinear Fokker-Planck equations: fundamentals and applications*. Springer Science & Business Media, 2005.

[72] G. E. Freire Oliveira. *Statistical Mechanics of the Kompaneets Equation*. Master's thesis, KU Leuven. Faculteit Wetenschappen, Leuven, 2021.

[73] G. E. Freire Oliveira, C. Maes, and K. Meerts. On the derivation of the kompaneets equation. *Astroparticle Physics*, 133:102644, Dec. 2021. DOI: 10.1016/j.astropartphys.2021.102644.

[74] G. E. Freire Oliveira, C. Maes, and K. Meerts. Photon frequency diffusion process. *Journal of Statistical Physics*, 189(1), July 2022. DOI: 10.1007/s10955-022-02960-0.

[75] G. E. Freire Oliveira, C. Maes, and K. Meerts. Resetting photons. *Journal of Physics A: Mathematical and Theoretical*, 55(41):414004, Oct. 2022. DOI: 10.1088/1751-8121/ac9261.

[76] T. Funaki. A certain class of diffusion processes associated with nonlinear parabolic equations. *Zeitschrift für Wahrscheinlichkeitstheorie und Verwandte Gebiete*, 67(3):331–348, 1984. DOI: 10.1007/bf00535008.

[77] M. Gondran and A. Gondran. Numerical simulation of the double slit interference with ultracold atoms. *American Journal of Physics*, 73(6):507–515, June 2005. DOI: 10.1119/1.1858484.

[78] W. Greiner et al. *Relativistic quantum mechanics*, volume 2. Springer, 2000.

[79] G. Grimmett and D. Stirzaker. *Probability and random processes*. Oxford University Press, London, England, 4th edition, July 2020.

[80] P. R. Holland. The dirac equation in the de broglie-bohm theory of motion. *Foundations of Physics*, 22(10):1287–1301, Oct. 1992. DOI: 10.1007/bf01889714.

[81] P. Holland. *The Quantum Theory of Motion: An Account of the de Broglie-Bohm Causal Interpretation of Quantum Mechanics*. Cambridge University Press, 1995. ISBN: 9780521485432.

[82] P. Holland and C. Philippidis. Implications of lorentz covariance for the guidance equation in two-slit quantum interference. *Physical Review A*, 67(6), June 2003. DOI: 10.1103/physreva.67.062105.

[83] W. T. Hu. *Wandering in the Background: A Cosmic Microwave Background Explorer*. PhD thesis, University of California at Berkeley, 1995.

[84] N. Itoh, Y. Kohyama, and S. Nozawa. Relativistic corrections to the sunyaev-zeldovich effect for clusters of galaxies. *The Astrophysical Journal*, 502(1):7, 1998.

[85] Itoh, N. and Nozawa, S. Relativistic corrections to the sunyaev-zeldovich effect for extremely hot clusters of galaxies*. *A&A*, 417(3):827–832, 2004. DOI: 10.1051/0004-6361:20034236.

[86] N. Iwamoto. Electron kinetic equations for Comptonization by isotropic photons. *The Astrophysical Journal*, 265:1021–1035, 1983.

[87] M. Jara, C. Landim, and S. Sethuraman. Nonequilibrium fluctuations for a tagged particle in one-dimensional sublinear rate zero-range processes, 2010. arXiv: 1011.1199 [math.PR].

[88] J. M. Jauch and F. Rohrlich. *The Theory of Photons and Electrons*. Springer Berlin Heidelberg, 1976. DOI: 10.1007/978-3-642-80951-4.

[89] O. Jefimenko. *Causality, Electromagnetic Induction, and Gravitation: A Different Approach to the Theory of Electromagnetic and Gravitational Fields*. Electret Scientific Company, 2000. ISBN: 9780917406232.

[90] T. Josset, A. Perez, and D. Sudarsky. Dark energy from violation of energy conservation. *Physical Review Letters*, 118(2), Jan. 2017. DOI: 10.1103/physrevlett.118.021102.

[91] M. Kac. A stochastic model related to the telegrapher's equation. *The Rocky Mountain Journal of Mathematics*, 4(3):497–509, 1974. ISSN: 00357596, 19453795. URL: http://www.jstor.org/stable/44236399 (visited on 03/16/2023).

[92] L. P. Kadanoff. *Quantum statistical mechanics*. CRC Press, 2018.

[93] J. I. Katz. High energy astrophysics. *Frontiers in Physics*, 1987.

[94] O. Kavian. Remarks on the Kompaneets equation, a simplified model of the Fokker-Planck equation. In *Nonlinear Partial Differential Equations and their Applications - Collège de France Seminar Volume XIV*, pages 469–487. Elsevier, 2002. DOI: 10.1016/s0168-2024(02)80022-4.

[95] L. Kellers. *Making Use of Quantum Trajectories for Numerical Purposes*. Master's thesis, LMU München, 2017.

[96] C. Kiefer. *Quantum Gravity*. en. International Series of Monographs on Physics. Oxford University Press, London, England, May 2004.

[97] J. Koch, A. A. Houck, K. L. Hur, and S. M. Girvin. Time-reversal-symmetry breaking in circuit-qed-based photon lattices. *Phys. Rev. A*, 82:043811, 4, Oct. 2010. DOI: 10.1103/PhysRevA.82.043811.

[98] V. N. Kolokoltsov. *Nonlinear Markov Processes and Kinetic Equations*. Cambridge Tracts in Mathematics. Cambridge University Press, 2010. DOI: 10.1017/CBO9780511760303.

[99] A. S. Kompaneets. The Establishment of Thermal Equilibrium between Quanta and Electrons. *Soviet Journal of Experimental and Theoretical Physics*, 4(5):730–737, May 1957.

[100] K. Kuchař. Canonical quantization of gravity. In *Astrophysics and Space Science Library*, pages 237–288. Springer Netherlands, 1973. DOI: 10.1007/978-94-010-2639-0_5.

[101] C. Kurtsiefer, T. Pfau, and J. Mlynek. Measurement of the wigner function of an ensemble of helium atoms. *Nature*, 386(6621):150–153, Mar. 1997. DOI: 10.1038/386150a0.

[102] C. D. Levermore, H. Liu, and R. L. Pego. Global dynamics of bose–einstein condensation for a model of the kompaneets equation. *SIAM Journal on Mathematical Analysis*, 48(4):2454–2494, 2016. DOI: 10.1137/15M1054377.

[103] D. A. Liedahl. The x-ray spectral properties of photoionized plasmas and transient plasmas. In *X-Ray Spectroscopy in Astrophysics*, pages 189–268. Springer Berlin Heidelberg, 1999. DOI: 10.1007/978-3-540-49199-6_3.

[104] A. P. Lightman. Double compton emission in radiation dominated thermal plasmas. *The Astrophysical Journal*, 244:392, Mar. 1981. DOI: 10.1086/158716.

[105] Liu, D.-B., Chen, L., Ling, J. J., You, J. H., and Hua, X. M. Evolution of x-ray spectra in down-comptonization. a comparison of the extended kompaneets equation with monte carlo simulation and the ross-mccray equation. *A&A*, 417(2):381–389, 2004. DOI: 10.1051/0004-6361:20031765.

[106] B. Loewe, A. Souslov, and P. M. Goldbart. Flocking from a quantum analogy: spin–orbit coupling in an active fluid. *New Journal of Physics*, 20(1):013020, Jan. 2018. DOI: 10.1088/1367-2630/aa9cdc.

[107] M. S. Longair. *High energy astrophysics*. Cambridge university press, 2010.

[108] C. Maes. Local detailed balance. *SciPost Physics Lecture Notes*, July 2021. DOI: 10.21468/scipostphyslectnotes.32.

[109] C. Maes, K. Meerts, and W. Struyve. Diffraction and interference with run-and-tumble particles. *Physica A: Statistical Mechanics and its Applications*, 598:127323, July 2022. DOI: 10.1016/j.physa.2022.127323.

[110] C. Maes, K. Meerts, and W. Struyve. Wave mechanics for gravity with point-particles. *Classical and Quantum Gravity*, 38(17):175003, Aug. 2021. DOI: 10.1088/1361-6382/ac12e3.

[111] C. Marletto and V. Vedral. Gravitationally induced entanglement between two massive particles is sufficient evidence of quantum effects in gravity. *Physical Review Letters*, 119(24), Dec. 2017. DOI: 10.1103/physrevlett.119.240402.

[112] J. Masoliver, J. M. Porrà, and G. H. Weiss. Solution to the telegrapher's equation in the presence of reflecting and partly reflecting boundaries. *Phys. Rev. E*, 48:939–944, 2, Aug. 1993. DOI: 10.1103/PhysRevE.48.939.

[113] D. P. A. Maurice. The quantum theory of the electron. *Proceedings of the Royal Society of London. Series A, Containing Papers of a Mathematical and Physical Character*, 117(778):610–624, Feb. 1928. DOI: 10.1098/rspa.1928.0023.

[114] H. P. McKean. A class of Markov processes associated with nonlinear parabolic equations. *Proceedings of the National Academy of Sciences*, 56(6):1907–1911, Dec. 1966. DOI: 10.1073/pnas.56.6.1907.

[115] K. Meerts. Photon diffusion process. https://gitlab.kuleuven.be/u0131889/photon-diffusion-process/-/tags/v1.0.

[116] K. Meerts. Zig-zag electrons, 2021. URL: https://github.com/kaspermeerts/zigzagelectrons.

[117] P. G. Merli, G. F. Missiroli, and G. Pozzi. On the statistical aspect of electron interference phenomena. *American Journal of Physics*, 44(3):306–307, Mar. 1976. DOI: 10.1119/1.10184.

[118] D.-A. Mihu, M.-A. Dariescu, and G. Amanoloaei. Generalized special solutions to modified kompaneets equation. *AIP Conference Proceedings*, 2071(1):020004, 2019. DOI: 10.1063/1.5090051.

[119] D. Millar. A calculation of the differential cross section for compton scattering in tree-level quantum electrodynamics, 2014. Lecture notes.

[120] J. Muga and C. Leavens. Arrival time in quantum mechanics. *Physics Reports*, 338(4):353–438, 2000. ISSN: 0370-1573. DOI: https://doi.org/10.1016/S0370-1573(00)00047-8. URL: https://www.sciencedirect.com/science/article/pii/S0370157300000478.

[121] D. I. Nagirner, V. M. Loskutov, and S. I. Grachev. Exact and numerical solutions of the kompaneets equation: evolution of the spectrum and average frequencies. *Astrophysics*, 40(3):227–236, July 1997. DOI: 10.1007/bf03035735.

[122] S. Nozawa and Y. Kohyama. Analytical study on the sunyaev-zeldovich effect for clusters of galaxies. *Physical Review D*, 79(8):083005, 2009.

[123] S. Nozawa and Y. Kohyama. Relativistic corrections to the kompaneets equation. *Astroparticle Physics*, 62:30–32, 2015.

[124] S. Nozawa, Y. Kohyama, and N. Itoh. Analytical study on the sunyaev-zeldovich effect for clusters of galaxies. ii. comparison of covariant formalisms. *Physical Review D*, 82(10):103009, 2010.

[125] K. B. Oldham, J. C. Myland, and J. Spanier. *The macdonald function kv(x)*. In *An Atlas of Functions: with Equator, the Atlas Function Calculator*. Springer US, New York, NY, 2009, pages 527–536. ISBN: 978-0-387-48807-3. DOI: 10.1007/978-0-387-48807-3_52.

[126] A. E. Patteson, A. Gopinath, M. Goulian, and P. E. Arratia. Running and tumbling with e. coli in polymeric solutions. *Scientific Reports*, 5(1), Oct. 2015. DOI: 10.1038/srep15761.

[127] W. Pauli. Über das thermische gleichgewicht zwischen strahlung und freien elektronen. *Zeitschrift für Physik*, 18(1):272–286, 1923.

[128] E. Pechersky, A. Yambartsev, and V. Zagrebnov. Stochastic dynamics of Einstein matter-radiation model with spikes, 2018. arXiv: 1803.08962 [math.PR].

[129] P. J. E. Peebles, L. A. Page Jr, and R. B. Partridge. *Finding the big bang*. Cambridge University Press, 2009.

[130] R. Penrose. *The road to reality : a complete guide to the laws of the universe*. Vintage, London, 2005. ISBN: 978-0-09-944068-0.

[131] C. Philippidis, C. Dewdney, and B. J. Hiley. Quantum interference and the quantum potential. *Il Nuovo Cimento B Series 11*, 52(1):15–28, July 1979. DOI: 10.1007/bf02743566.

[132] N. Pinto-Neto and E. S. Santini. Must quantum spacetimes be euclidean? *Physical Review D*, 59(12), May 1999. DOI: 10.1103/physrevd.59.123517.

[133] N. Pinto-Neto and E. Santini. The accelerated expansion of the universe as a quantum cosmological effect. *Physics Letters A*, 315(1-2):36–50, Aug. 2003. DOI: 10.1016/s0375-9601(03)01000-4.

[134] N. Pinto-Neto and W. Struyve. Bohmian quantum gravity and cosmology. In X. O. Pladevall and J. Mompart, editors, *Applied Bohmian Mechanics*, chapter 10. Jenny Stanford Publishing, May 2019.

[135] C. Pitrou. Radiative transport of relativistic species in cosmology. *Astroparticle Physics*:102494, 2020.

[136] D. Pozar. *Microwave Engineering*. Wiley, 2004. ISBN: 9780471448785.

[137] P. Procopio and C. Burigana. A numerical code for the solution of the kompaneets equation in cosmological context. *Astronomy & Astrophysics*, 507(3):1243–1256, 2009.

[138] S. Ramaswamy. The mechanics and statistics of active matter. *Annual Review of Condensed Matter Physics*, 1(1):323–345, Aug. 2010. DOI: 10.1146/annurev-conmatphys-070909-104101.

[139] P. Romanczuk, M. Bär, W. Ebeling, B. Lindner, and L. Schimansky-Geier. Active brownian particles. *The European Physical Journal Special Topics*, 202(1):1–162, Mar. 2012. DOI: 10.1140/epjst/e2012-01529-y.

[140] R. R. Ross, R. Weaver, and R. McCray. The comptonization of iron x-ray features in compact x-ray sources. *The Astrophysical Journal*, 219:292–299, 1978.

[141] P. Roushan, C. Neill, A. Megrant, Y. Chen, R. Babbush, R. Barends, B. Campbell, Z. Chen, B. Chiaro, A. Dunsworth, A. Fowler, E. Jeffrey, J. Kelly, E. Lucero, J. Mutus, P. J. J. O'Malley, M. Neeley, C. Quintana, D. Sank, A. Vainsencher, J. Wenner, T. White, E. Kapit, H. Neven, and J. Martinis. Chiral ground-state currents of interacting photons in a synthetic magnetic field. *Nature Physics*, 13(2):146–151, Oct. 2016. DOI: 10.1038/nphys3930.

[142] D. Roy. Two-photon scattering by a driven three-level emitter in a one-dimensional waveguide and electromagnetically induced transparency. *Phys. Rev. Lett.*, 106:053601, 5, Feb. 2011. DOI: 10.1103/PhysRevLett.106.053601.

[143] D. Roy, C. M. Wilson, and O. Firstenberg. Colloquium: strongly interacting photons in one-dimensional continuum. *Rev. Mod. Phys.*, 89:021001, 2, May 2017. DOI: 10.1103/RevModPhys.89.021001.

[144] G. B. Rybicki and A. P. Lightman. *Radiative processes in astrophysics*. John Wiley & Sons, 2008.

[145] A. S. Sanz and S. Miret-Artés. A trajectory-based understanding of quantum interference. *Journal of Physics A: Mathematical and Theoretical*, 41(43):435303, Sept. 2008. DOI: 10.1088/1751-8113/41/43/435303.

[146] A. Sanz, M. Davidović, and M. Božić. Full quantum mechanical analysis of atomic three-grating mach–zehnder interferometry. *Annals of Physics*, 353:205–221, Feb. 2015. DOI: 10.1016/j.aop.2014.11.012.

[147] Á. S. Sanz and S. Miret-Artés. *A Trajectory Description of Quantum Processes. II. Applications*. Springer Berlin Heidelberg, 2014. DOI: 10.1007/978-3-642-17974-7.

[148] M. J. Schnitzer. Theory of continuum random walks and application to chemotaxis. *Phys. Rev. E*, 48:2553–2568, 4, Oct. 1993. DOI: 10.1103/PhysRevE.48.2553.

[149] E. Schrödinger. Über die kräftefreie bewegung in der relativistischen quantenmechanik. *Preuss. Akad. Wiss. Berlin*, 24:418–428, 1930.

[150] S. S. Schweber. Feynman and the visualization of space-time processes. *Rev. Mod. Phys.*, 58:449–508, 2, Apr. 1986. DOI: 10.1103/RevModPhys.58.449.

[151] F. Schweitzer, W. Ebeling, and B. Tilch. Complex motion of brownian particles with energy depots. *Phys. Rev. Lett.*, 80:5044–5047, 23, June 1998. DOI: 10.1103/PhysRevLett.80.5044.

[152] M. Seiffert, D. J. Fixsen, A. Kogut, S. M. Levin, M. Limon, P. M. Lubin, P. Mirel, J. Singal, T. Villela, E. Wollack, and C. A. Wuensche. Interpretation of the ARCADE 2 absolute sky brightness measurement. *The Astrophysical Journal*, 734(1):6, May 2011. DOI: 10.1088/0004-637x/734/1/6.

[153] S. Sethuraman. On diffusivity of a tagged particle in asymmetric zero-range dynamics, 2004. arXiv: math/0410181 [math.PR].

[154] D. Shirk. A Practical Review of the Kompaneets Equation and its Application to Compton Scattering. Technical report, Los Alamos National Lab. (LANL), May 2006. DOI: 10.2172/891567.

[155] J. Silvester. An examination of differential cross sections for compton scattering, 2014. Lecture notes.

[156] H. Spohn. *Dynamics of Charged Particles and their Radiation Field*. Cambridge University Press, Aug. 2004. DOI: 10.1017/cbo9780511535178.

[157] E. J. Squires. A quantum solution to a cosmological mystery. *Physics Letters A*, 162(1):35–36, Jan. 1992. DOI: 10.1016/0375-9601(92)90955-1.

[158] W. Struyve. On the zig-zag pilot-wave approach for fermions. *Journal of Physics A: Mathematical and Theoretical*, 45(19):195307, Apr. 2012. DOI: 10.1088/1751-8113/45/19/195307.

[159] W. Struyve. Pilot-wave approaches to quantum field theory. *Journal of Physics: Conference Series*, 306:012047, July 2011. DOI: 10.1088/1742-6596/306/1/012047.

[160] W. Struyve. Semi-classical approximations based on bohmian mechanics. *International Journal of Modern Physics A*, 35(14):2050070, May 2020. DOI: 10.1142/s0217751x20500700.

[161] W. Struyve. Towards a novel approach to semi-classical gravity. In *The Philosophy of Cosmology*, pages 356–374. Cambridge University Press, Jan. 2017. DOI: 10.1017/9781316535783.019.

[162] W. Struyve. Wheeler–DeWitt quantization for point-particles. *General Relativity and Gravitation*, 53(3), Mar. 2021. DOI: 10.1007/s10714-021-02802-6.

[163] P. A. Sturrock. Stochastic acceleration. *Phys. Rev.*, 141:186–191, 1, Jan. 1966. DOI: 10.1103/PhysRev.141.186.

[164] R. A. Sunyaev and Y. B. Zeldovich. Distortions of the background radiation spectrum. *Nature*, 223(5207):721–722, Aug. 1969. DOI: 10.1038/223721a0.

[165] R. A. Sunyaev and Y. B. Zeldovich. The Observations of Relic Radiation as a Test of the Nature of X-Ray Radiation from the Clusters of Galaxies. *Comments on Astrophysics and Space Physics*, 4:173, Nov. 1972.

[166] Y. Suwa, H. W. Tahara, and E. Komatsu. Kompaneets equation for neutrinos: application to neutrino heating in supernova explosions. *Progress of Theoretical and Experimental Physics*, 2019(8):083E04, 2019.

[167] J. Terrall. Elementary treatment of relativistic cross sections. *American Journal of Physics*, 38(12):1460–1474, 1970.

[168] S. Teufel and D. Dürr. *Bohmian Mechanics*. Springer Berlin Heidelberg, 2009. DOI: 10.1007/b99978.

[169] H. Tong, C. Faloutsos, and J.-Y. Pan. Random walk with restart: fast solutions and applications. *Knowledge and Information Systems*, 14(3):327–346, July 2007. DOI: 10.1007/s10115-007-0094-2.

[170] H. Tong, R.-X. Xu, Q.-H. Peng, and L.-M. Song. Resonant cyclotron scattering in pulsar magnetospheres and its application to isolated neutron stars. *Research in Astronomy and Astrophysics*, 10(6):553, 2010.

[171] A. Tonomura, J. Endo, T. Matsuda, T. Kawasaki, and H. Ezawa. Demonstration of single-electron buildup of an interference pattern. *American Journal of Physics*, 57(2):117–120, Feb. 1989. DOI: 10.1119/1.16104.

[172] R. Toral and P. Colet, editors. *Stochastic Numerical Methods*. Wiley-VCH Verlag GmbH & Co. KGaA, July 2014. DOI: 10.1002/9783527683147.

[173] C. Univ, M. Brin, W. on Dynamical Systems, R. Topics, K. Burns, D. Dolgopyat, and Y. Pesin. *Fermi acceleration*. In *Geometric and Probabilistic Structures in Dynamics: Workshop on Dynamical Systems and Related Topics in Honor of Michael Brin on the Occasion of His 60th Birthday, March 15-18, 2008, University of Maryland, College Park, MD*. Contemporary mathematics - American Mathematical Society. American Mathematical Society, 2008, page 149. ISBN: 9780821842867.

[174] C. van Weert, W. van Leeuwen, and S. de Groot. Elements of relativistic kinetic theory. *Physica*, 69(2):441–457, 1973. ISSN: 0031-8914. DOI: https://doi.org/10.1016/0031-8914(73)90082-7. URL: https://www.sciencedirect.com/science/article/pii/0031891473900827.

[175] H. van Hees. Introduction to relativistic transport theory, 2020. Lecture notes.

[176] R. M. Wald. *General Relativity*. University of Chicago Press, Chicago, IL, June 1984.

[177] T. Wang and A. Burrows. Generalized kompaneets formalism for inelastic neutrino-nucleon scattering in supernova simulations. *Physical Review D*, 102(2):023017, 2020.

[178] G. H. Weiss. Some applications of persistent random walks and the telegrapher's equation. *Physica A: Statistical Mechanics and its Applications*, 311(3):381–410, 2002. ISSN: 0378-4371. DOI: https://doi.org/10.1016/S0378-4371(02)00805-1. URL: https://www.sciencedirect.com/science/article/pii/S0378437102008051.

[179] R. Weymann. Diffusion approximation for a photon gas interacting with a plasma via the compton effect. *Physics of Fluids*, 8(11):2112, 1965. DOI: 10.1063/1.1761165.

[180] Y. B. Zel'dovich. Interaction of free electrons with electromagnetic radiation. *Soviet Physics Uspekhi*, 18(2):79–98, Feb. 1975. DOI: 10.1070/pu1975v018n02abeh001947.

[181] X. Zhang and X. Chen. Extend the Kompaneets Equation to Down-Comptonization Process in a Novel Way. *arXiv e-prints*, Sept. 2015. eprint: arXiv:1509.00140.

List of publications

1. C. Maes, K. Meerts, and W. Struyve. Wave mechanics for gravity with point-particles. *Classical and Quantum Gravity*, 38(17):175003, Aug. 2021. DOI: 10.1088/1361-6382/ac12e3

2. G. E. Freire Oliveira, C. Maes, and K. Meerts. On the derivation of the kompaneets equation. *Astroparticle Physics*, 133:102644, Dec. 2021. DOI: 10.1016/j.astropartphys.2021.102644

3. C. Maes, K. Meerts, and W. Struyve. Diffraction and interference with run-and-tumble particles. *Physica A: Statistical Mechanics and its Applications*, 598:127323, July 2022. DOI: 10.1016/j.physa.2022.127323

4. G. E. Freire Oliveira, C. Maes, and K. Meerts. Photon frequency diffusion process. *Journal of Statistical Physics*, 189(1), July 2022. DOI: 10.1007/s10955-022-02960-0

5. G. E. Freire Oliveira, C. Maes, and K. Meerts. Resetting photons. *Journal of Physics A: Mathematical and Theoretical*, 55(41):414004, Oct. 2022. DOI: 10.1088/1751-8121/ac9261



FACULTY OF SCIENCE
DEPARTMENT OF PHYSICS AND ASTRONOMY
INSTITUUT VOOR THEORETISCHE FYSICA
Celestijnenlaan 200D box 2415
B-3001 Leuven